Distinct protective roles of CD4 and CD8 T cells in vaccine-mediated immunity against *Mycobacterium tuberculosis*

Holly Barrett

A dissertation

submitted in partial fulfillment of the

requirements for the degree of

Doctor of Philosophy

University of Washington

2024

Reading Committee:

Kevin Urdahl, Chair

Thomas Hawn

Rhea Coler

Program Authorized to Offer Degree:

Pathobiology

University of Washington

Abstract

Distinct protective roles of CD4 and CD8 T cells in vaccine-mediated immunity against *Mycobacterium tuberculosis*

Holly Barrett

Chair of the Supervisory Committee:

Kevin Urdahl

Department of Immunology and Department of Global Health

Despite widespread vaccination with Bacille Calmette-Guerin (BCG) globally, tuberculosis (TB) remains a major global health concern. A new vaccine is urgently needed, but our limited understanding of immunity against *Mycobacterium tuberculosis* (Mtb) infection is a major barrier to designing more effective vaccines. Mice are commonly used to study TB immunity but deficiencies in the current conventional dose (CD) (50-100 CFU) mouse model have left little confidence in its translation to humans. Our lab has overcome these limitations by developing a physiologic ultra-low dose (ULD) (1-3 CFUs) Mtb infection, which resembles several aspects of human Mtb infection**.** Here, we assess vaccine-mediated protection using the ULD model and identify three parameters of BCG-mediated protection: 1. Durable reduction in overall lung burden, 2. Prevention of dissemination to the contralateral lung, and 3. Prevention

of detectable infection in a subset of BCG vaccinated mice. Importantly, this is the first evidence that BCG vaccination can mediate sterilizing immunity in any mouse model of TB.

Next, we sought to determine the lymphocyte subsets responsible for BCG-mediated immunity. We investigated the impact of BCG vaccination on early Mtb immunity before confounding differences in bacterial burden occurred. We found that BCG induced a robust effector CD4 and CD8 T cell response in the lung during early Mtb infection while changes in lung B cells were less pronounced. Furthermore, T cell depletion reversed the protection conferred by BCG, whereas B cell deficiency had no effect. Finally, we assessed the relative roles of CD4 and CD8 T cells in BCG-mediated immunity and found that CD4 and CD8 T cells promoted distinct aspects of immunity. CD4 T cells played larger roles in control of lung burden and prevention of dissemination to the contralateral lung, whereas CD8 T cells were more important for prevention of infection and played a minor role in control of lung burden. These newfound roles of CD8 T cells in BCG-mediated protection were masked using the supraphysiologic conventional dose challenge and could only be detected in the ULD model.

Together, these studies further our understanding of vaccine-mediated protection against Mtb and highlight the ULD model as a superior platform for pre-clinical vaccine testing. Additionally, our work demonstrates distinct roles for CD4 and CD8 T cells in vaccine-mediated immunity. Targeting both aspects of immunity could be key to designing a more effective TB vaccine.

Table of Contents

List of Figures

List of Tables

Acknowledgements

There are many people I would like to thank, as this work would not have been possible without them. First and foremost, thank you to Kevin Urdahl for being an amazing advisor throughout my graduate career. I have learnt so much about TB and immunology from Kevin, who seems to have an endless wealth of knowledge in this field. His creativity and dedication to my project at all times of the day continuously motivated me to push through the bad days and celebrate the good days. His guidance and support helped me become a more confident researcher. I also want to thank Courtney Plumlee for her mentorship throughout every stage of my project. I turned to Courtney with every possible question swirling in my brain, no matter how big or small. She was also essential for translating Kevin's thoughts to me as I would often appear in her office after our weekly meeting and ask what Kevin meant when he said x, y, or z.

I want to thank the entire Urdahl lab for their emotional and experimental support. No one in our lab would survive without Courtney Plumlee and Sara Cohen, who we all agree run the day-to-day of the lab, and who we all depend upon for experimental and ABSL-3 support. Thank you to Ben Gern, my former desk neighbor, and his lab for support and guidance as I learned confocal microscopy. Thank you to all of the lab techs that have cycled through the lab during my graduate career. From help with plate pouring, to reagent ordering, to harvest prep and harvest help, to plate counting and DNA extractions, our lab techs were crucial for their behind-the-scenes work in all of my giant mouse experiments. Also, a big thank you to all of the Urdahl and Gern lab members for their help during my giant harvests. In particular, thank you to Sara Cohen, Lauren Cross (my current desk neighbor), Kim Foster, and Elya Shamskhou for their mouse injection expertise and assistance. I would not have been able to get through even one of these experiments without all of you. Lastly, thank you to the other Urdahl graduate students, Kim Foster and Elya Shamskhou, for their emotional support on the good and bad days. It was so helpful to have other students in the lab who understood the unique struggles of

TB research. Thank you, Kim, for all of the lunches we had together and for always being willing to take a break with me when I needed it the most.

I thank the SCRI OAC staff for their technical support and the UW Cell Analysis Facility for their flow cytometry support. I would like to thank our collaborators Danica Shao and Paul Edlefsen at Fred Hutch Cancer Center and Vitaly Ganusov at Texas Biomedical Research Institute for their statistical analysis and mathematical modeling expertise. Their contributions are specified in the acknowledgement sections at the end of chapters 2 and 3. Thank you to all of students in the Pathobiology program, particularly my 2019 cohort, for all of the fun, support, and great science. Thank you to the Pathobiology program manager Ernie Lefler and program directors Jennifer Lund (current) and Lee Ann Campbell (former). I would like to thank my supervisory committee members: Thomas Hawn, Rhea Coler, Michael Gerner, and Joshua Woodward for their feedback and guidance on this project.

Finally, I would like to thank my friends and family for their unwavering support throughout graduate school. My family is always there for me to lean on through the ups and downs. Their constant belief in me has helped me push forward and motivates me to keep going. Thank you to my other half, Monisha, for always having my back and understanding me better than anyone. In this particular stage of our lives, you remind me that no matter how hard grad school gets, medical school is ten times worse. Even though I am often anxious about the future, I look forward to the next stage with you.

Chapter 1. Introduction

1.1 Tuberculosis burden of disease

Tuberculosis (TB), caused by the bacterium *Mycobacterium tuberculosis* (Mtb), is still a major global health challenge. In 2022, there were 10.6 million new cases and 1.3 million deaths from TB disease, making it the second leading cause of death from an infectious disease after COVID-19 (1). Most of these cases were in South-East Asia, Africa, and the Western Pacific. The high burden and mortality of TB occurs despite the existence and global use of the Bacille Calmette-Guérin (BCG) vaccine against TB.

1.2 BCG vaccine

BCG has been used to vaccinate humans against TB since 1921 (2). It is a live attenuated vaccine derived from *Mycobacterium bovis,* which causes tuberculous disease in cows. Scientists Albert Calmette and Camille Guérin developed BCG from a strain of virulent *M. bovis* that became attenuated by passaging it in culture for over 10 years (3). BCG remains the only licensed vaccine against TB, and it is still used globally, typically administered intradermally (i.d.) at birth. This is because BCG consistently confers protection against disseminated TB such as TB meningitis and miliary TB during infancy and childhood (4)**.** However, the efficacy of BCG widely varies from 0-80% in adults (5, 6). Some studies have shown that BCG can sometimes provide long-term protection. For example, one major follow up study of a placebo-controlled trial among American Indians and Alaska Natives demonstrated that BCG vaccine efficacy persisted for 50 to 60 years (7). Other studies have shown no protective effect of BCG. A recent meta-analysis study proposed that the variability in BCG efficacy across studies could be due to the timing of exposure to Mtb as the results suggested BCG provided persistent protection in settings of declining TB burden but not in settings of sustained high TB

transmission (8). Other potential explanations for variable BCG efficacy include pre-exposure to environmental mycobacteria, variations in BCG vaccine strains, route of administration, and geographical location**,** however, specific mechanisms of this variable BCG efficacy are not fully understood (9). In order to develop more effective TB vaccines, we not only need a better understanding of TB immunity, but we also need a better understanding of BCG-mediated immunity.

1.3 Tuberculosis infection and disease outcomes

TB is transmitted via the airborne route when an individual inhales droplet nuclei expelled from a person with active TB who coughs, sneezes, speaks, or sings. Exposure to TB has a variety of outcomes. An estimated 20-25% of individuals become immunoreactive to Mtb antigens, which is measured as a positive TB immunoreactivity test (TST) or IFN-γ release assay (IGRA), however these tests are not 100% specific or sensitive (10, 11). Most of these individuals have actually cleared Mtb infection suggesting that a positive IGRA is not equivalent to infection or disease (11, 12). Because of this, there has been a recent shift towards recognizing the spectrum of infection and disease and very recent work aimed to address the inconsistency and confusion in the current definitions and terminology and develop a new consensus (13). This group proposed that while all states of infection and disease have viable Mtb and host responses, distinct TB states have differences in pathology, infectiousness, and symptoms and signs. For example, individuals with subclinical TB have macroscopic TB pathology and do not have TB symptoms or signs and are further divided into infectious or non-infectious sub-clinical TB states (13).

Most cases of clinical TB manifest as pulmonary tuberculosis (~85%) and individuals experience symptoms such as a persistent cough, fever, weight loss, night sweats, and fatigue (14, 15). The other 15% of cases clinically manifest as extrapulmonary tuberculosis which is

when Mtb disseminates to other anatomical sites including the lymph nodes, pleura, bone, and joints (15). It is important to consider these different outcomes of the TB infection and disease spectrum because vaccines may target different aspects of immunity that can prevent or control these different clinical manifestations.

1.4 Kinetics of the early host immune response to Mtb infection

Mtb infection begins when droplet nuclei between 1 to 5 μm containing Mtb bacilli are inhaled (16), travel through the airway, and reach the terminal alveoli where the first immune cells they encounter are alveolar macrophages (AM) (17). AM have many important functions in the lung to maintain homeostasis and to act as the first line of defense against inhaled pathogens by surveying the alveoli environment and phagocytosing pathogens including Mtb (18). However, Mtb has multiple mechanisms to evade degradation, such as prevention of phagolysosome fusion, and instead use AM as an early niche for infection (19, 20). Murine studies have shown that Mtb almost exclusively infect airway-resident AM the first days post-infection (p.i.) (17). The infected AM re-localize to the lung interstitium at which point Mtb are transferred to other immune cells including recruited monocyte-derived macrophages (MDM) and neutrophils between days 10-14 p.i., which leads to production of inflammatory cytokines and chemokines resulting in more recruitment of immune cells to the site of infection (17).

One such type of immune cell, neutrophils, are an active area of research in TB. Neutrophils may not contribute to the direct control of Mtb, but their influx is important for dendritic cell (DC) priming and therefore the initiation of the adaptive immune response (21, 22). However, patients with active TB have a high level of neutrophils in the blood and bronchoalveolar fluid and lung neutrophil frequencies correlate with lung burden early in infection (23, 24). A recent study from Gern *et al*. using a mouse model that recapitulates two

distinct types of TB lesions, necrotizing granulomas and alveolitis, discovers that neutrophils are required for lesion necrosis at both early and late stages of TB infection (25).

These innate cells become organized and form a lesion that will become a granuloma. Pulmonary granulomas are a hallmark feature or TB. The classically described composition of early granulomas includes a central core of uninfected and Mtb-infected macrophages surrounded by a cuff of T cells (26). B cells aggregates also form structures on the periphery of the granuloma called tertiary lymphoid structures (TLS), which also contain T follicular helper cells (Tfh), follicular dendritic cells, and high endothelial venules (26-28). The function of the granuloma is complex as historically it is thought that TB granulomas are protective to the host by containing the Mtb from the rest of the lung. However, more recently it has been shown that granulomas can be protective to Mtb by being a permissive environment and by limiting effector immune cells from infiltrating the core of the granuloma (29-31).

The initiation of the adaptive immune response to Mtb is slow as it takes 9-11 days for T cell responses to be initiated and several weeks for the T cell responses to peak (32). T cells recognize Mtb in the lung-draining lymph nodes (LN) so before T cell responses can be initiated, live Mtb bacteria must be transported to the lung-draining LN and Mtb antigen must be presented to T cells by DCs at this site (33-35). The slow kinetics of early immune response to TB, resulting, in part, from the localization of AM to the lung interstitium to the priming of T cells in the lung draining LN, all contribute to persistence of the Mtb infection as the bacteria has ample opportunity to replicate. There are other strategies Mtb uses to delay the immune response such as evading immune detection in the AM, inhibiting apoptosis, and an early induction of Mtb specific Tregs (32, 36). Activated lymphocytes migrate from the LN back to the lungs and have different roles in TB immunity including participating in granuloma formation. The functions of CD4 T cells, CD8 T cells, and B cells in TB immunity and vaccine-induced immunity are described in more depth below.

1.5 CD4 T cells and TB

It has been well established in mice and humans that CD4 T cells are critical for TB immunity. For example, antibody depletion of CD4 T cells has been used to show that CD4 T cells are required for control of bacterial burden in the lung and spleens (37, 38). In humans, HIV-infected individuals depleted of CD4 T cells are also restricted in their ability to contain Mtb infection (39). Th1 cells are the major CD4 T cell responding to TB infection primarily through production of IFN-γ which is thought to activate macrophages to enhance killing of Mtb via induction of iNOS and autophagy (40). Accordingly, IFN-γ knockout in mice and IFN-γ signaling deficits in humans result in increased susceptibility to mycobacterial disease, including TB (41-43). However, T cell production of IFN-γ in vaccine candidates does not consistently correlate with protection (44-47), and there has also been more focus on the importance of IFN-γ-independent CD4 T cell functions (48-50). The relative importance of T cell-derived IFN-γ has only been recently confirmed when Maciag *et al*. used a bone marrow chimera model with T cell deficient mice to determine that T cell-derived IFN-γ is critical for immune protection against pulmonary Mtb (51). IFN-γ-independent mechanisms of CD4 T cell control of Mtb are also being discovered. For example, work from Van Dis *et al.* used a co-culture model with murine bone marrow-derived macrophages (BMDMs) to find that CD4 T cells can activate macrophages in the absence of IFN-γ signaling that is dependent on activation of the transcription factor HIF-1α and CD4 T cell-derived GM-CSF (50).

Th1 CD4 T cells can also produce other cytokines including TNF-α and IL-2. TNF-α, in addition to activating macrophages, also plays a role in formation of mature granulomas (52). IL-2 is thought to be important in TB immunity by expanding and maintaining the T cell response as it induces proliferation and promotes survival of TCR-activated T cells (53, 54). Polyfunctional CD4 T cells produce a combination of IFN-γ, TNF-α, and IL-2. The role of polyfunctional CD4 T cells during natural TB infection in humans is unclear as some studies

reported that active disease was associated with increased Mtb-specific CD4 T cells expressing mono or bifunctional cytokines while those with immunoreactivity against Mtb antigens, who did not get sick, had more trifunctional cytokine production (55, 56). Other studies, however, have found the exact opposite – active TB disease was accompanied by increased trifunctional cytokines (57-60). Therefore, any causal role of polyfunctional CD4 T cells remains unclear. Consistently though, during active disease, Mtb-specific IL-2-expressing CD4 T cell frequencies decline and TNF-expressing CD4 T cell frequencies increase (61, 62). The IL-2-expressing CD4 T cells are KLRG1- PD-1+. These cells produce less proinflammatory cytokines but are less differentiated and have higher proliferative capacity (61). As infection proceeds, they differentiate into the TNF-α and/or IFNγ-expressing CD4 T cells that are KLRG1+ PD-1-. These cells robustly produce proinflammatory cytokines but are short-lived and terminally differentiated (62). Additionally, PD-1+ CD4 T cells can migrate into the lung parenchyma, while KLRG1+ CD4 T cells accumulate in the vasculature (63-65). Therefore, during active TB, it makes sense that as the chronic disease progresses, the quality of CD4 T cells, and therefore function, declines.

BCG and other TB vaccine candidates elicit polyfunctional CD4 T cells in mouse and non-human primate (NHP) models and in humans. In mice, BCG induces polyfunctional CD4 T cells that are present in the first 2-4 months and CD44+ memory T cells as early as 3 weeks after vaccination (66-68). However, these polyfunctional cells were not seen past 14 months post-vaccination and therefore may not last long-term (66). The causal relationship between vaccine-induced polyfunctional CD4 T cell responses and control of Mtb is uncertain with some studies providing strong correlative evidence for polyfunctional CD4 T cells being protective (66, 69, 70) and others showing evidence for bifunctional T cells having a stronger correlation with vaccine-induced protection (61, 68, 70). It is possible that other factors including lung residency and long-lasting vaccine-induced CD4 T cells (71) may be important in addition to polyfunctionality for the strongest vaccine-induced CD4 T cell response to TB.

Finally, other CD4 T cell subsets are also implicated in TB immunity. Th17 cells produce IL-17 and IL-17 signaling is important for proper neutrophil responses, as dysregulated IL-17 production led to immunopathology driven by excess neutrophil recruitment (72). In the context of vaccination, IL-17 responses are important for protective CD4 T cell responses after vaccination (73, 74). Recently Th1/Th17 (Th1* cells) have been associated with protection in NHP and latent infection in humans (75-77). Conversely, Tregs suppress the Th1 immune response via IL-10 and are linked to poor TB immunity (32).

CD4 T cells clearly play an essential role in TB immunity, especially in controlling Mtb replication. However, the frequency of circulating Mtb-specific Th1 T cells does not correlate with protection (46, 78, 79). Therefore, other adaptive immune players must also play underappreciated roles in TB and vaccine-induced immunity.

1.6 CD8 T cells and Mtb

While mouse antibody depletion studies confirmed that CD4 T cells were important for controlling Mtb burden and extending survival, CD8 T cells in those same studies played little to no role in controlling bacterial burden or survival (37, 38). In humans, there are few situations where humans are deficient in CD8 T cells and are exposed to TB (like CD4 deficiencies including HIV infection). Therefore, the complex role of CD8 T cells in TB immunity has overall been underappreciated.

CD8 T cells recognize Mtb-specific antigens presented by classical and non-classical MHC molecules. Classically restricted CD8 T cells recognize peptides presented on MHC Ia (HLA-A, -B, -C). CD8 T cells, like CD4 T cells, can produce IL-2, IFN-γ, TNF-α, and therefore contribute to the crucial Th1 response against TB (80). However, little work has been done to determine the importance of specifically CD8 T cell-derived cytokines on Mtb infection. Cytotoxic CD8 T cells can kill infected cells by releasing perforin, granzymes, and granulysin (in

humans only) from granules (81, 82). Perforin creates a pore in the target cell to deliver other molecules, and in Mtb-infected mice, perforin was required for lysing infected macrophages (82). Granzymes induce pro-apoptotic pathways to trigger cell death in target cells and are expressed by CD8 T cells, natural killer cells (NK), and NKT cells. CD8 T cells also can have Fas-Fas ligand interactions to induce apoptosis (80). Humans have 5 granzymes and mice have 11 granzymes. Granzyme B is the most extensively studied granzyme that is detected in the blood of Mtb infected patients and has higher expression in immunoreactve, asymptomatic individuals than those with active TB (83). Mice deficient in perforin or granzyme B are not more susceptible to Mtb infection (84, 85), however, again suggesting that their roles in TB immunity cannot be appreciated using the current models.

Non-classical CD8 T cells are not restricted by specific peptides presented on MHC Ia but rather recognize either nonpeptidic antigens via genetically conserved antigen presentation molecules, disrupted homeostasis, or stress responses. They therefore bridge the innate and adaptive immune responses together and can mount an early response even if classical CD8 T cells are not yet sufficiently primed and need more time to interact with cognate antigen. Non-classical CD8 T cells are also able to home to mucosal surfaces (80) and therefore could be an important vaccine-induced cell type mediating immunity against TB.

There are many types of non-classically restricted CD8 T cells (broadly known as MHC Ib-restricted CD8 T cells) including HLA-E-restricted T cells, lipid- or glycolipid- specific CD1d-restricted T cells, mucosal-associated invariant T (MAIT) MR1-restricted cells, and TCR $\gamma\delta$ BTN3A1-restricted T cells (80). There are a few differences in non-classical CD8 T cells that exist in humans and mice. Humans have group 1 CD1 molecules (CD1a, b, c, d, and e) while mice only have CD1d-restricted T cells (86, 87). Mice also have H2-M3-restricted T cells that humans lack (88). Nevertheless, it is still important to understand the roles of various non-classical CD8 T cells in Mtb infection and each of these types of non-classical CD8 T cells have different functions during Mtb infection.

One example is the class Ib molecule HLA-E, which is highly conserved in humans and has an orthologue called QA-1^b in mice (89, 90). HLA-E is a ligand for CD94/NKG2C which are receptors expressed by NK cells (91). When HLA-E binds CD94/NKG2C, it inhibits NK-cell cytolytic function under homeostatic conditions (89, 92). However, during infection, HLA-E instead binds and presents antigenic peptides, allowing NK cells to become activated (93). During Mtb infection, HLA-E presents mycobacterial peptides and glycopeptides to CD8 T cells. HLA-E-restricted T cells were detected in active TB patients, patients co-infected with HIV, and lower frequencies were found in latently infected individuals (94, 95). A study from Bian *et al.* dissected the functions of Qa-1 using Mtb-infected Qa-$1^{-/-}$ mice and found that Qa-1 presented multiple Mtb peptides to CD8 T cells during Mtb infection (96). Qa-$1^{-/-}$ mice had increased bacterial burden and mortality compared to wild-type mice but only with high dose Mtb challenge. Other work suggests that HLA-E-restricted T cells can indirectly activate B cells via IL-4 production and express IFN-γ and therefore have a polyfunctional response during TB infection (97, 98).

Because of inconsistencies and caveats of studying the role of CD8 T cells in mouse models, studies turned to the NHP model to look at the role of CD8 T cells in TB immunity. Winchell *et al.* recently dissected the role of CD8 T cells in cynomolgus macaques (99). CD8 is expressed as a dimer and it is thought that in NHPs, the CD8αb heterodimer is predominantly expressed by classical CD8 T cells while CD8$\alpha\alpha$ homodimer is predominantly expressed by non-classical innate-like CD8 T cells such as $\gamma\delta$ T cells, NK T cells, MAITs, and NK cells. Winchell found using antibody depletion of CD8α or CD8β that CD8 T cells play important protective roles during early Mtb infection by inhibiting establishment of infection, dissemination, and disease (99). Additionally, a couple of NHP studies have looked at the role of CD8 T cells in BCG-mediated immunity. Chen *et al.* showed that CD8 T depletion reduced protection against high dose Mtb challenge in i.d. BCG vaccinated and unvaccinated rhesus macaques compared to non-depleted NHPs (100). Recently, Simonson *et al.* demonstrated in IV BCG vaccinated

NHPs that depletion of CD4 T cells or all CD8α T cells diminished BCG-mediated protection against Mtb including increased disease, bacterial burden, and dissemination (101). However, a major caveat to CD8 depletion studies in NHPs is that CD8α is expressed by some CD4 T cells, and phenotypes could be a result of diminished CD4 T cell responses (101, 102). Therefore, more work needs to be done to understand the roles of CD8 T cells in TB and vaccine-mediated immunity.

1.7 B cells and Mtb

The role of B cells in TB immunity, like CD8 T cells, remains inconclusive. The impact of B cell deficiency in mice on bacterial burden seems to widely vary depending on mouse strain, and Mtb strain, dose, and route of challenge (103, 104). Two different studies using $\mu MT^{-/-}$ B cell deficient mice showed no difference in lung or spleen burdens after challenge with ~100 CFU of Mtb (105, 106). In NHPs, B cell depletion with rituximab resulted in an increase in bacterial burden and altered cytokine production in only some granulomas (107). In humans, patients with rheumatoid arthritis treated with rituximab do not have an increased risk of TB reactivation (108, 109).

B cells can have numerous functions during TB infection. B cells were shown to contribute to the macrophage responses during TB infection by producing type I interferons that modulate polarization towards M2 anti-inflammatory macrophages (110). B cells also delay neutrophil influx to the site of infection by regulating the Th17/IL-17 response (111, 112). B cells can also act as antigen presenting cells to generate Mtb-specific CD4 T cells (113, 114). Chen *et al.* used $\mu MT^{-/-}$ mice to show that during chronic TB infection, B cells contribute to pulmonary inflammation by increasing the numbers of IFN-γ producing CD4 T cells in the lung via restriction of IL-10 expression and that the resulting enhanced Th1 response may lead to the pulmonary inflammation (115).

B cells are best known for their role in producing antibodies, and the role of humoral immunity against TB has been of more recent focus. Studies have shown that antibodies originating from the lung tissue have weak reactivity to mycobacterial antigens compared to antibodies originating from serum and only a few of the monoclonal antibodies from lung B cells have specificity to mycobacterial antigens (114). However, B cells from the peritoneal cavity produced high levels of IgM antibodies after stimulation from Mtb or BCG lipids (116). NHP models have shown that animals with asymptomatic Mtb infection progress more rapidly to symptomatic disease if they exhibit low antibody responses (117). In humans, many observational studies have highlighted the protective potential of specific antibodies to TB. For example, lower titers of IgG antibodies against the mycobacterial surface glycolipid lipoarabinomannan (LAM) were associated with disseminated TB disease in children (118).

Antibodies have many potential functions during TB immunity including opsono-phagocytosis of Mtb, complement activation, and cellular cytotoxicity (119). For example, antibodies have been shown to opsonize Mtb via FcR signaling which targets Mtb for degradation via the lysosomal pathway (120-122). Antibodies also play an important role in mucosal immunity against Mtb. Mtb is a pulmonary infection, and Ig isotypes, especially secretory IgA, are found in the mucosal lining. Belay *et al.* showed that healthy individuals exposed to TB have increased anti-HBHA IgA titers compared to untreated TB patients suggesting that Mtb-specific IgA could be a protective marker of control (123). Mucosal and IV BCG vaccination in NHPs also both resulted in increased IgA levels associated with protection (124, 125). Other roles of BCG-induced antibodies have also been observed. For example, the levels of Ag85A-specific IgG associated with reduced risk of TB disease in BCG-vaccinated South African infants (126).

1.8 BCG-mediated immunity

After immunization, BCG is recognized by pathogen-associated molecular patterns (PAMPs) which include mycobacterial cell wall components such as peptidoglycans, arabinogalactan, and mycolic acids (127). These PAMPs interact with Toll-like receptors and other pattern recognition receptors (PRRs) including NOD2. This induces a rapid innate immune response where local resident innate cells and infiltrating mononuclear cells produce inflammatory cytokines including IL-1β, TNFα, MCP-1, and IL-8 (128). Resident dendritic cells (DCs) presenting antigen or live BCG initiate adaptive immunity by activating antigen-specific CD4 T cells in the presence of IL-12 and IL-18, leading to a strong Th1 response with IFNγ secretion (129, 130). BCG-induced T and B cell responses were described in the previous sections.

BCG has also been shown to provide non-specific protection via trained innate immunity by inducing epigenetic modifications and metabolic reprogramming of monocytes that lead to increased cytokine production and antimicrobial function upon secondary *Mycobacterium tuberculosis* (Mtb) or heterologous infection (131-133). However, trained immunity is still actively being defined, and mechanisms of BCG-induced immune responses that result in protection against Mtb infection are incompletely understood.

While there are many studies on the immune responses elicited after BCG vaccination, few studies look how BCG impacts the immune response after Mtb infection. Work from Delahaye *et al*. investigated the BCG-induced immune responses early after Mtb infection in mice (134). They first found that BCG accelerates the translocation of AM to the lung interstitium and transfer of Mtb from AM to MDM and neutrophils within the first two weeks after infection. Delahaye then determined that BCG-induced lung resident CD4 T cells are responsible for promoting the accelerated transfer of Mtb from AM. They find that these differences in BCG-induced immune responses occur before a divergence in bacterial burdens which occurs after day 14 p.i. This is because BCG-induced CD4 T cells are activated distal to the site of infection

so they can function to transfer Mtb from AM but still need to co-localize with infected cells to curb Mtb replication and reduce the bacterial burden (134). These data provide new insights into very early impacts of BCG on the immune response to TB. However, there are still large gaps in our knowledge of BCG-induced immune responses, particularly in the adaptive immune response, that result in protection against Mtb infection.

1.9 BCG and the TB vaccine pipeline

There are many TB vaccine candidates in various stages of development and clinical trials. Many of these vaccine candidates use or modify BCG in their vaccination strategies, showing that BCG is still relevant in the current TB vaccine pipeline. These include different types of vaccines such as live attenuated vaccines, recombinant BCG vaccines, viral vector vaccines, inactivated vaccines, and subunit vaccines that are each described in more detail below.

The two live attenuated vaccine candidates are BCG (for revaccination) and MTBVAC. BCG is currently being evaluated as a method of revaccination in adolescents and children. Safety, immunogenicity, and efficacy of BCG revaccination was evaluated in a randomized, placebo-controlled, phase II clinical trial of healthy adolescents in Cape Town, South Africa (135). BCG revaccination induced a robust, multifunctional BCG-specific CD4 T cell response and was immunogenic. QuantiFERON-TB Gold In-tube assay (QFT) conversion, which detects Mtb infection, showed that BCG was not efficacious in preventing initial Mtb conversion, but it did significantly reduce the rate of sustained conversion (135). This suggests that BCG revaccination doesn't prevent initial Mtb infection but may help prevent sustained infection. The other live attenuated TB vaccine candidate, MTBVAC, is an attenuated version of Mtb and has gene defects to remove key virulence factors including ESAT-6 (136). MTBVAC is being targeted as a replacement for BCG vaccination of newborns and boosting adolescents and

adults. A phase Ib trial in South Africa showed that MTBVAC has comparable safety to BCG in clinical trials and high dose MTBVAC induced strong Th1 CD4 T cell responses (137). However clinical trials to further determine immunogenicity and efficacy are still ongoing.

The protective efficacy of other vaccine candidates has yet to surpass BCG in clinical trials. Therefore, recombinant BCG (rBCG) vaccines that modify and improve the current BCG vaccine are also being investigated. One rBCG candidate, VPM1002, substituted the urease C gene with the listeriolysin (LLO) encoding gene from Listeria monocytogenes, leading to the secretion of LLO which promotes the entry of antigens and DNA into the cytoplasm of host cells (138). VPM1002 enhances the production of antigen-specific CD4 and CD8 T cells and induces Th1 and Th17 immune responses (139). Larger Clinical III phase trials are ongoing to determine the effectiveness and safety of VPM1002.

Viral vector vaccine candidates aim to enhance immune effect of BCG. Viral vector-based vaccines such as ChAdOx185A+MVA85A, TB/FLU-01L, and TB/FLU-04L transfer protective Mtb-specific antigens to a safe viral vector. ChAdOx1.85A is a simian-adenovirus vector-based vaccine and MVA85A is a replication-deficient modified Vaccinia virus Ankara vaccine (140). Both express the Mtb-specific antigen Ag85A and were tested in pre-clinical murine studies with BCG. Researchers found that ChAdOx1.85A and MVA85A alone did not significantly reduce Mtb bacterial burdens, however, prior immunization with BCG before ChAdOx1.85A and MVA85A (B-C-M) improved immune protection. Additionally, the B-C-M prime-boost regime was more protective than BCG alone(140, 141). The authors hypothesize that ChAdOx1.85A-MVA85A might induce central memory responses not induced by BCG alone and enhance protection. They also found that B-C-M increased in antigen-specific CXCR3+ KLRG1- CD4 T cells in the lung parenchyma compared to BCG alone, which could contribute to the better protection (141). The safety and protective efficacy of the ChAdOx1.85A vaccine and the B-C-M prime-boost regime are currently being assessed in phase IIa trials. TB/FLU-01L and TB/FLU-04L use replication-deficient influenza virus A to express the Mtb-

specific antigen ESAT-6 or truncated NS1 that expresses ESAT-6 and Ag85A, respectively (140, 142). Pre-clinical murine studies show that TB/FLU-04L enhances BCG using a BCG prime – TB/FLU-04L boost regimen, however, clinical phase 1 trials are still underway (143).

There are also other TB vaccine candidates including inactivated vaccines and subunit vaccines that could play complementary roles to BCG vaccination. Inactivated vaccines use whole Mtb, lysed Mtb, or fragments of Mtb and induce strong Th1 cell and humoral immune responses to a wide variety of Mtb antigens. They are primarily being developed for TB treatment in patients with active pulmonary TB or latent infection. For example, *Mycobacterium indicus pranii* (MIP) is a non-pathogenic, non-tuberculosis mycobacteria (NTM) tested as a therapeutic vaccine in category II TB patients in India (144, 145). After four weeks, treatment of MIP resulted in faster sputum culture conversion than the placebo group, indicating that MIP can clear Mtb(145).

Finally, there are six current subunit vaccines in clinical trials. Subunit vaccines consist of immunologically active component isolated from Mtb. For example, M72/AS01E consists of immunogenic Mtb proteins Mtb39A and Mtb32A and the adjuvant AS01E and induces a robust IFNγ-producing Th1 immune response and antibody response (146). M72/AS01E was designed to protect against TB disease and a phase II clinical trial showed an initial 54% efficacy against TB infection with a ~50% efficacy after 36 months of follow-up of preventing latent infections from developing into active TB (147, 148). Some of these subunit vaccines have also been investigated as booster vaccines to enhance protection after initial BCG vaccination. For example, GamTBvac is a recombinant subunit vaccine with multiple Mtb antigens including Ag85A, ESAT-6, and CFP10 and a CpG oligodeoxynucleotide adjuvant that activates Toll-like receptor 9 signaling which enhances the innate immune response and response to the antigens (149). Pre-clinical testing in mouse and guinea pig models showed that GamTBvac had strong immunogenicity and a strong protective effect particular as a BCG-prime/GamTBvac-boost regime. Phase I and II clinical trials demonstrated acceptable safety and strong immunogenicity

including high levels of antigen-specific IFNγ and antibodies in uninfected, BCG vaccinated healthy volunteers (150). Current phase III trials will determine the efficacy of GamTBvac in preventing pulmonary TB. Finally, new vaccine approaches including DNA vaccines, RNA vaccines, and virus-like particle-based vaccines are also being explored and developed.

From revaccination with BCG, to improving BCG, to boosting BCG with new vaccines, BCG remains relevant in the current TB vaccine pipeline. Therefore, not only is it important to study BCG-mediated immunity to create more effective vaccines that could replace BCG, it is also important to understand how BCG works to further improve its efficacy or to create vaccines to be used in tandem with BCG that enhance or complement BCG-induced immune responses.

1.10 Conventional dose and ultra-low dose murine infection models

After reviewing the roles and functions of lymphocytes against natural and vaccine-mediated immunity to Mtb in animal models and humans, it is clear that there are gaps in our knowledge about the immune responses, especially vaccine-induced responses, that lead to protection against TB. Our understanding of TB immunity and BCG-mediated immunity has been hampered by a lack of a gold standards for defining control or eradication of Mtb in a tractable animal model. The current conventional dose (CD) mouse model (50-100 CFU), which is the model used in the mouse studies described above, has limitations that have left little confidence in its translation to humans (151). For example, infection with CD Mtb in mice results in uniformly high lung bacterial burdens associated with progressive inflammatory disease and ultimately, death (152). In contrast, human TB infection results in a wide spectrum of outcomes from infection to active TB disease (described above). BCG immunization within the CD mouse model confers a transient 10-fold reduction in bacterial burdens that is lost by late timepoints post-infection (153, 154). Most importantly, the mouse immune system is thought to lack

immune effectors needed to eradicate, or even contain Mtb. It is unclear if the mechanisms by which BCG-immunized mice transiently reduce their bacterial burdens in the setting of an ultimately unsuccessful immune response have any relevance to human protective immunity. However, Mtb droplet transmission research suggests that humans are only exposed to about 1-3 CFU, therefore, a conventional dose of Mtb is higher than a physiologic dose of Mtb which could contribute to differences in mouse TB immunity (155-157).

The deficiencies in the CD model led our lab to develop the ultra-low dose model (ULD) where mice are infected with only ~1-3 CFU of Mtb (152)**.** To achieve an ULD infection, the Mtb dose is reduced so that, based on Poisson distribution, approximately 37% of mice remain uninfected. We have previously shown that an ULD infection recapitulates key features of human TB infection including heterogeneous bacterial burdens across tissues and timepoints post-infection as well as single, organized lung granulomas that resemble those found in non-human primates and humans (152). However, protection conferred by BCG within the ULD model, and how this model could be used to investigate mechanisms of vaccine-mediated protection was unknown when I initiated my thesis research.

1.11 Dissertation objectives and significance

This dissertation aims to use the ULD murine Mtb infection model to investigate mechanisms of BCG-mediated immunity. In **Chapter 3**, we test the ability of the ULD model to assess BCG-mediated protection. In this chapter, we identify three parameters of BCG-mediated protection within the ULD model: 1. Reduction in overall lung burden, 2. Prevention of dissemination to the contralateral lung, and 3. Prevention of detectable infection in a subset of BCG vaccinated mice. Importantly, our model provides the first evidence that BCG vaccination is capable of mediating sterilizing immunity in any mouse model of TB and suggests that the prevailing idea that mice cannot control or eliminate Mtb was fostered by challenging mice with

a non-physiological, high Mtb inoculum to which even vaccinated mice succumb. The ULD model therefore provides an unprecedented opportunity to dissect immune pathways that lead to protection in a highly tractable system.

Having shown in Chapter 3 that we can can investigate distinct protective parameters, that cannot be assessed in conventional dose experiments (i.e, inhibition of dissemination and prevention of detectable infection), in **Chapter 4**, we will examine the roles of T cells and B cells in vaccine-mediated immunity in this model. We first determine that T cells are required for all parameters of BCG-mediated immunity while B cells are not required. We then dissect the relative roles of CD4 and CD8 T cells in BCG-mediated immunity. We discover that CD4 T cells play major roles in control of lung burden and prevention of dissemination while CD8 T cells play a major role in prevention of infection. Furthermore, we find that mechanisms of protection that are masked using the supraphysiologic aerosol dose that is standard in the field are revealed in the ULD model, suggesting that the ULD model may provide a superior platform for triaging TB vaccine candidates for human clinical trials.

Determining how and when BCG provides protection as well as dissecting the immune responses that lead to protection against TB could lead to a greater understanding of protective TB immunity, which could inform design of effective TB vaccines. Furthermore, the work described in my thesis helped convince the Bill & Melinda Gates Foundation to fund our lab to be a site for pre-clinical vaccine testing using the ULD model. We hope this will help identify promising TB vaccine candidates and speed up their clinical development. Accelerating the development of an effective TB vaccine would save millions of human lives.

Chapter 2. Assessing vaccine-mediated protection in an ultra-low dose Mycobacterium tuberculosis murine model

This chapter was published in "PLoS Pathogens" in 2023 and was reproduced here (154). I was co-first author in this manuscript and the contributions of each author can be found in the acknowledgments and author contributions sections at the end of this chapter.

2.1 Introduction

New and effective tuberculosis (TB) vaccines are urgently needed. Although BCG vaccination can provide protection in infants and older children in some clinical settings (8, 158-160), it has proven to be inadequate to combat the global pandemic. There are numerous TB vaccine candidates in the developmental pipeline (161), but it will not be feasible to conduct human efficacy trials for most of them. The standard for assessing vaccine efficacy is prevention of disease, which occurs in only a small percentage of infected individuals, resulting in daunting sample sizes and costs needed to complete human trials. Prevention of infection would also be a highly desirable outcome of vaccination, but in human populations this endpoint is very difficult to assess independently from prevention of disease. Unfortunately, identifying promising vaccine candidates to prioritize for human efficacy trials has been hindered by the lack of reliable animal models that can measure immune parameters relevant to preventing disease or infection, as evidenced by their poor ability to adequately predict human TB vaccine efficacy (162, 163).

Historically, mice have been the most commonly used model for testing TB vaccine candidates due to their ease of use, cost-effectiveness, and the relative conservation of the mammalian immune system. However, limitations in the current mouse model, in which mice are infected with ~50-100 CFU by aerosol, have shaken confidence regarding how well findings in mice can be translated to humans (162, 163). There is minimal variability in the performance of different vaccines in the current model. Most TB vaccines confer ~1 log of protection,

reducing the lung burden from ~10^6 to ~10^5 CFU, but only if assessed 4-6 weeks after aerosol challenge. This protection is transient and usually dissipates by 3-4 months post-infection (p.i.) (61, 153). Furthermore, it is unclear if the vaccine-induced mechanisms that enable mice to transiently reduce their bacterial burdens in the setting of an ultimately unsuccessful immune response are relevant to the types of immunity required for long lasting protection against the clinical manifestations of human TB. Because mice in this model are unable to eradicate, or even durably control Mtb, some have suggested that mice may lack the fundamental immune effector molecules needed for Mtb control (164). The failure of mouse vaccine testing to reliably predict results in human TB vaccine trials have reinforced these concerns about the relevance of the mouse model for TB vaccine testing (162, 163).

Recently we developed an ultra-low dose (ULD) (i.e., 1-3 CFUs) Mtb mouse infection model that more closely resembles several aspects of human Mtb infection (29). Here we test the ability of the ULD challenge model to assess immunity conferred by BCG vaccination, the vaccine for which the most human efficacy data exists. In contrast to the conventional dose model, we show that BCG-vaccinated mice challenged with 1-3 Mtb CFU exhibit a more durable reduction in lung bacterial burdens. Vaccinated mice had an increased ability to contain infection to a single lung and prevent Mtb dissemination to the contralateral lung. Finally, vaccinated mice exhibited a significantly higher proportion of animals with no detectable infection. Thus, the ULD model provides a promising platform for TB vaccine testing, as it affords the opportunity to measure distinct parameters of vaccine-mediated immunity that are relevant to preventing disease and/or infection that cannot be assessed in the current mouse model.

2.2 Results

2.2.1 BCG-mediated reduction of lung bacterial burdens is transient in the current mouse model.

The capacity of BCG to mediate protection in C57BL/6 (B6) mice infected with 50-100 Mtb CFU has been assessed by many labs, but we sought to repeat this experiment in our own hands to directly compare the conventional dose with the ULD model. We subcutaneously immunized B6 mice with 10^6 BCG-Pasteur 8 weeks prior to aerosol challenge with H37Rv Mtb and determined the lung bacterial burdens at days 42 and 120 post-infection. As previously shown (61, 153), BCG immunization provided about one log of protection against lung bacterial burden at day 42, but this protection was transient and dissipated at later timepoints; there was no significant difference in bacterial burdens between unimmunized and BCG-immunized mice at day 120 post-infection (**Figure 2.1**).

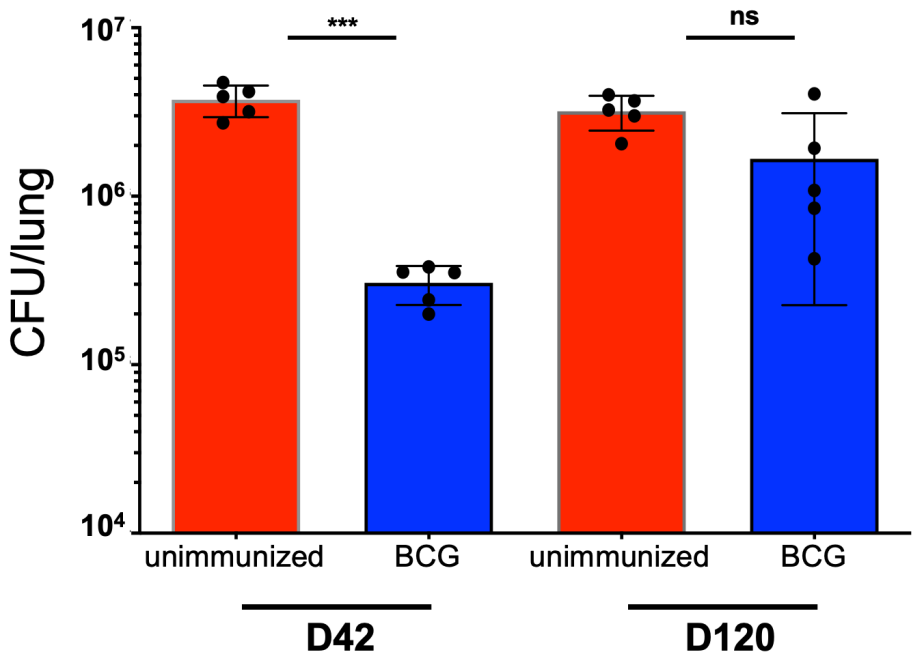

Figure 2. 1. BCG-mediated reductions in Mtb lung burdens are not durable in a conventional-dose infection. C57BL/6 (B6) mice were aerosol infected with a conventional dose (CD) (50-100 CFU) of H37Rv Mtb eight weeks following either subcutaneous (s.c.) immunization with 10^6 BCG-Pasteur (BCG) or no immunization (unimmunized). On day 42 or 120 post-infection, CFU were enumerated from lung homogenates plated onto 7H10 plates. These data represent 5 mice per group and are shown as mean ± SEM. Single-group comparisons were analyzed using an unpaired t test. ***p<0.001.

2.2.2 Measuring vaccine-mediated immunity in the ULD Mtb model.

Next, we assessed the efficacy of BCG in the ULD aerosol Mtb challenge model, a model in which the aerosolized dose is reduced with a goal of infecting only ~60-80% of the mice in the infection chamber (152). As previously described using an ULD infection of a pool of bar-coded Mtb strains, the number founding strains detected using bar-codes after ULD infection approximates a Poisson distribution; most mice are infected with a single founding Mtb strain, whereas fewer are infected with two or three founding strains (152). In all of the experiments performed in this manuscript (shown in **Supplementary Table S2.1**), in addition to assessing CFU values from serial dilutions of lung homogenates, we also plated out 100% of the neat homogenates. Thus, the limit of detection for bacterial burdens in these experiments is defined only by the Mtb that may have stuck to the dilution tubes or pipet tips. **Figure 2.2** depicts a BCG immunization experiment in which we assessed the bacterial burdens in the right and left lungs separately and in the spleen 9 weeks after aerosol ULD challenge. Amongst those mice with detectable infection (>0 CFU), we observed that, compared to unimmunized mice, BCG-immunized mice had lower overall lung bacterial burdens (pooling right and left lungs) (**Figure 2.2A**), and lower spleen bacterial burdens (**Figure 2.2B**). We also observed that 7/20 of the unimmunized mice and 10/20 of the BCG-immunized mice had no detectable infection in either lung (**Figure 2.2A**), a difference that was not statistically significant in this single experiment ($p=0.53$). While the same seven mice with undetectable lung bacterial burdens also had no detectable splenic bacterial burdens, two mice that did have detectable lung infection in the BCG-immunized group failed to show evidence of splenic bacterial burdens (12/20 BCG-immunized mice had no recoverable Mtb from their spleen, compared to 10/20 from the lungs). Thus, BCG immunization may prevent Mtb dissemination to the spleen or promote splenic Mtb clearance.

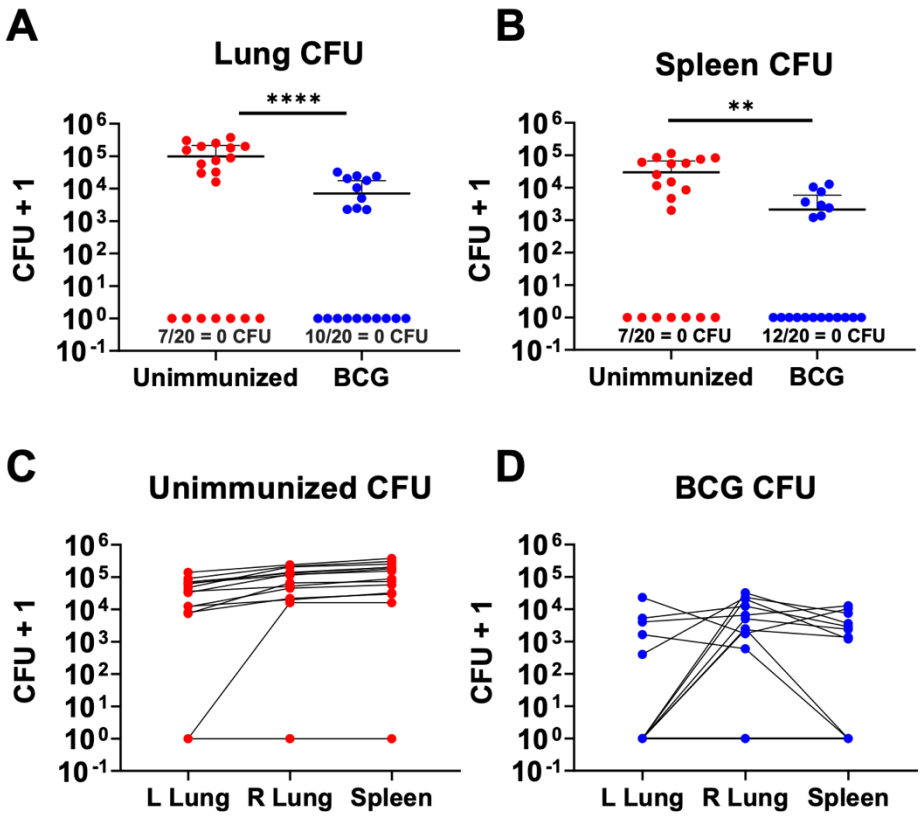

Figure 2. 2. Assessing BCG efficacy in the ultra-low dose Mtb model. B6 mice were aerosol infected with an ULD (1-3 CFU) of H37Rv Mtb 8 weeks following either s.c. immunization with 10^6 BCG-Pasteur (n=20) or no immunization (n=20). On day 63 post-infection, CFU were enumerated from left lung, right lung, or spleen homogenates plated onto 7H10 plates. **A)** Combined lung CFUs or **B)** spleen CFUs from unimmunized and BCG-immunized mice are graphed. Counts from left lungs, right lungs and spleen are graphed separately from, **C)** unimmunized mice or **D)** BCG-immunized mice. There were 20 mice per group, and the data are graphed as mean ± SD. Single-group comparisons were analyzed using an unpaired t test and excluding mice with 0 CFU. **p<0.01, ****p<0.0001.

To further assess the capacity of BCG immunization to restrict Mtb dissemination, we also assessed bacterial burdens separately in the right and left lungs. In the ULD model, since infection is usually established by a single founding Mtb strain, the lungs are often infected unilaterally; most commonly, the right lung is infected because the right lung and bronchus are larger than the left (152) Our previous ULD studies using bar-coded Mtb strains showed that bilateral lung infection usually represents the dissemination of a single Mtb strain from the infection-seeded lung to the contralateral lung. In the experiment shown in **Figure 2.2**, we observed that 5/10 of the BCG-immunized mice exhibited unilateral lung infection compared to only 1/13 of the infected unimmunized mice (p= 0.023; **Figure 2.2C and 2.2D**). Of the two BCG-immunized mice with pulmonary Mtb infection but no detectable splenic bacterial burdens, one

was infected in the right lung only while the other had bilateral lung infection (**Figure 2.2D**). Thus, the ULD model has the capacity to assess a vaccine's ability to prevent dissemination, a parameter of protection that cannot be assessed in conventional dose infections because dissemination occurs in all mice regardless of vaccination status.

2.2.3 BCG confers durable reductions in lung bacterial burdens in ULD-challenged mice.

As previously shown (61, 153), and as demonstrated in **Figure 2.1**, BCG-mediated reductions in lung bacterial burdens are abrogated by 100-120 days post-challenge. To assess the durability of BCG-mediated protection in the ULD model, we performed a time course and assessed bacterial burdens in the lungs and spleen of ULD-infected mice at an early (d14), intermediate (d42), and late timepoint (d115). Because ULD challenge results in some mice with no detectable lung bacteria, even in the absence of immunization, we assessed bacterial burdens only in mice with detectable bacterial burdens and performed a separate analysis to determine the proportion of mice with undetectable bacteria (the latter is shown in **Figure 2.5**). At day 14 post ULD-infection, bacterial burdens were similar in both unimmunized and BCG-immunized infected mice, but at days 42 and 115, bacterial burdens were reduced by approximately one log ($p=0.002$ and $p<0.001$, respectively, excluding those with 0 CFU; **Figure 2.3A**). These data suggest that BCG-mediated reductions of lung bacterial burdens are more durable in ULD-infected mice compared to conventional dose-infected mice, but the intentional heterogeneous nature of the model makes it difficult to draw conclusions based on a single experiment.

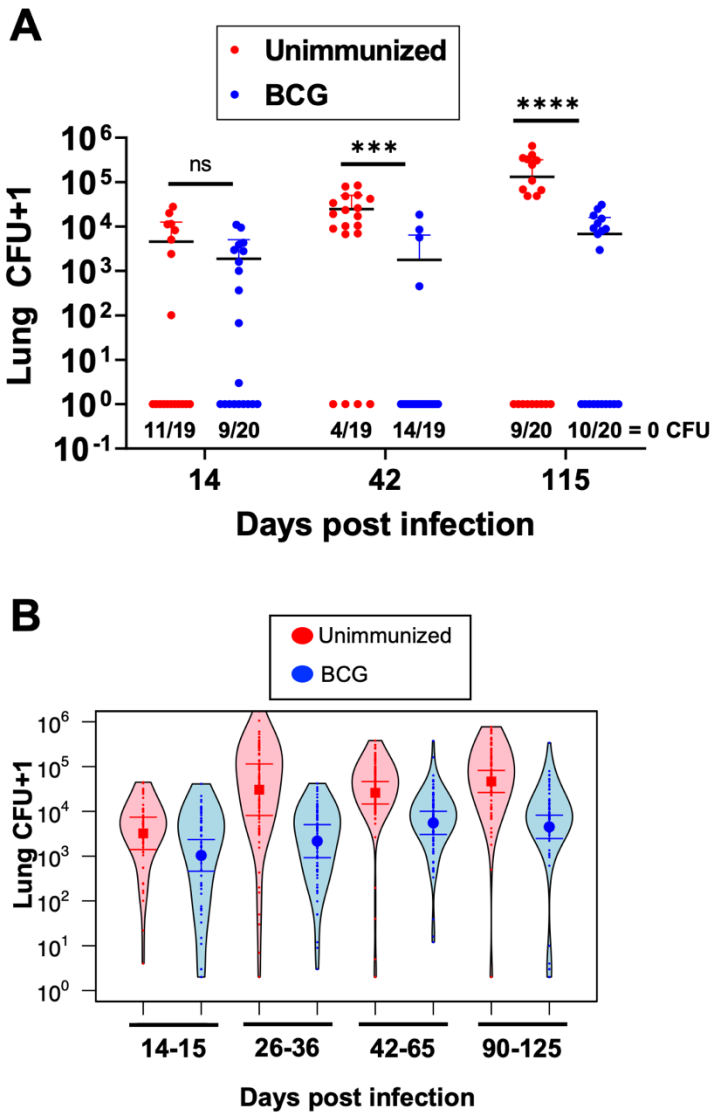

Figure 2. 3. BCG-mediated reductions in Mtb lung burden are more durable in the ULD model. **A)** Combined lung CFU from a single experiment time course of ULD-infected B6 mice with or without BCG immunization. Combined lung CFU were enumerated on days 14, 42, and 115 post-infection. There were 19 or 20 mice per group, and the data are graphed as mean ± SD. Single-group comparisons were analyzed using an unpaired t test (excluding mice with 0 CFU). ***p<0.001, ****p<0.0001. **B)** Combined lung CFU from a compilation of 31 experiments, excluding mice with 0 CFU, separated by timepoint post-infection of ULD-infected B6 mice with or without BCG immunization. Error bars are 95% confidence intervals in a fixed effects negative regression model. All timepoints except days 14-15 post-infection have a $p < 0.001$.

Next, we performed multiple ULD challenge experiments comparing BCG immunized vs. unimmunized mice to rigorously assess the reproducibility of our findings. **Supplementary Table S2.1** shows results from 31 individual experiments assessing BCG efficacy in the ULD model, representing a total of 537 unimmunized and 543 BCG-immunized mice with lung

bacterial burdens assessed at timepoints ranging from days 14-125 post-infection. **Figure 2.3B** shows the combined (right and left lungs pooled) bacterial burdens from all experiments binned by similar timepoints post-infection. Similar to prior reports using a conventional dose Mtb challenge (134, 165), BCG had no effect on bacterial burdens at the earliest timepoints assessed, days 14-15 post-infection. However, BCG-immunized mice had lower lung bacterial burdens than unimmunized mice at every later timepoint (excluding those with 0 CFU). This reduction remained robust (~1 log) even at days 90-125 post-infection. Thus, unlike the transient reduction of bacterial burdens observed in the conventional dose Mtb challenge model (61, 153), BCG durably reduces the lung bacterial burdens in ULD-challenged mice for at least 4 months post-infection.

2.2.4 BCG prevents Mtb dissemination to the contralateral lung.

To better assess the reproducibility of BCG's capacity to prevent dissemination, we assessed the proportion of mice with bilateral vs. unilateral lung infection in all experiments shown in **Supplementary Table S2.1**. Based on raw CFU data, there was no difference in the proportion of mice with bilateral lung infection between unimmunized vs. BCG-immunized groups at days 14-15 post-infection. At this early timepoint, the proportion of mice with bilateral lung infection was low even in unimmunized mice, suggesting that dissemination had not yet occurred in either group. At all later timepoints, however, the proportion of mice with bilateral lung infection was higher in unimmunized compared to BCG-immunized mice even out to days 90-125 post-infection (**Figure 2.4A**). Although bilateral lung infection in the ULD model usually reflects Mtb dissemination from the initially infected lung to the contralateral lung, it can sometimes represent separate aerosolized infections by distinct bacilli in each individual lung. To assess true dissemination more accurately, we ULD-infected mice with a pool of 50 bar-coded H37Rv Mtb strains that we have previously characterized (152). Amplified genomic DNA

extracted from bacterial colonies of each infected mouse lung were sequenced to determine the number of unique founding Mtb strains in each lung (**Figure 2.4B**). Because the probability of separate infections with the same bar-coded strain is only ~1 in 78 when using the 50 bar-coded Mtb pool in the ULD model (152), bilateral lung infection with a single Mtb strain in both lungs likely represents true dissemination (e.g. BCG 36L and 36R). In contrast, when mice have different Mtb strains in each lung (e.g. BCG 28L and 28R), this reflects separate infections of each lung. Thus, if dissemination to the contralateral lung is assessed by bacterial burden alone without assessing Mtb bar-codes, the ability of a vaccine to prevent dissemination will be underestimated due to falsely categorizing separate infections in each lung as dissemination events. In this experiment, BCG was deemed to have 50.2% efficacy ($p = 0.002$); **Figure 2.4C**) in preventing dissemination when measured as the proportion of mice with bilateral Mtb infection. However, if dissemination was defined as the proportion of mice that possessed at least one identical bar-coded Mtb strain in both lungs, then BCG exhibited an efficacy of 73.5% ($p = 0.001$, **Figure 2.4D**). Compiling data from all experiments in which we performed bar-coded infection and sequencing (n=5) revealed that BCG exhibited 79.7% efficacy in preventing dissemination of Mtb to the contralateral lung ($p < 0.001$; **Figure 2.4E**).

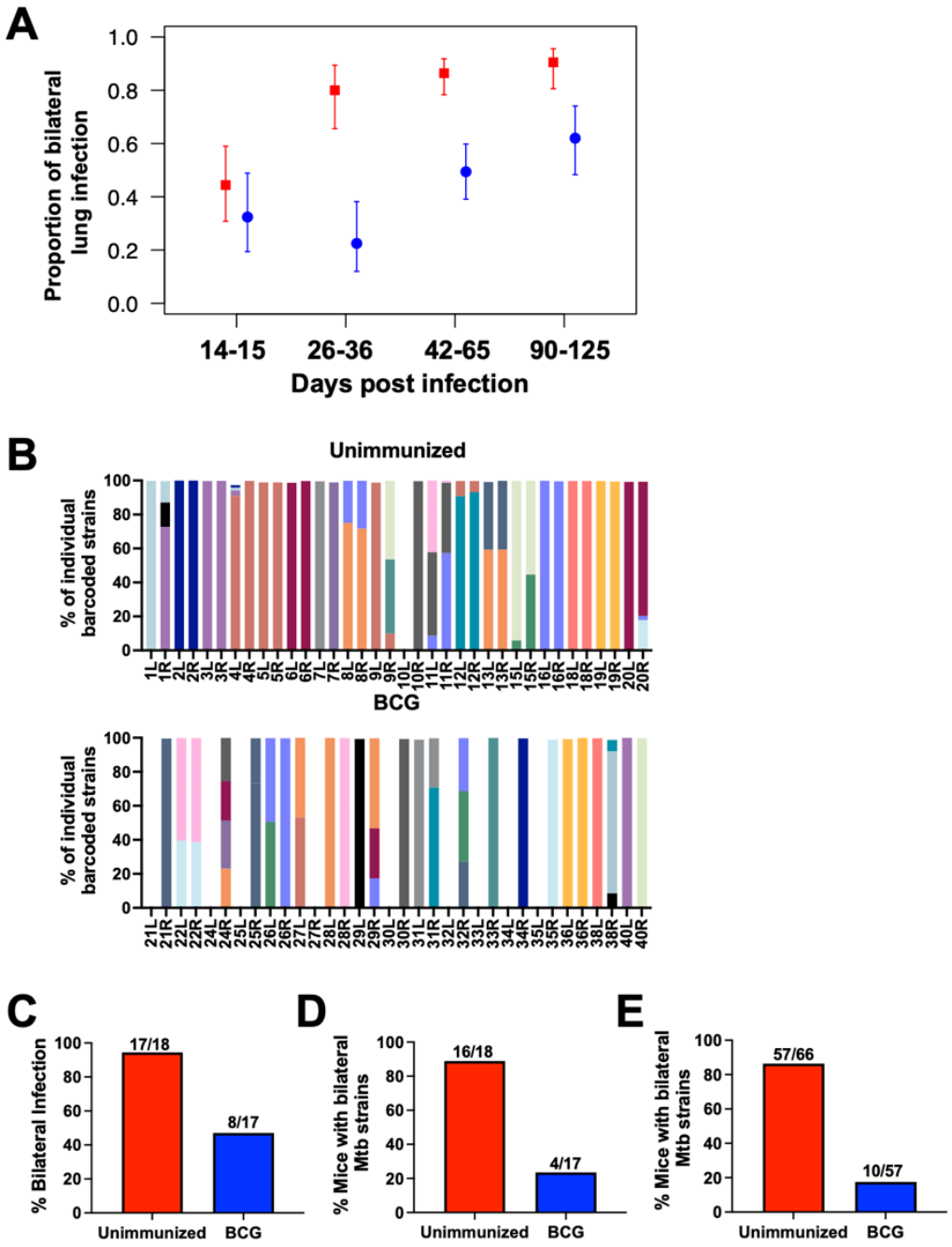

Figure 2. 4. BCG-immunization prevents Mtb dissemination to the contralateral lung. A) Proportion of mice with bilateral lung infection (CFU in left and right lung) from a compilation of 31 experiments separated by timepoint post-infection of ULD-infected B6 mice with or without BCG immunization. Error bars are 95% confidence intervals in a mixed effects logistic regression model, with experiment as a grouping variable. All timepoints except days 14-15 post-infection have a $p \leq 0.001$. **B)** A single ULD experiment using bar-coded Mtb strains is shown. On day 65 post-infection, right and left lung homogenates were plated onto 7H10 plates and Mtb colonies from infected lungs were scraped to make genomic DNA. DNA was sequenced, and the identity of each bar-coded Mtb strain is graphed for each lung separately. The percentage of bilateral infection for unimmunized and BCG-immunized mice from this experiment was calculated by the proportion of mice with CFUs in both lungs **(C)** or the proportion of mice with at least one common Mtb strain in both lungs **(D)**. **(E)** The percentage of mice with bilateral Mtb strains was compiled from 5 independent experiments, excluding day 14 post-infection. Vaccine efficacy for preventing dissemination to the contralateral lung was calculated as 1-(% BCG mice with bilateral infection)/(% Unimmunized mice with bilateral infection).

2.2.5 BCG immunization can prevent detectable infection.

Finally, we compared the proportion of unimmunized and BCG-immunized mice that presented with undetectable pulmonary infection. Pooling the data from all experiments assessed at D14-15 after Mtb challenge (n=6), we observed no difference in the proportion of mice with undetectable bacterial burdens in the BCG-immunized vs. unimmunized groups (**Figure 2.5A**). However, at all later timepoints through day 125 post-infection, we observed more mice with undetectable bacterial burdens in BCG-immunized mice than in unimmunized mice. Excluding the six experiments assessed at D14-15 when no difference was seen, we plotted the remaining 25 experiments at timepoints from D26-125 as the proportion of mice with undetectable bacterial burdens in the unimmunized vs. BCG-immunized group (**Figure 2.5B**). Although only three experiments (15-20 mice/group/experiment) reached statistical significance on their own (all in the BCG-immunized group), most experiments (18 of 25) had a higher proportion of mice with undetectable bacterial burdens in the BCG-immunized group. When the compiled data from all 25 of these experiments were assessed (**Figure 2.5B**, black filled circle), the difference in the proportion of mice with undetectable bacterial burdens in the BCG-immunized compared to the unimmunized group was relatively modest (13% efficacy in preventing detectable infection), but highly statistically significant ($p = 0.001$).

A

	# mice with undetectable CFU (Unimmunized)	# mice with undetectable CFU (BCG)
All timepoints w/o D14-15	154/440 (35.0%)	191/443 (43.1%)
14-15 dpi	41/97 (42%)	41/100 (41%)
26-36 dpi	34/118 (29%)	40/116 (35%)
42-65 dpi	54/164 (33%)	65/162 (40%)
90-125 dpi	66/158 (42%)	86/165 (52%)

B

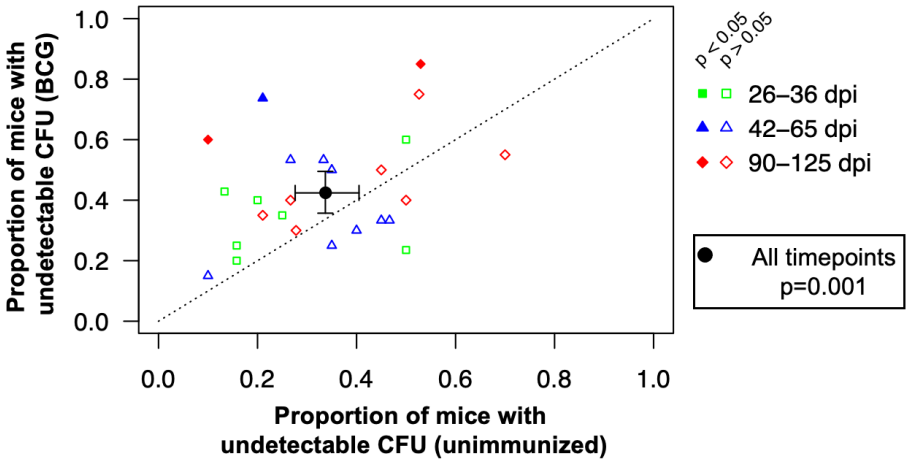

C

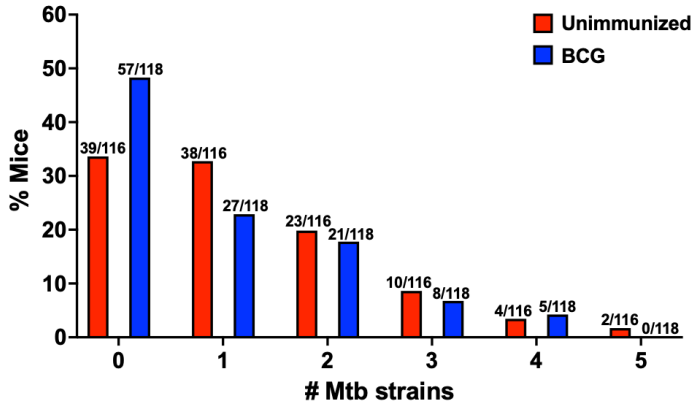

Figure 2. 5. BCG immunization prevents detectable infection in some mice. A) Table of all mice, showing the percentage with 0 CFU in the unimmunized vs BCG-immunized groups separated by timepoint post-infection. **B)** The proportion of unimmunized mice with 0 CFU (x-axis) vs the proportion of BCG-immunized mice with 0 CFU (y-axis) for each experiment from a compilation of 25 experiments (days 26-125) separated by timepoint post-ULD infection. Each colored symbol is an independent experiment, and the larger black circle is the compilation of all the data, which was statistically significant (mixed effects logistic regression p = 0.001). Post-hoc analyses indicated that, if each infection cohort had been analyzed separately, the 3 filled in symbols would have attained statistical significance if they had been analyzed using the same regression model (p<0.05), see **Figure S2.1C Table)** In ULD-Mtb experiments in which bar-coded strains were used for infection (n=6 for unimmunized, n=6 for BCG-immunized), the mice are graphed according to the number of unique Mtb strains recovered from each mouse's lungs.

We also examined the number of founding strains in each mouse for all ULD experiments using the pool of bar-coded strains (6 experiments) (**Figure 2.5C**). As expected from the Poisson distribution, most unimmunized mice were infected with only one strain, and fewer mice were infected with two or more strains. Although these experiments were underpowered to fully assess differences in the distribution of founding strain numbers, there appeared to be similar proportions of unimmunized and BCG-immunized mice infected with two or more Mtb strains. However, fewer BCG-immunized mice were infected with one founding Mtb strain (32.8% of unimmunized mice versus 22.9% of BCG-immunized mice), whereas more BCG-immunized mice had zero Mtb strains (33.6% of unimmunized mice versus 48.3% of BCG-immunized mice). This suggests that infection attributable to a single founding Mtb strain may be more readily prevented by BCG-mediated immunity than infection due to two or more strains, but further investigation is needed to test this possibility more rigorously.

The demonstration that vaccine-induced immunity can prevent detectable Mtb infection in ULD-infected mice opens the possibility of assessing a new and important immune parameter for TB vaccine testing that was not known to be achievable in mice. However, BCG had a very low capacity to mediate this type of protection (13% efficacy, $p = 0.001$); large numbers of mice were required to reach statistical significance, which would not be practical for routine testing of TB vaccine candidates. Because the overarching goal is to identify vaccines that are more efficacious than BCG, we performed a power calculation to determine what level of vaccine efficacy would be required to feasibly measure prevention of infection with a reasonable number of mice (**Table 2.1)**. This analysis showed that a vaccine with 50-60% efficacy could be assessed with a sample size of 28-55 mice per group, which would be achievable by pooling results from 2-3 experiments. Such a pipeline could be feasible, as Vidal et al. recently reported that a novel live attenuated Mtb vaccine was dramatically more effective than BCG using the ULD challenge model in C3HeB/FeJ mice, and prevention of detectable infection could be measured in a statistically significant manner with only 18 mice per group (166). Taken together

with our findings, these results suggest that the ULD challenge model provides a larger window to measure differences between TB vaccine candidates and to measure parameters of protection, including inhibition of dissemination and prevention of detectable infection, that cannot be assessed in currently used mouse models.

Table 2. 1. Group sizes needed to assess vaccine-mediated prevention of detectable infection.

		Min. sample size per group	
Prevalence	**Vaccine efficacy**	**80% Power**	**90% Power**
61.6%	20%	259	342
61.6%	30%	112	155
61.6%	40%	66	84
61.6%	50%	40	55
61.6%	60%	28	37
61.6%	70%	21	25
61.6%	80%	16	18
61.6%	90%	12	16

Minimum sample size required per group for specified power to detect a given vaccine efficacy (prevalence in unimmunized mice assumed to be 61.6%).

2.3 Discussion

There is an abundance of evidence supporting the idea that humans are typically infected with an aerosolized inoculum of 1-3 Mtb bacilli (156, 157, 167). In a classic study, Wells demonstrated that only the smallest water droplet nuclei (1-5 microns in diameter), capable of harboring 1-3 bacilli (156), could optimally infect an animal. Although an individual with TB may expel many larger Mtb-laden water droplets, these droplets, even if inhaled, are unlikely to remain airborne through the respiratory tree and reach the terminal alveoli to infect an alveolar macrophage, a requisite event to initiate infection (17).

Recent literature suggests that TB patients in TB-endemic areas are exposed to a much higher dose. Wood, R. and Warner, D.F. developed the Respiratory Aerosol Sampling Chamber (RASC) to quantify and characterize aerosol particles emitted from patients during normal breathing, coughing, and talking in real-time while in a small personal cleanroom (168). Further studies found a high prevalence of Mtb bioaerosol release in a randomly selected community cohort from TB-endemic Cape Town, South Africa, with 79.5% of participants producing at least one positive bioaerosol sample and an average of 2.9 viable Mtb CFU per sample (169). In a subsequent longitudinal study, 74% of participants were constant low-level producers of Mtb over 2 months (169). These data suggest that in hyperendemic communities, there is more repeated exposure to Mtb-containing particles than previously thought.

Other work has shown that TB patients can produce a large amount of culturable Mtb even in small aerosols. These researchers use the cough aerosol sampling system (CASS), originally developed by Fennelly, K.P., to capture and quantify culturable cough generated aerosols of Mtb from active pulmonary TB patients who coughed into a closed chamber (170). Initial studies in Uganda and recent studies in Kenya have shown that about 30% of subjects with positive sputum cultures produce culture-positive cough aerosols (171, 172). One study in Uganda showed that among the CASS-positive patients, the median cultured bacteria was 16 CFU and a more recent large study in South Africa showed that 30% of CASS-positive patients cultured more than 10 CFU from cough aerosols and 60% of the CFUs were in droplets smaller than 4.7μm which could be deposited in the smallest airways (172, 173). These data suggest that TB patients can generate aerosols with large amounts of culturable TB in a short measurement interval, including TB cultured from small, 1-5 μm aerosols. The studies using CASS argue that one component of infectiousness is the ability of the host and pathogen to generate infectious quanta and that this can be approximated by measuring culturable Mtb CFU from respirable cough aerosols. Other studies have shown that cough-generated aerosol

cultures predict tuberculosis transmission to household contacts better than microbiological or clinical markers (174, 175).

It is important to remember, however, that Mtb culturability from cough aerosols may not necessarily correlate with infectivity. For an aerosolized infectious particle to establish Mtb infection in a way that leads to disease, it must remain airborne through the entire respiratory tree until it reaches the terminal alveoli, be taken up by an alveolar macrophage, and undergo productive replication without being cleared by immunity.

The best evidence that human exposure to truly infectious Mtb particles is a relatively rare event is the observation that primary TB usually manifests as a single focus of infection, or Ghon complex. In Anton Ghon's original post-mortem series of 170 children with primary TB, 72% had a single lung granuloma, and subsequent studies reported that up to 94% of primary TB cases presented with single granulomas (176). Studies in non-human primates have shown that granulomas are initiated by a single founding bacilli (177, 178), and animal studies in NHPs and mice routinely show that higher infectious doses result in numerous primary lesions involving both lungs. The fact that human lesions usually develop as a solitary lesion in the most well-ventilated regions of a single lung, suggest that these foci are initiated by aerosol deposition of a single infectious particle. If multiple infectious particles were inhaled in manner that led to true infectivity, one would expect to find multiple lesions in both lung, consistent with animals models (both NHP and mice). Using the ULD model, the proportion of mice with a single lung granuloma is very similar to that described by Ghon, strongly suggesting that the ULD model provides a reasonable reflection of the physiologic infectious dose in humans.

This estimate is consistent with conclusions about the relatively rare concentration of infectious particles shown in another classic study by Riley et al. Riley evaluated the frequency with which contacts of active TB patients are exposed to infectious aerosols, effluent air from a TB ward was delivered to guinea pigs over a two-year period and the acquisition of infection was assessed (179, 180). Based on the estimated volume of air breathed by each animal, the

effluent air from the TB ward was calculated, on average, to contain one infectious unit per 340 m^3 of air (12,000 ft^3). Subsequent studies of Mtb infectivity support these estimations by Riley (181-183). Given that the average human adult breaths ~10 m^3 of air each day, this suggests that a household contact of an individual with active TB would inhale an Mtb-bearing droplet capable of successfully initiating infection only every few weeks. The contrast between the high frequency of particles exhibiting Mtb culturability and those demonstrating the infectivity in animals (guinea pigs) or humans (Ghon foci) suggests that most of the culturable Mtb does not lead to infectivity. It is for these reasons that we believe that the ULD model represents a more physiologic infectious dose.

To triage the growing number of TB vaccine candidates and move those with the most promise into clinical trials, there is an urgent need to develop small animal models that reliably assess parameters of immunity with relevance to human protection. There is growing concern that the current mouse model, in which mice are infected with 50-100 Mtb CFU by aerosolization, is not up to this task (162, 163). This model provides too small a window to discern differences between vaccine candidates; most confer a transient reduction in the lung bacterial burden by about one log if measured between 4-6 weeks post-infection. Durable reductions in lung bacterial burdens and other clinically relevant parameters of immunity, including the ability to curb Mtb dissemination or prevent detectable infection, are difficult or impossible to assess. Indeed, the inability of the current model to predict how well vaccine candidates will perform in human efficacy trials is becoming increasingly apparent (162, 163). In this study, we utilize the current TB vaccine, BCG, for which there is abundant human efficacy data, to assess the utility of the ULD model for TB vaccine testing. We demonstrate that ULD infection provides a promising new challenge model in which three distinct parameters of protection can be assessed: 1) reductions in lung bacterial burdens that are more durable than after conventional dose challenge, 2) inhibition of Mtb dissemination, and 3) prevention of detectable infection.

Of these, reduction in bacterial burdens is the only parameter of protection that can readily be assessed in current mouse models. In contrast to transient protection that dissipates within 3-4 months in the current model (61, 153), we have shown durable lung bacterial burden reductions for at least four months in the ULD model. Importantly, the types of immune responses that mediate reductions in lung bacterial burdens in mice infected with high doses (>250 CFUs) are sometimes different than those that do so at conventional doses (50–100 CFU) (104, 184). Although this has not yet been rigorously assessed in the ULD model, it is reasonable to hypothesize that the immune responses that are optimal for reducing lung bacterial burdens after an infectious inocula of 1-3 CFU may also be different than those required for a 50-100 CFU challenge. Thus, vaccine candidates may vary in their capacity to control bacterial burdens to a challenge dose that is more physiological compared to a challenge dose that is artificially high, a hypothesis that needs further investigation.

The second parameter of immunity that can be measured in the ULD model is the ability to prevent dissemination. Because most ULD-infected mice are infected by a single founding bacillus (152), infection is usually initiated at a single site in one lung. Thus, most bilateral lung infection is the result of Mtb dissemination from the initially infected lung to the contralateral lung and CFU determinations of each individual lung can provide an estimation of a vaccine's ability to block dissemination, which we have termed containment. This approach underestimates containment, however, because some mice may have Mtb in each lung not because of dissemination, but due to independent infection events of each lung by two or more distinct aerosolized strains. By infecting mice with a pool of bar-coded strains, we have shown that we can distinguish between disseminated infection and separate infections with different strains by sequencing the Mtb bar-codes in each lung. Using this approach, we have shown that BCG immunization can prevent Mtb dissemination to the contralateral lung in ~80% of ULD-infected mice. These results in the murine ULD model parallel results in BCG vaccinated humans showing that BCG vaccination is most effective at preventing disseminated forms of TB (185).

The third parameter of immunity that can be assessed in the ULD model is the prevention of detectable infection. There are several lines of evidence that the human immune system can prevent or eradicate Mtb infection. Some individuals with high exposure to index cases with active TB disease, including household contacts, fail to develop an Mtb-specific IFNγ-producing T cell response, suggesting that long-term Mtb infection is sometimes not established despite intense exposure (186). Furthermore, many individuals that do develop a T cell IFNγ response against Mtb may eventually eradicate infection, as the incidence of active TB is quite low amongst IGRA+ individuals (usually less than 5%) even when their immune systems are potently immunosuppressed or ablated (12). Recently there have been several high-profile TB vaccine studies showing that some vaccines can prevent detectable infection in non-human primates (124, 125, 187). This had not been previously shown in mice, and it has been postulated that mice lack the fundamental immune effectors needed to prevent sustained Mtb infection (164). In this study we showed no difference in the proportion of BCG-immunized mice with detectable infection compared to controls at d14-15 after Mtb challenge, suggesting that vaccination did not block the initial Mtb infection. At all later timepoints, however, BCG vaccinated animals had a modest, but highly statistically significant increase in the proportion of mice with undetectable infection compared to unimmunized controls (overall 13% efficacy, p=0.001). This suggests that a small proportion of the vaccinated mice that may have been initially infected were able to clear Mtb to undetectable levels. Even though BCG can do this only modestly, these results suggest that vaccine-mediated immunity can prevent sustained infection in mice exposed to a more physiologic Mtb dose, challenging the longstanding belief stemming from experiments with an artificially high Mtb exposure dose, that mice are unable to eradicate Mtb infection.

One limitation of the ULD model for vaccine testing is the number of animals that are required in each group. This is exacerbated by the fact that not all animals are initially infected

in the model, and currently it is not possible to discern animals that were never infected from those that were initially infected, but subsequently eradicated Mtb. We have attempted to develop both immunologic and molecular assays to distinguish between these possible outcomes, but this has proven difficult to achieve. We initially assessed Mtb-specific CD4 T cell responses against an Mtb antigen (ESAT-6) that is not present in BCG. We identified a couple unvaccinated mice that were exposed to aerosolized ULD Mtb and had measurable Mtb ESAT-6-specific CD4 T cell responses despite having no detectable lung bacterial burdens. These results suggested that even a few unvaccinated ULD-infected mice may clear Mtb to undetectable levels, but mice exhibiting this phenotype were rare. However, this approach was not successful in BCG-immunized mice because BCG immunization suppressed the development of Mtb ESAT-6-specific T cells to undetectable or almost undetectable levels even in ULD Mtb-challenged mice that were demonstrably infected, providing minimal window to discern differences between uninfected and infected mice. We next attempted to measure anti-ESAT6 IgG antibody as a biomarker of infection. However, in initial studies we obtained non-specific responses from uninfected mice and weak responses even from some high-dose infected mice. It is possible we could further optimize the protocol for these ELISAs but given the background noise and weak responses from higher dose infected mice, it seemed unlikely that this assay would be sensitive enough to detect potentially even weaker responses from ULD-infected mice. We also attempted to amplify Mtb DNA from lung homogenate using previously published Mtb-specific PCR primers (178). Unfortunately, the sensitivity of this assay was not sufficient to reliably detect below 1,000 viable bacteria, and we were unable to obtain a signal from mice with undetectable bacterial burdens. Despite our inability to differentiate mice that were never infected from those who cleared infection, we were able to build strong statistical evidence for prevention of detectable infection by assessing large numbers of mice.

Our results are consistent with findings that BCG can sometimes provide long-term protection against human TB, and are consistent with studies showing BCG-mediated protection

in individuals without prior Mtb exposure (tuberculin skin test-negative or IGRA-negative individuals) or in low Mtb transmission settings (8, 158-160). The low overall observed efficacy (~13%) in preventing detectable infection also reflects the suboptimal nature of BCG-mediated immunity. Reliably assessing this parameter of protection for a vaccine with such low efficacy would require hundreds of mice per group, as in this study, which would not be feasible for routine pre-clinical evaluation of TB vaccine candidates. However, the goal is to identify promising vaccine candidates that are significantly more efficacious than BCG to move into human trials. Our power analysis showed that a vaccine with 50% efficacy could be readily assessed by repeating studies with 15-20 mice per group 2-3 times and compiling the results. We believe this is feasible and would be worthwhile if further studies show that results obtained in the ULD model are superior to those obtained in the conventional murine model for distinguishing vaccine efficacies in clinical meaningful ways. We are encouraged that a recent study assessing a novel TB vaccine candidate (ΔLprG, a live-attenuated Mtb vaccine) in C3HeB/FeJ mice after ULD challenge showed that ΔLprG was dramatically better than BCG at preventing detectable infection and achieved statistical significance with only 18 mice per group (166). In this same study, ΔLprG was only slightly better than BCG in reducing lung bacterial burdens in mice challenged with 100 CFU, suggesting that the ULD challenge model provides a larger window to discriminate differences between vaccines.

This study has several limitations. We used a single experimental Mtb strain (H37Rv) and a single inbred mouse strain (C57BL/6); different bacterial or host strains could result in changes in vaccine efficacy. In addition, the immune system is more quiescent in mice reared under specific pathogen free (SPF) conditions compared to “dirty” mice (188); thus, the SPF setting may be less reflective of protective immunity in humans, as humans also live in dirty environments. To reproducibly deliver an ULD of Mtb that infects 60-80% of mice, we used freshly thawed Mtb stocks at an established concentration. However, freshly thawed Mtb may have differences in metabolic state or cell wall composition compared to droplet-laden Mtb

expelled from an infected individual, which could impact vaccine responses. In future studies, different Mtb strains, including those obtained from clinical settings, and different inbred mouse strains could be incorporated into the model; however, some of these limitations may remain due to the inherent mouse-to-mouse variability in the ULD model and the large number of mice needed to perform the experiments. For example, using genetically heterogeneous mice, such as diversity outbred mice, or “dirty” mice, would introduce even more variability, and the number of mice needed to see meaningful differences between groups may be impractical. Of course, no animal model will precisely mirror the complexities that lead to human TB protection vs. susceptibility. Nevertheless, animal models are needed and should be used to assess parameters of protection that are relevant to humans to help prioritize vaccine candidates and thus de-risk human clinical trials.

Overall, the ULD challenge model holds promise as a new and improved platform for evaluating TB vaccine candidates. The model can assess distinct parameters of vaccine-mediated immunity that cannot be assessed in the current mouse model and has potential to improve discrimination between the protective capacities of different vaccines. Each of the three parameters of immunity that can be assessed in the ULD model may be relevant to different clinical TB outcomes. For example, the ability of vaccines to durably reduce lung bacterial burdens and prevent dissemination may reflect their capacity to prevent different aspects of TB disease, whereas the ability to prevent detectable infection may reflect prevention of sustained infection. Because each of these parameters are likely mediated by different aspects of immunity, it is possible that different vaccines will differ in the relative capacity to control Mtb burdens, inhibit dissemination, and prevent detectable infection. For these reasons, the advantages of assessing vaccine-mediated protection in a more physiologic infectious challenge may outweigh the limitations listed above. Future studies are needed to assess a variety of TB vaccine candidates in the ULD model, and whenever possible, determine whether the results correlate with clinical outcomes in human vaccine trials.

2.4 Materials and Methods

2.4.1 Ethics Statement

All animal studies were performed in compliance with the SCRI Animal Care and Use Committee, protocol IACUC00499.

2.4.2 Mice

C57BL/6J mice were purchased from Jackson Laboratories (Bar Harbor, ME). Female mice between the ages of 9-12 weeks were used. All animals were housed and maintained in specific-pathogen-free conditions at Seattle Children's Research Institute (SCRI).

2.4.3 BCG Immunizations

BCG-Pasteur was cultured in Middlebrook 7H9 with OADC supplement and 0.05% Tween-80 at 37˚C with constant agitation for five days. BCG was back diluted in 7H9 for two days and grown to an OD of 0.2-0.5. Bacteria was diluted in PBS and mice were injected subcutaneously with 200µl of 10^6 CFU. After immunization, mice were rested for 8 weeks prior to Mtb infection.

2.4.4 ULD Mtb Aerosol Infections

H37Rv or bar-coded H37Rv Mtb were used for infections (29). Mtb stocks were grown in Middlebrook 7H9 with OADC supplement and 0.05% Tween-80 at 37˚C with constant agitation to an OD = 1. Cultures were filtered through a 5µm filter to remove clumps and aliquots were frozen at -80˚C. Frozen filtered stocks were thawed and titered side by side with stocks used for conventional dose infection to determine how to dilute the ULD stocks with the goal of leaving 37% of mice uninfected. Mice were infected by injecting 5mls of diluted Mtb into the nebulizer of

a Glas-Col aerosol infection chamber. The nebulization cycle was set to 45 minutes followed by 45 minutes of cloud decay.

2.4.5 CFU Plating

Mouse organs (right lung, left lung, or spleen) without perfusion were homogenized separately in M tubes containing 1mL PBS+0.05% Tween-80 (PBS-T) using a Miltenyi GentleMACS machine (Miltenyi). Homogenates were then diluted in PBS-T and plated onto 7H10 plates. For ULD infections, undiluted homogenates were also plated between two 7H10 plates. Plates were incubated at 37˚C for at least 21 days before quantification of CFU.

2.4.6 Genomic DNA Extraction

Bacterial colonies grown from infected left lungs or right lungs were scraped into resuspension buffer (25mM Tris-HCl pH 7.9, 10mM EDTA, 50mM glucose, water) plus 10mg/mL lysozyme and were incubated at 37˚C overnight. Samples were resuspended in 10% sodium dodecyl sulfate and 10mg/mL Proteinase K and were heated at 55˚C for 30 minutes. Samples were then resuspended in 5M NaCl followed by Cetrimide saline solution and heated at 65˚C for 10 minutes. Genomic DNA was extracted twice with 24:1 chloroform:isoamyl alcohol. DNA was precipitated with 0.7x volume of isopropanol and washed with 70% ethanol. Finally, DNA was eluted with DEPC water.

2.4.7 Barcoded Sequencing

Mice were infected with a pool of 50 bar-coded strains. Sequencing of bacterial bar-codes has been previously described (152, 189). Briefly, genomic DNA was pre-amplified with pooled barcoded primers before libraries were prepared with NEBNext Ultra DNA Library Prep Kit for

Illumina (New England Biolabs) using the AMPure XP reagent (AgenCourt Bioscience) for size selection and cleanup. The NEBNext Multiplex Oligos for Illumina (New England Biosciences) were used to barcode DNA libraries and enabled multiplexing of 96 libraries per sequencing run. Samples were sequenced using the NextSeq 500 Mid Output v2 kit (Illumina) at the University of Washington Northwest Genomics Center. Read alignment was carried out using a custom processing pipeline that has been previously described (189).

2.4.7 Statistics

All statistical analysis was done in R v.4.2.0 with packages Exact (v3.1) and lme4 (v1.1-30). When comparing values between two groups in a single experiment, we used Barnard's exact test for differences in proportions and simple linear regression on log-transformed CFU values for differences in bacterial burden (excluding those with 0 CFU). For analyses compiling more than one experiment, we used mixed effects logistic regression with experiment as the grouping variable for differences in proportions, and mixed effects linear regression on log-transformed CFU values for differences in bacterial burden. In all analyses, mice were considered protected when the CFU was undetectable in both lungs, and analyses of dissemination and overall bacterial burden were performed conditional on absence of protection.

2.5 Acknowledgements

The authors would like to thank Bridget Alexander, Lindsay Engels, Samuel Schrader, Kaitlin Durga and the Seattle Children's OAC staff for technical support. This work was supported by NIH contract 75N93019C00070 (K.B.U), the Bill and Melinda Gates Foundation, INV-026296 (K.B.U) and NIH grant U19AI135976 (K.B.U).

2.6 Author contributions

C.P. and H.B. contributed equally to this manuscript.

Conceptualization and writing – original draft: C.P., H.B., K.U.

Investigation and validation: C.P., H.B., S.C., K.L., L.C., K.U.

Visualization, formal analysis, and writing – review & editing: C.P., K.B., S.C., D.S., P.E., K.U.

Funding acquisition: C.P., S.C., K.U.

Supervision: K.U.

Chapter 3. CD4 and CD8 T cells mediate distinct aspects of vaccine-induced immunity against Mycobacterium tuberculosis

This chapter is an adaptation of a manuscript draft where I am first author, currently being prepared for publication. The contributions of each author can be found in the acknowledgments section at the end of this chapter.

3.1 Introduction

Tuberculosis (TB) is still a major global health challenge despite global vaccination with Bacille-Calmette-Guérin (BCG), currently the only licensed vaccine against TB. While BCG consistently confers protection against disease such as TB meningitis and miliary TB in infants and during childhood**,** vaccine efficacy widely ranges from 0-80% in adults (4-6)**.** Some studies have shown that BCG can provide long-term protection for as long as 50 to 60 years, but other studies have shown no protective effect of BCG, particularly in endemic regions (7, 8). Overall, BCG is clearly not sufficient to curb the global TB pandemic. To develop more effective TB vaccines, we not only need a better understanding of immunity against *Mycobacterium tuberculosis* (Mtb), we also need a better understanding of successful vaccine-mediated immunity against TB.

Our understanding of TB immunity, especially vaccine-mediated immunity, has been hampered by a lack of gold standards for defining control or eradication of Mtb in a tractable animal model. BCG vaccination in the current conventional dose (CD) (50-100 CFUs) Mtb mouse infection model confers ~1 log reduction in lung bacterial burdens that is transient and dissipates by 3-4 months post-infection (153, 154). This 1 log reduction in lung bacterial burden is the only measurable parameter in the CD model and it is unclear if the vaccine-induced mechanisms that enable mice to transiently reduce their bacterial burdens are relevant to the mechanisms of immunity required for long lasting protection in human TB infection. Our lab

developed an ultra-low dose (ULD) (1-3 CFUs) Mtb mouse model and recently described three novel parameters of BCG-mediated protection within the ULD model: 1. Durable reduction in lung bacterial burdens, 2. Prevention of Mtb dissemination to the contralateral lung, and 3. Prevention of detectable infection in a subset of BCG vaccinated mice (152, 154). These parameters are relevant to preventing disease and/or infection that cannot be assessed in the CD model. Furthermore, each parameter may be mediated by different aspects of immunity, and we can use BCG vaccination within the ULD model to begin to dissect mechanisms of BCG-mediated protection against Mtb.

Historically, the roles of T cells in TB immunity were defined in studies that used antibody depletion of mice infected with CD Mtb. CD4 T cells are critical for protective TB immunity as depletion of CD4 T cells results in higher lung and spleen bacterial loads and rapid mortality (37, 38). This is consistent in humans as HIV-infected individuals are depleted of CD4 T cells and are restricted in their ability to contain Mtb infection (39). In the same mouse studies, CD8 T cells appeared to play a minimal role in controlling bacterial burden or survival. Studies using $\mu MT^{-/-}$ B cell deficient mice challenged with 100-300 CFU of Mtb also concluded that B cells are not required for controlling lung or spleen burdens (105, 106). However, recently there has been a surge of interest in looking at the importance of B cells, and there has been correlative and *in vitro* data showing the contribution of different types of antibodies in people infected with TB (116-118). However, these studies did not investigate the relative roles of these lymphocyte subsets in vaccine-mediated immunity and need to be re-addressed in tractable animal models infected with a more physiologic dose of Mtb, as the mechanisms of immunity that curb infection to a supraphysiologic dose may not be the same as those that operate in response to a more physiologic infectious dose of 1-3 CFU.

Here we determined the roles of T cell subsets and B cells in vaccine-mediated immunity. We first characterized the BCG-induced T cells that are responding early after CD Mtb infection but before the divergence in lung bacterial burdens via flow cytometry, confocal

microscopy, and 10x single cell RNA sequencing and found that BCG induces antigen-specific, activated and proliferative CD4 and CD8 T cells in the lung early after Mtb infection with distinct transcriptional profiles. Then, using antibody co-depletion of CD4 and CD8 T cells or $\mu MT^{-/-}$ B cell deficient mice in the ULD model, we found that T cells were required for all three parameters of BCG-mediated protection while B cells were not required. We further investigated the relative roles of CD4 and CD8 T cells using single antibody depletion experiments and discovered that CD4 T cells played predominant roles in controlling Mtb replication in the lungs regardless of vaccination status and preventing BCG-mediated dissemination to the contralateral lung but played a minor role in preventing the initial infection by inhaled Mtb strains. In contrast, CD8 T cells played a modest but still significant role in BCG-mediated control of lung burden and a minor role in prevention of dissemination to the contralateral lung. Importantly, CD8 T cells played a predominant role in BCG-mediated prevention of infection of Mtb strains. Therefore, CD4 and CD8 T cells play distinct roles in vaccine-mediated immunity against Mtb and targeting both aspects of immunity could be key to designing an effective TB vaccine.

3.2 Results

3.2.1 BCG-induces Mtb-specific, effector CD4 and CD8 T cells that respond to early pulmonary Mtb infection.

Our lab previously published data showing that Bacille-Calmette-Guérin (BCG) vaccination in C57Bl/6 (B6) mice accelerates the recruitment of both CD4 and CD8 Mtb-specific T cells to the lung as early as day 10 post-infection (p.i.) (134). To extend these findings and look at additional T cell phenotypes, we compared lung parenchymal cells in unvaccinated versus BCG-vaccinated B6 mice infected with a conventional dose (CD) (50-100 CFU) of mCherry-expressing H37Rv Mtb via flow cytometry (**Figure 3.1A**). At day 12 p.i., CFU burdens from the lung are equivalent in unvaccinated and BCG-vaccinated mice (**Figure 3.1B**), indicating that this is a timepoint just prior to the BCG-induced divergence in bacterial burdens. We therefore used day 12 p.i. to investigate immune responses induced by BCG early after Mtb infection but before the data were confounded by differences in bacterial burdens. BCG vaccination increased the numbers of activated and proliferative CD4 T cells and CD8 T cells in the lung parenchyma that were $CD44^{hi}Ki67^{+}$ (**Figure 3.1C**). There were also more cytotoxic CD8 T cells characterized by granzyme B expression (**Figure 3.1D**). Consistent with prior findings, BCG increased the numbers of both Ag85B specific CD4 T cells and TB10.4 specific CD8 T cells (**Figure 3.1E**). Therefore, BCG induces activated and proliferative antigen-specific effector T cells early after Mtb infection.

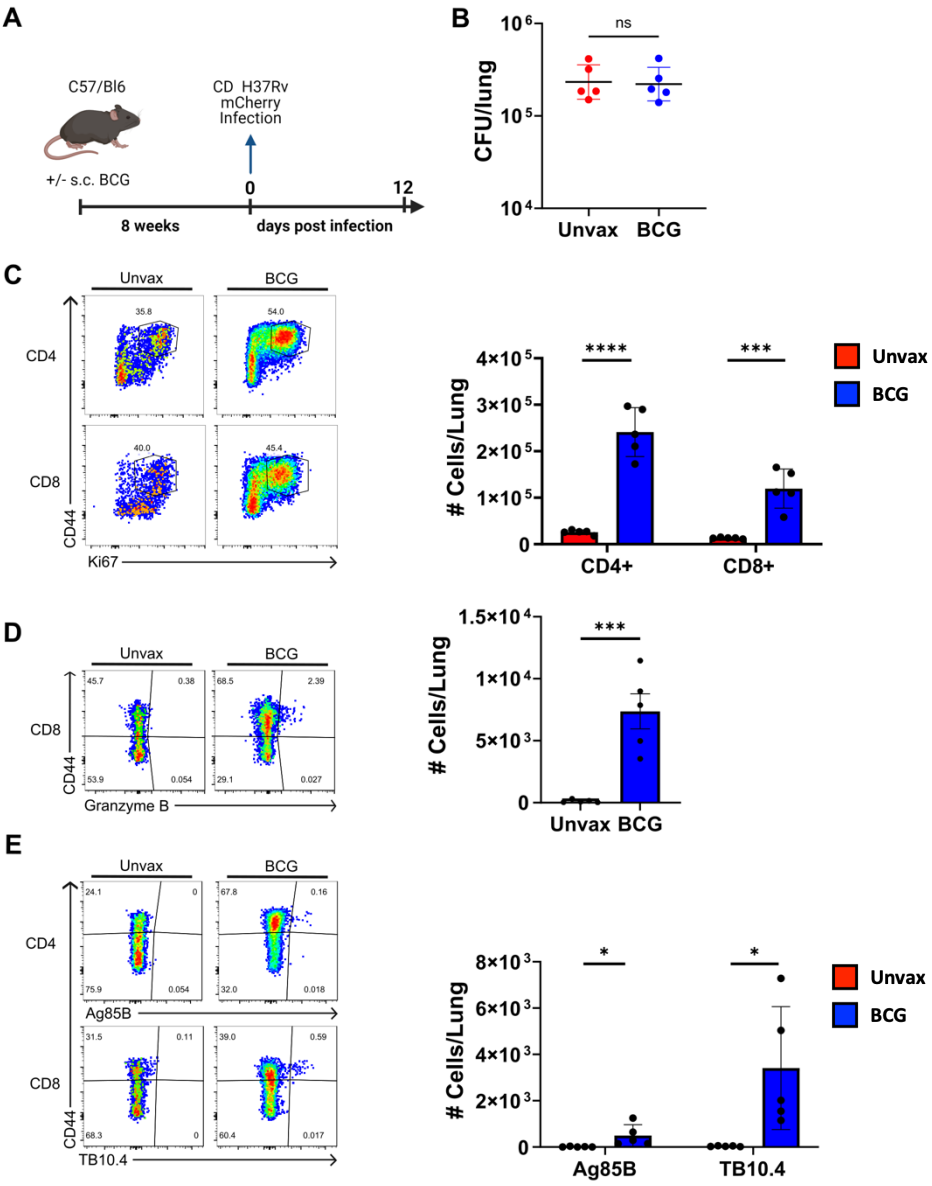

Figure 3. 1. Antigen specific effector CD4 and CD8 T cells induced by BCG respond early after Mtb infection. **(A)** Schematic of experimental timeline. C57Bl/6 (B6) mice were infected with a conventional dose (50-100 CFU) of bar-coded H37Rv Mtb 8 weeks post vaccination with s.c. 10^6 BCG-Aeras Pasteur or no vaccination. At day 12 post-infection, the inferior lobe was taken for microscopy, the rest of the right lobe was taken for flow cytometry, and the left lobe was plated for CFU. **(B)** CFU of unvaccinated (red) or BCG vaccinated mice (blue). **(C)** Representative flow cytometry plots and quantification of IV- CD4 and CD8 T cells with $CD44^{hi}Ki67^{+}$ expression. **(D)** Representative flow plots and quantification of granzyme B expressing CD8 T cell subsets. **(E)** Representative flow plots and quantification of IV- $CD44^{hi}$Ag85b+ CD4 T cells and IV- TB10.4+ CD8 T cells. Prior gating: Lymphocytes, single cells, live, CD3+ dump-, IV-, TCRb+, CD4+ or CD8+. Significance was determined using unpaired t-test on GraphPad Prism. ns = not significant, *p<0.05, **p<0.01, ***, p<0.001.

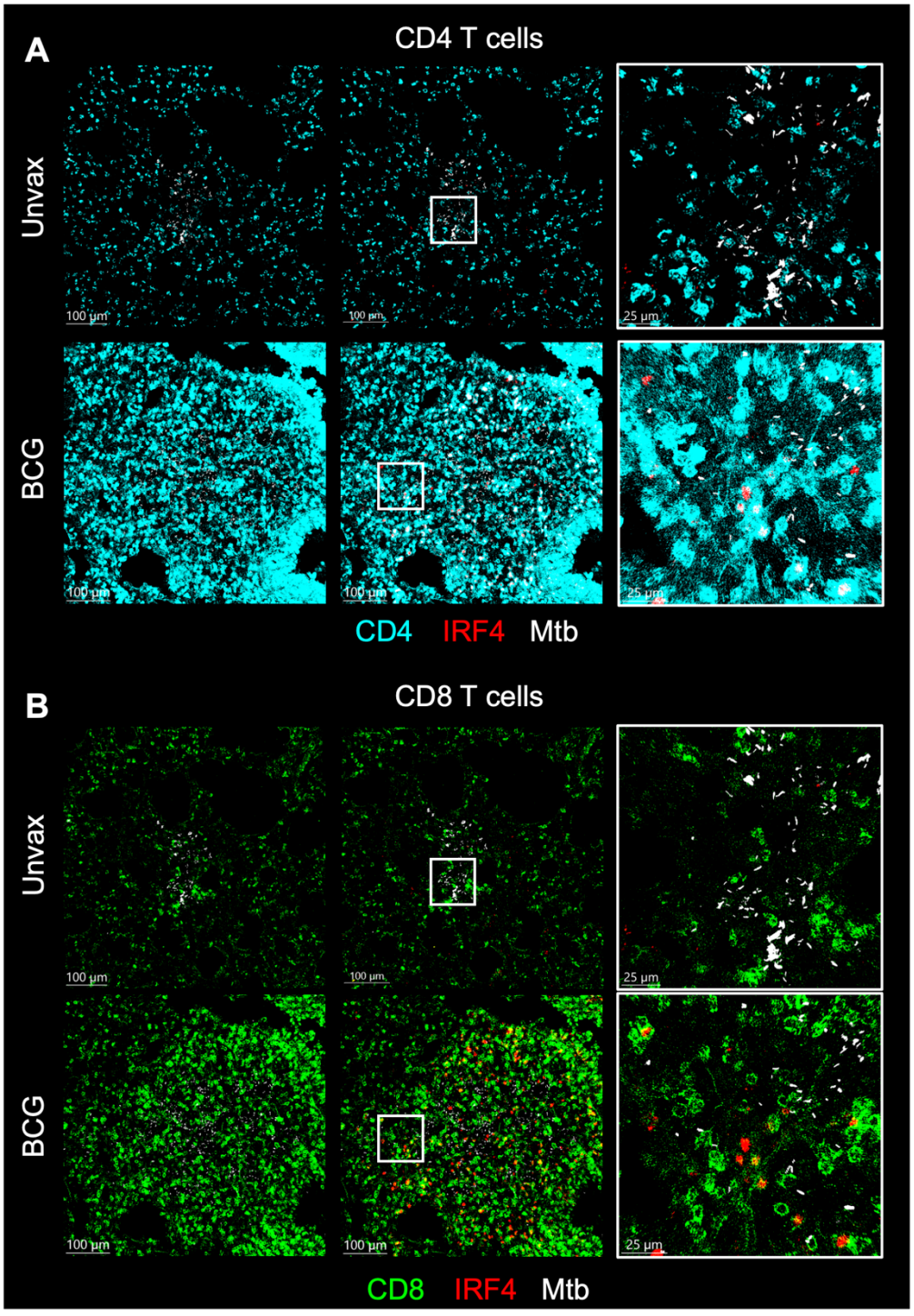

Figure 3. 2. BCG accelerates activated CD4 and CD8 T cell influx into lesions early after Mtb infection. Representative confocal microscopy images showing lesions and zoom-ins highlighting CD4 T cells **(A)** or CD8 T cells **(B)** and IRF4 expression. Day 12 post CD mCherry-expressing H37Rv infection, n = 15 per group.

We next performed confocal microscopy of the right inferior lung lobes to observe the spatial localization of CD4 and CD8 T cells within lesions of the unvaccinated versus BCG vaccinated mice (**Figure 3.2**). There were large influxes of both CD4 and CD8 T cells into the lesions of BCG vaccinated mice compared to unvaccinated mice (**Figure 3.2**). Importantly, BCG vaccinated lesions, but not unvaccinated lesions, had T cells expressing IRF4, a marker of recent antigen sensing and activation (**Figure 3.2**). While there were a few IRF4+ CD8+ cells, most IRF4+ cells were CD4+ (**Figure 3.2**). Quantitative analysis is ongoing to determine if these observations are statistically significant and to determine the distance of these cells to infected cells. These data are consistent with the increase in CD4 and CD8 T cells found in the flow cytometry data and suggests that the increase in abundance of T cells occurs within the newly forming lesions. Additionally, the data suggest that BCG vaccination accelerates recent antigen sensing of a few CD8 T cells and of many CD4 T cells.

3.2.2 BCG-induced T cells are activated with effector properties while B cells are responding to the environment early after Mtb infection.

We complemented the flow cytometry and microscopy data with 10x single-cell RNA sequencing (scRNAseq) where 4 unvaccinated and 12 BCG vaccinated B6 mice were harvested at days 12 or 13 post CD H37Rv infection and we confirmed no difference in lung bacterial burdens between unvaccinated and BCG vaccinated mice (**Figure 3.3A-B**). Viable lung parenchymal cells were FACS-sorted using a fluorescent IV-injected antibody then prepared for 10x sequencing. After initial lymphocyte identification, cells were re-clustered to identify cell subsets with distinct gene expression profiles (**Figure S3.15 and 3.3C**). We identified clusters 4 and 0 that matched profiles for naïve and activated CD4 T and clusters 1 and 4 that matched profiles for naïve and activated CD8 T cells. Cluster 11 mapped to Tregs and cluster 7 was driven by proliferation and had expression of both CD4 and CD8. We also

identified clusters 3 and 2 that matched profiles for B cells and activated B cells, clusters 6 and 10 that matched $\gamma\delta$ T cells and NKT cells, and clusters 8 and 9 that matched innate-like ILC2s and NK cells. (**Figures S3.15 and 3.3C**).

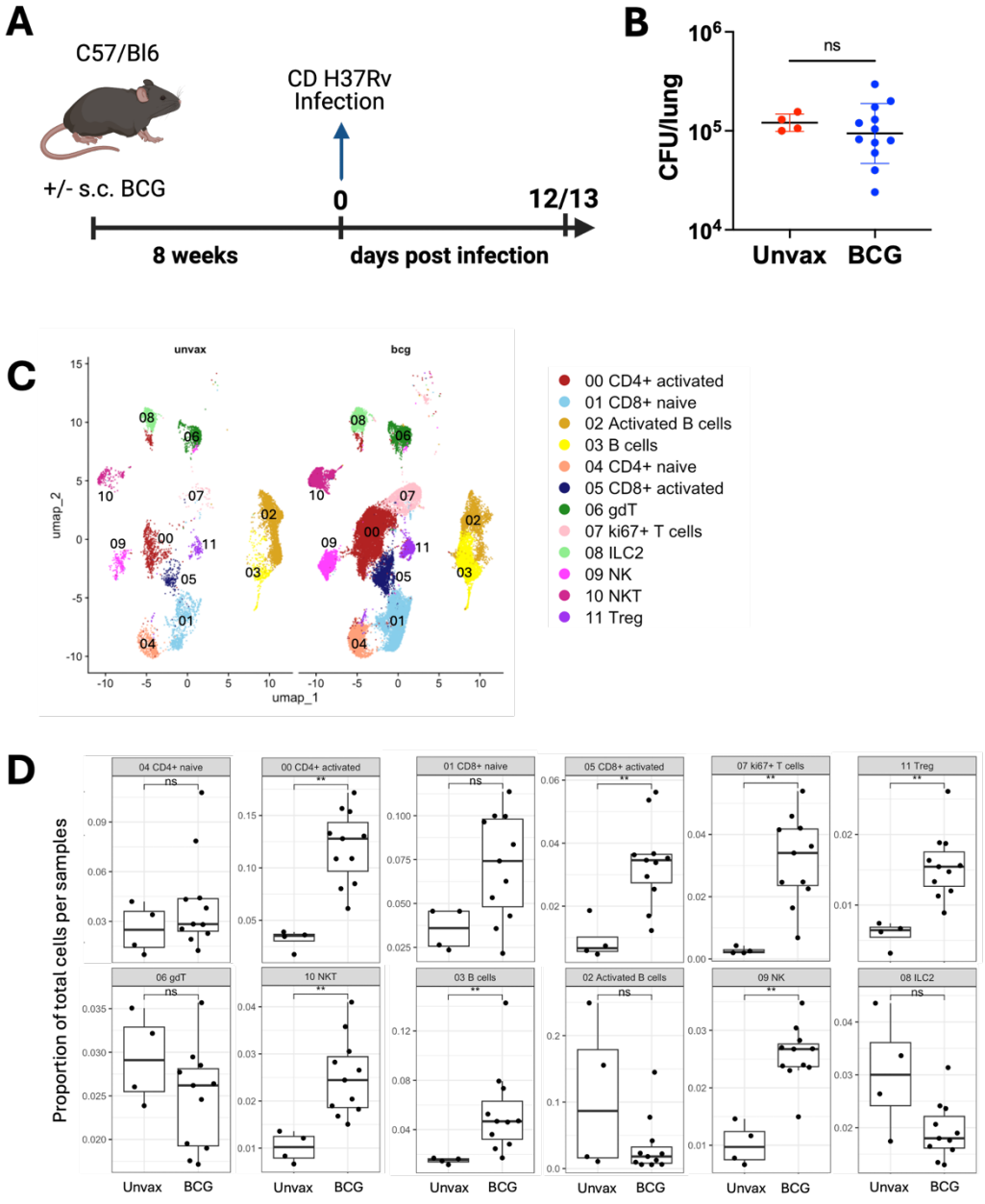

Figure 3. 3. Unvaccinated versus BCG vaccinated lymphocyte cell profiles in lungs early after Mtb infection. (A) Schematic of experimental timeline. C57Bl/6 (B6) mice were infected with a conventional dose (50-100 CFU) of H37Rv Mtb 8 weeks post vaccination with s.c. 10^6 BCG-Aeras Pasteur or no vaccination. At day 12 and 13 post-infection, the right lung was processed for scRNA sequencing, and the left lung was plated for CFU. **(B)** CFU of unvaccinated (red) or BCG vaccinated mice (blue). Significance was determined using unpaired t-test in GraphPad Prism; ns = not significant. **(C)** Lymphocyte subclusters compiled for unvaccinated or BCG vaccinated samples using the R Seurat package. **(D)** Relative frequency of each cell cluster per sample for unvaccinated or BCG vaccinated samples. Significance was determined using Wilcoxon test; ns = not significant, **p<0.01.

We then compared the cell clusters in unvaccinated versus BCG vaccinated samples (**Figure 3.3**). Importantly, we started with more BCG vaccinated mice (4 unvaccinated mice and 12 BCG vaccinated mice) which contributes to the overall increase in recovered cells from BCG vaccinated mice. We saw a consistent distribution of cells throughout most clusters in unvaccinated and BCG vaccinated mice. Interestingly, there were different distributions in the activated T cell clusters (clusters 0 and 5) and B cell cluster (cluster 3) with unvaccinated cells from those clusters being present in the bottom half and mostly absent in the top half of the cluster while BCG vaccinated cells were dispersed throughout the clusters (**Figure 3.3C**). Thus, BCG may induce cells with unique phenotypes from these clusters. We also normalized samples to account for differences in numbers of unvaccinated versus BCG vaccinated cells to look at the proportion of cells per sample. BCG increased the proportions of activated CD4 T cell, activated CD8 T cell, Ki67+ T cell, Treg, NKT, B cell, and NK cell clusters (**Figure 3.3D**). These data suggest that multiple types of lymphocytes, particularly activated and proliferative T cells, are induced by BCG vaccination and respond early after Mtb infection.

We wondered about the functional profiles of the cell clusters and used a R package (RIRA) with defined signatures for classification of phenotypes of immune cell subsets identified in NHPs and translated into mouse gene orthologs (**Figure 3.4**). Median signature scores were calculated for unvaccinated and BCG vaccinated samples of each cluster (**Figure 3.4A**). Interferon response had a higher median signature score in BCG samples compared to unvaccinated samples across all cell clusters. The BCG group of the Ki67+ T cell cluster also had increases in median signature scores for T and NK activation (0.086 vs 0.14) and glycolysis (0.088 vs 0.12), consistent with the proliferative phenotype of this cluster. The cytotoxicity signature scores were increased in BCG samples for the CD4 activated (0 vs 0.063), Ki67+ T cells (0 vs 0.075), NK (0.076 vs 0.1), and NKT (0.19 vs 0.23) clusters. Surprisingly, the activated CD8 T cell cluster did not have very different cytotoxic signature scores (0.14 vs 0.15) (**Figure 3.4A**).

Because it was difficult to identify other differences using median signature scores, we looked at the signature scores of unvaccinated versus BCG vaccinated samples on a per cell basis (**Figure 3.4B-F**). Again, there were more BCG vaccinated mice, resulting in more BCG vaccinated cells than unvaccinated cells, so we were interested in comparing the location of signature expression within sub-regions of clusters. Expression of the T and NK activation signature overlapped with expression of the glycolysis signatures as both were predominant in the Ki67+ T cells and CD4+ activated clusters, particularly for BCG vaccinated cells (**Figure 3.4B and D**). The pattern of interferon signature expression was most predominant in specific sub-regions of CD4+ activated, CD8+ activated, Treg, and NK clusters, and the pattern of expression was similar for unvaccinated and BCG vaccinated cells (**Figure 3.4C**). There was also some interferon signature expression in the BCG vaccinated CD4+ naïve cluster that did not seem to be expressed by the unvaccinated CD4+ naïve cluster. The pattern of cytotoxicity signature expression was most predominant in specific sub-regions of CD8+ activated, Ki67+ T cells, NK, and NKT clusters (**Figure 3.4F**). The sub-regions of cytotoxicity expression were different than the sub-regions of interferon signature expression, particularly for the activated CD8+ activated and NK clusters (**Figure 3.4C and F**). For the BCG vaccinated activated CD8+ cluster, some of the cells with cytotoxicity signature expression were located in the sub-region of the activated CD8+ cluster absent in the unvaccinated samples.

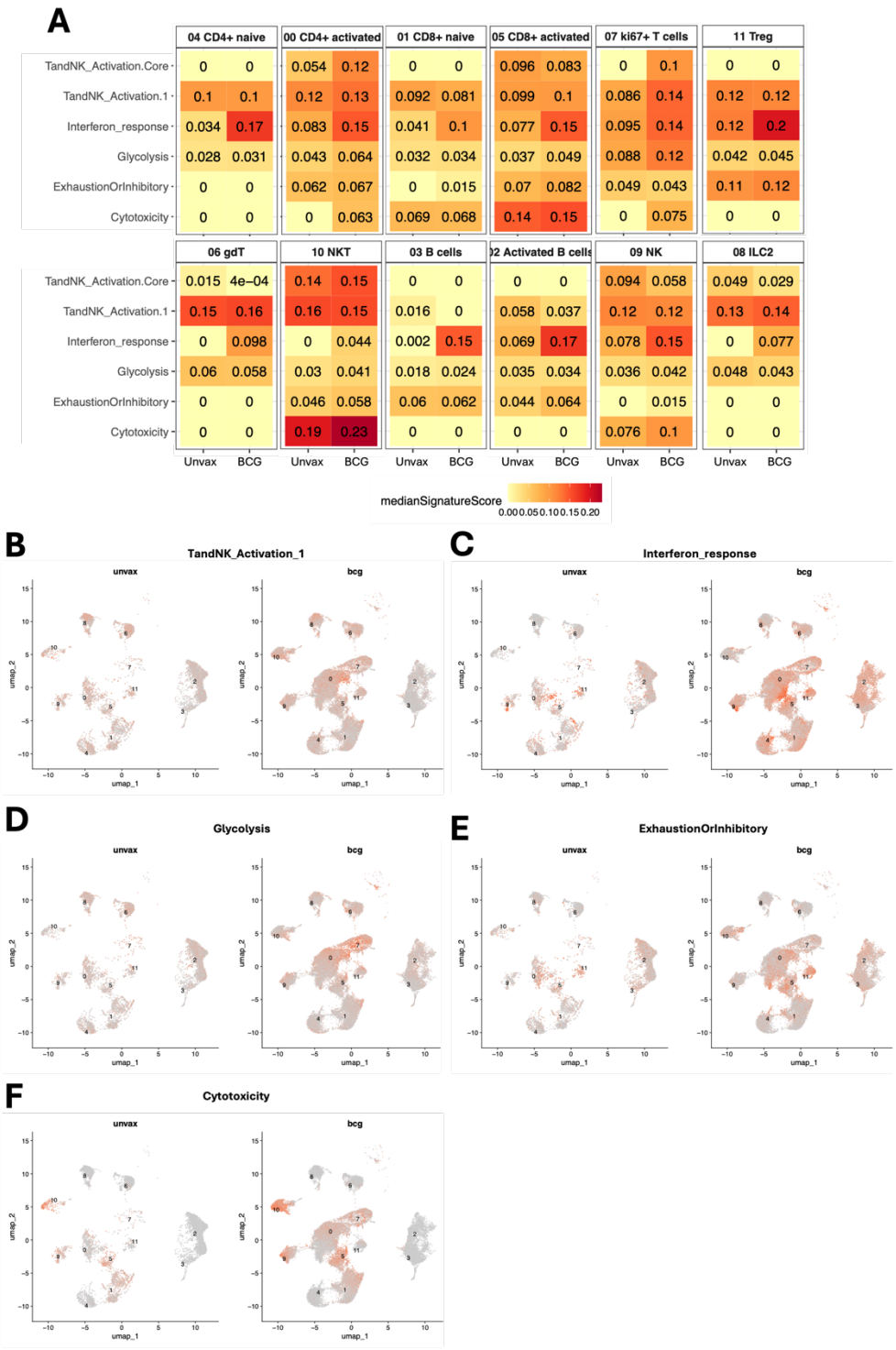

Figure 3. 4. BCG-induced effector gene signatures in lymphocyte clusters early after Mtb infection. A) Heatmap showing mean signature score of unvaccinated versus BCG vaccinated samples for each cell cluster. Heatmap of signature expression visualized on the cellular level for **(B)** T and NK activation, **(C)** interferon response, **(D)** glycolysis, **(E)** exhaustion or inhibitory, or **(F)** cytotoxicity signatures. Signature scores calculated using the R UCell package.

Finally, the pattern of exhaustion or inhibitory signature expression was most predominant in sub-regions of CD4+ activated, CD8+ activated, Treg, Ki67+ T cells, and NKT clusters (**Figure 3.4E**). For the BCG vaccinated CD4+ activated cluster, there seemed to be two different sub-regions with expression of the exhaustion or inhibitory signature. One sub-region overlapped with unvaccinated cells while the other sub-region was in a location that lacked unvaccinated cells. However, the location of the strongest interferon response signature seemed to avoid both exhaustion or inhibitory signature expression sub-regions (**Figure 3.4C and E**). This may suggest that BCG induces activated CD4 T cells with stronger glycolysis and T and NK activation signatures that become exhausted or inhibitory early after Mtb infection. For the CD8+ activated cluster, the sub-region of exhaustion or inhibitory signature expression was different than the sub-region of the cytotoxicity signature expression (**Figure 3.4E and F**). While predominant cytotoxicity expression seemed to be in the sub-region that lacked unvaccinated activated CD8+ cells, the predominant exhaustion or inhibitory expression seemed to be in the sub-region that overlaps in unvaccinated and BCG vaccinated activated CD8+ cells. This may suggest that the BCG-induced, activated CD8 T cells are more cytotoxic with a less exhausted or inhibitory phenotype.

Since activated CD4 T cells, activated CD8 T cells, and B cells were enriched in BCG samples, we further investigated gene expression profiles of these clusters using an unbiased approach by first identifying differentially expressed genes (DEGs) enriched in BCG-vaccinated samples and then determining BCG vaccination-associated enriched pathways for each cluster by quantifying the overlap of DEGs with defined blood transcriptional modules (BTMs) using a hypergeometric test (**Figure 3.5A, 3.6A, and 3.7A**). Overall, the pathways with significant DEG overlap for the activated CD4 cluster and activated CD8 cluster relate to activation and effector function (**Figure 3.5B and 3.6B**). For activated CD4 T cells, the DEGs that overlap with these pathways include IFNg, Il18rap, Il12rb2, Ccr5, Nkg7, and Ctsw (**Figure 3.5C**). For activated CD8 T cells, the DEGs that overlap with these pathways include CD8a, CD3g, Gzmb, Ctsw, and

Stat1, which also suggests BCG-induced cytotoxic function (**Figure 3.6C**). The predominant pathways with significant DEG overlap for the B cell cluster demonstrate B cells responding to IFN in the environment (**Figure 3.7B**). The DEGs that overlap with these pathways include Irf1, Stat1, Ifi213, and Ifi47 (**Figure 3.7C**). However, whether BCG upregulates specific pathways is less clear. Overall, the scRNAseq data suggest that BCG alters the transcriptional profiles of the activated CD4 and activated CD8 clusters to become even more activated and effector-like while inducing the B cell cluster to respond to the inflammatory environment early after Mtb infection.

A

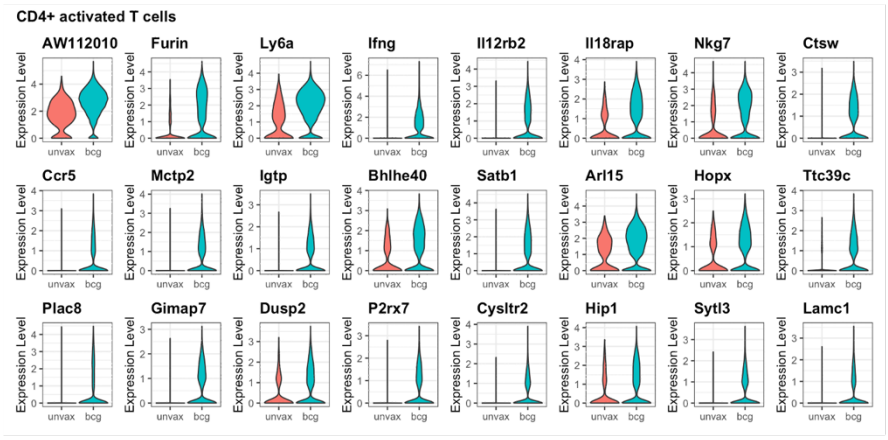

B

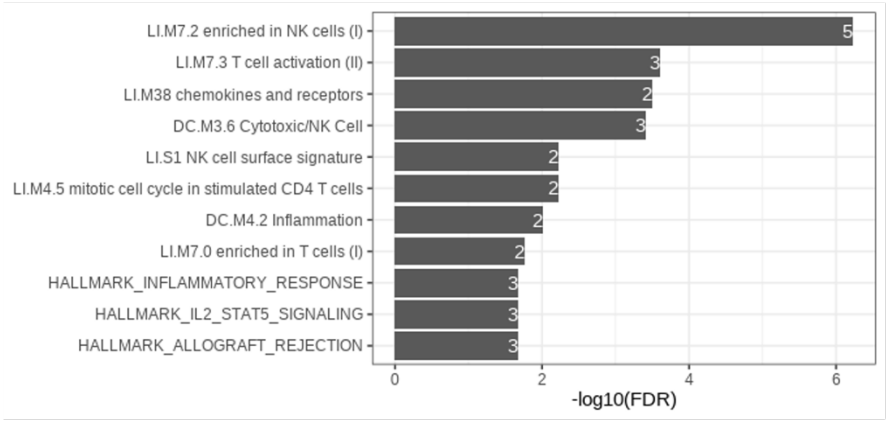

C

gset	genes
HALLMARK_ALLOGRAFT_REJECTION	Ccr5
HALLMARK_ALLOGRAFT_REJECTION	Ifng
HALLMARK_ALLOGRAFT_REJECTION	Il18rap
HALLMARK_IL2_STAT5_SIGNALING	Bhlhe40
HALLMARK_IL2_STAT5_SIGNALING	Furin
HALLMARK_IL2_STAT5_SIGNALING	Gadd45b
HALLMARK_IL2_STAT5_SIGNALING	Hopx
HALLMARK_IL2_STAT5_SIGNALING	Ifitm3
LI.M7.0 enriched in T cells (I)	Gimap7
LI.M7.0 enriched in T cells (I)	Nkg7
LI.M7.2 enriched in NK cells (I)	Hopx
LI.M7.2 enriched in NK cells (I)	Gimap7
LI.M7.2 enriched in NK cells (I)	Ctsw

gset	genes
LI.M7.2 enriched in NK cells (I)	Il18rap
LI.M7.2 enriched in NK cells (I)	Nkg7
LI.M7.3 T cell activation (II)	Ifng
LI.M7.3 T cell activation (II)	Ccr5
LI.M7.3 T cell activation (II)	Nkg7
LI.S1 NK cell surface signature	Il12rb2
LI.S1 NK cell surface signature	Il18rap
DC.M3.6 Cytotoxic/NK Cell	Ifng
DC.M3.6 Cytotoxic/NK Cell	Ctsw
DC.M3.6 Cytotoxic/NK Cell	Nkg7
DC.M4.2 Inflammation	Mctp2
DC.M4.2 Inflammation	Il18rap

Figure 3. 5. BCG induces effector functions in activated CD4 T cell cluster early after Mtb infection. (A) Differentially expressed genes (DEGs) in the activated CD4 T cell cluster enriched in BCG samples. **(B)** Blood transcriptional module (BTM) pathways with significant overlap with DEGs. Significance determined by hypergeometric test. The number on each bar graph indicates the number of DEGs that overlap with the BTM. **(C)** List of DEGs that overlapped with each BTM pathway.

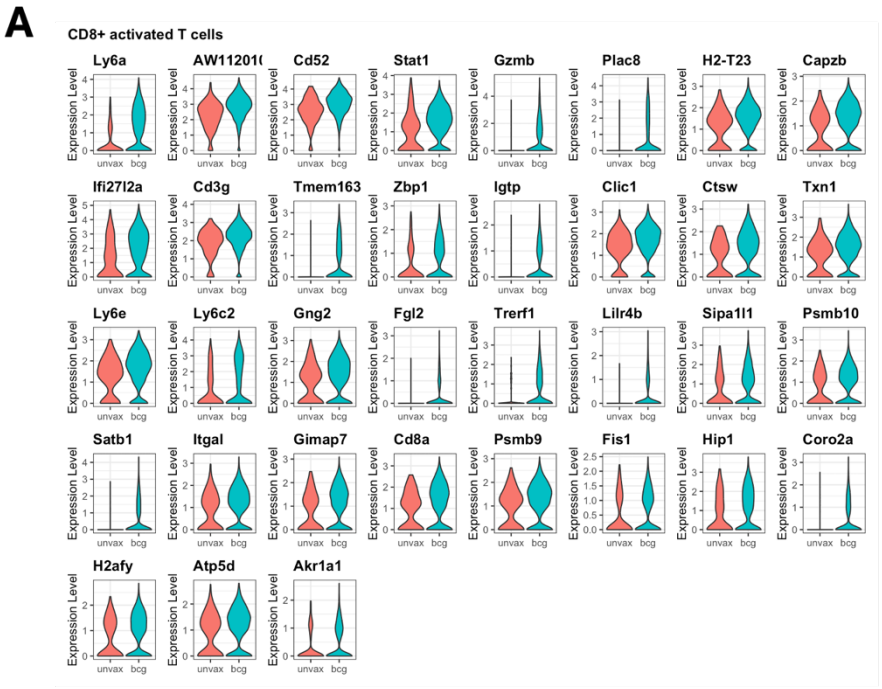

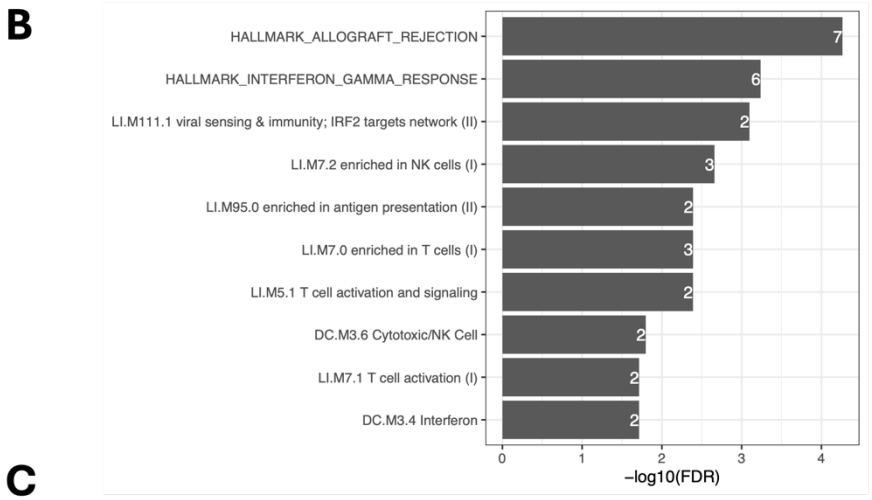

C

gset	genes
HALLMARK_ALLOGRAFT_REJECTION	Cd3g
HALLMARK_ALLOGRAFT_REJECTION	Cd8a
HALLMARK_ALLOGRAFT_REJECTION	Gzmb
HALLMARK_ALLOGRAFT_REJECTION	H2-T23
HALLMARK_ALLOGRAFT_REJECTION	Itgal
HALLMARK_ALLOGRAFT_REJECTION	Psmb10
HALLMARK_ALLOGRAFT_REJECTION	Stat1
HALLMARK_INTERFERON_GAMMA_RESPONSE	Fgl2
HALLMARK_INTERFERON_GAMMA_RESPONSE	Ly6e
HALLMARK_INTERFERON_GAMMA_RESPONSE	Psmb10
HALLMARK_INTERFERON_GAMMA_RESPONSE	Psmb9
HALLMARK_INTERFERON_GAMMA_RESPONSE	Stat1
HALLMARK_INTERFERON_GAMMA_RESPONSE	Zbp1
LI.M5.1 T cell activation and signaling	Cd3g
LI.M5.1 T cell activation and signaling	Cd52

gset	genes
LI.M7.0 enriched in T cells (I)	Gimap7
LI.M7.0 enriched in T cells (I)	Gzmb
LI.M7.0 enriched in T cells (I)	Cd3g
LI.M7.1 T cell activation (I)	Cd8a
LI.M7.1 T cell activation (I)	Cd3g
LI.M7.2 enriched in NK cells (I)	Gimap7
LI.M7.2 enriched in NK cells (I)	Gzmb
LI.M7.2 enriched in NK cells (I)	Ctsw
LI.M95.0 enriched in antigen presentation (II)	Fgl2
LI.M95.0 enriched in antigen presentation (II)	Itgal
LI.M111.1 viral sensing & immunity; IRF2 targets network (II)	Psmb10
LI.M111.1 viral sensing & immunity; IRF2 targets network (II)	Zbp1
DC.M3.4 Interferon	Stat1
DC.M3.4 Interferon	Zbp1
DC.M3.6 Cytotoxic/NK Cell	Cd8a
DC.M3.6 Cytotoxic/NK Cell	Ctsw

Figure 3. 6. BCG induces effector and cytotoxic functions in activated CD8 T cell cluster early after Mtb infection. (A) Differentially expressed genes (DEGs) in the activated CD8 T cell cluster enriched in BCG samples. **(B)** Blood transcriptional module (BTM) pathways with significant overlap with DEGs. Significance determined by hypergeometric test. The number on each bar graph indicates the number of DEGs that overlap with the BTM. **(C)** List of DEGs that overlapped with each BTM pathway.

A

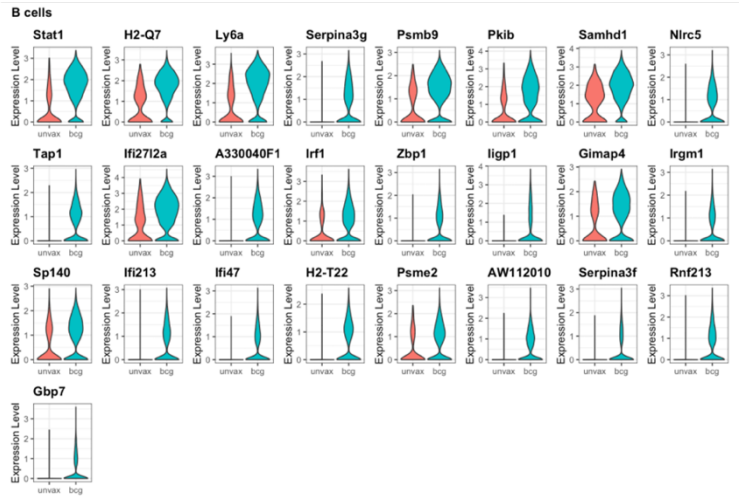

B

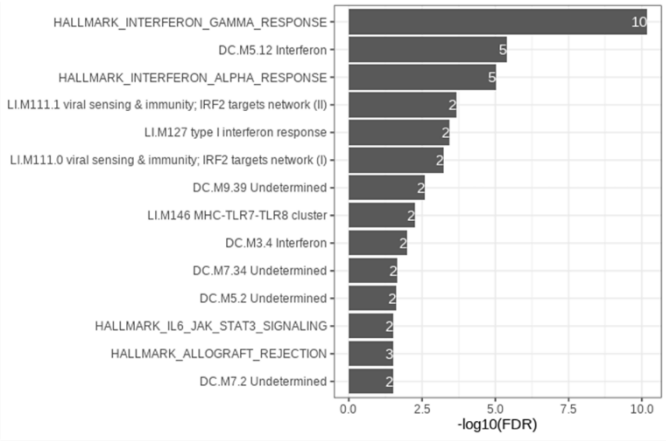

C

gset	genes
HALLMARK_ALLOGRAFT_REJECTION	Gbp2
HALLMARK_ALLOGRAFT_REJECTION	H2-Q7
HALLMARK_ALLOGRAFT_REJECTION	Stat1
HALLMARK_ALLOGRAFT_REJECTION	Tap1
HALLMARK_IL6_JAK_STAT3_SIGNALING	Irf1
HALLMARK_IL6_JAK_STAT3_SIGNALING	Stat1
HALLMARK_IL6_JAK_STAT3_SIGNALING	Stat2
HALLMARK_INTERFERON_ALPHA_RESPONSE	Gbp2
HALLMARK_INTERFERON_ALPHA_RESPONSE	H2-Q7
HALLMARK_INTERFERON_ALPHA_RESPONSE	Irf1
HALLMARK_INTERFERON_ALPHA_RESPONSE	Parp14
HALLMARK_INTERFERON_ALPHA_RESPONSE	Parp9
HALLMARK_INTERFERON_ALPHA_RESPONSE	Psmb9
HALLMARK_INTERFERON_ALPHA_RESPONSE	Psme2
HALLMARK_INTERFERON_ALPHA_RESPONSE	Stat2
HALLMARK_INTERFERON_ALPHA_RESPONSE	Tap1
HALLMARK_INTERFERON_GAMMA_RESPONSE	Gbp4
HALLMARK_INTERFERON_GAMMA_RESPONSE	H2-Q7
HALLMARK_INTERFERON_GAMMA_RESPONSE	Irf1
HALLMARK_INTERFERON_GAMMA_RESPONSE	Nampt
HALLMARK_INTERFERON_GAMMA_RESPONSE	Nlrc5
HALLMARK_INTERFERON_GAMMA_RESPONSE	Parp14
HALLMARK_INTERFERON_GAMMA_RESPONSE	Psmb9
HALLMARK_INTERFERON_GAMMA_RESPONSE	Psme2
HALLMARK_INTERFERON_GAMMA_RESPONSE	Rnf213
HALLMARK_INTERFERON_GAMMA_RESPONSE	Samhd1
HALLMARK_INTERFERON_GAMMA_RESPONSE	Stat1
HALLMARK_INTERFERON_GAMMA_RESPONSE	Stat2
HALLMARK_INTERFERON_GAMMA_RESPONSE	Tap1
HALLMARK_INTERFERON_GAMMA_RESPONSE	Zbp1

gset	genes
LI.M111.0 viral sensing & immunity; IRF2 targets network (I)	Tap1
LI.M111.0 viral sensing & immunity; IRF2 targets network (I)	Zbp1
LI.M111.1 viral sensing & immunity; IRF2 targets network (II)	Tap1
LI.M111.1 viral sensing & immunity; IRF2 targets network (II)	Zbp1
LI.M127 type I interferon response	Stat1
LI.M127 type I interferon response	Tap1
LI.M127 type I interferon response	Parp9
LI.M146 MHC-TLR7-TLR8 cluster	H2-T22
LI.M146 MHC-TLR7-TLR8 cluster	H2-Q7
DC.M3.4 Interferon	Stat1
DC.M3.4 Interferon	Stat2
DC.M3.4 Interferon	Gbp4
DC.M3.4 Interferon	Gbp2
DC.M3.4 Interferon	Gbp6
DC.M3.4 Interferon	Parp14
DC.M3.4 Interferon	Parp9
DC.M3.4 Interferon	Zbp1
DC.M5.2 Undetermined	H2-T22
DC.M5.2 Undetermined	H2-Q7
DC.M5.12 Interferon	Psmb9
DC.M5.12 Interferon	Tap1
DC.M5.12 Interferon	Gbp2
DC.M5.12 Interferon	C130026I21Rik
DC.M5.12 Interferon	Sp140
DC.M5.12 Interferon	Rnf213
DC.M5.12 Interferon	Ifi213
DC.M7.2 Undetermined	H2-T22
DC.M7.2 Undetermined	H2-Q7
DC.M7.34 Undetermined	H2-T22
DC.M7.34 Undetermined	H2-Q7
DC.M9.39 Undetermined	Serpina3f
DC.M9.39 Undetermined	Serpina3g

Figure 3. 7. BCG induces B cells responding to inflammatory environment early after Mtb infection. (A) Differentially expressed genes (DEGs) in the B cell cluster enriched in BCG samples. **(B)** Blood transcriptional module (BTM) pathways with significant overlap with DEGs. Significance determined by hypergeometric test. The number on each bar graph indicates the number of DEGs that overlap with the BTM. **(C)** List of DEGs that overlapped with each BTM pathway.

3.2.3 T cells are required for vaccine-mediated immunity in the ULD model.

Since BCG induces both CD4 and CD8 T cells that are responding early after Mtb infection, it is possible that each cell type may play an important and distinct role in restricting infection. We therefore wanted to determine the relative contributions of CD4 and CD8 T cells in BCG-mediated immunity against Mtb infection, however, we've previously shown that it is difficult to define measures of BCG-mediated protection within the CD model (154). Here, we sought to dissect mechanisms of BCG-mediated immunity to each of the parameters of protection that we previously defined in the ULD model (154). First, we re-examined the roles of T cells by depleting mice of both CD4 and CD8 T cells (co depletion). Unvaccinated or BCG vaccinated B6 mice were injected intraperitoneally (i.p.) with either IgG isotype (Ctrl) or α-CD4 and α-CD8α (α-CD4/8) depleting antibodies weekly, starting day 1 post bar-coded ULD infection and mice were harvested at days 27-30 p.i. (**Figure 3.8A**). Half of the right lung was prepared for flow cytometry to confirm that CD4 and CD8α T cells were successfully depleted in lung tissues at the time of harvest (**Figure S3.16A**). Data were compiled across two independent experiments.

For control of bacterial burden, consistent with our previous findings, BCG non-depleted (control) mice had significantly lower lung bacterial burdens compared to unvaccinated control mice 25.5-fold reduction ($p<0.0001$, excluding those with 0 CFU) (**Figure 3.8B**). In unvaccinated mice, T cell depletion led to increased lung burden compared to control mice (3.5-fold increase, $p = 0.017$). In BCG vaccinated mice, T cell depleted mice had significantly higher lung and spleen bacterial burden compared to BCG control mice (lung: 31-fold increase, $p<0.0001$; spleen: 26.5-fold increase, $p<0.0001$) (**Figure 3.8B and S3.16C**). These data suggest that T cells are required for BCG-mediated control of bacterial burden.

We next determined the role of T cells in preventing dissemination to the contralateral lung (**Figures 3.8C-E**). The mice were ULD-infected with a pool of 50 bar-coded H37Rv Mtb

strains so we could more accurately measure dissemination of unique Mtb strains to both lungs as we previously described (152, 154). We determined the left lung and right lung bacterial burdens separately (**Figure 3.8C**) and amplified and sequenced the Mtb bar-coded strains to quantify the percentage of mice with at least one bilateral Mtb strain and the percentage of all Mtb bar-coded strains detected in each group that were found bilaterally (in both lungs) (**Figure 3.8D-E**). BCG control mice prevented dissemination to the contralateral lung compared to unvaccinated control mice with 73.5% efficacy using percentage mice with at least one bilateral Mtb strain (Unvax Ctrl = 70%, BCG Ctrl = 18.5%, $p<0.01$) and 71% efficacy using percentage of bilateral Mtb bar-coded strains (Unvax Ctrl = 53.3%, BCG Ctrl = 15.4%, $p<0.01$), consistent with our published findings (154). T cell depletion in BCG vaccinated mice reversed this phenotype with 18.5% of BCG control vs 68% BCG depleted mice having bilateral strains ($p = 0.0009$) (Bilateral strains: BCG control = 15.4% vs BCG depleted = 56.25%, $p = 0.0002$) and resulted in dissemination similar to the unvaccinated depleted mice, which had 71.4% of mice with bilateral strains ($p = 0.94$) (Bilateral strains: BCG depleted = 56.25% vs unvax depleted = 47.5%, $p = 0.55$) (**Figure 3.8D-E**). This was highly consistent between both independent experiments and there were similar trends when looking at the percent of mice with dissemination to the spleen (**Figure S3.16B and D**). Together, this suggests that T cells are required for BCG-mediated prevention of dissemination.

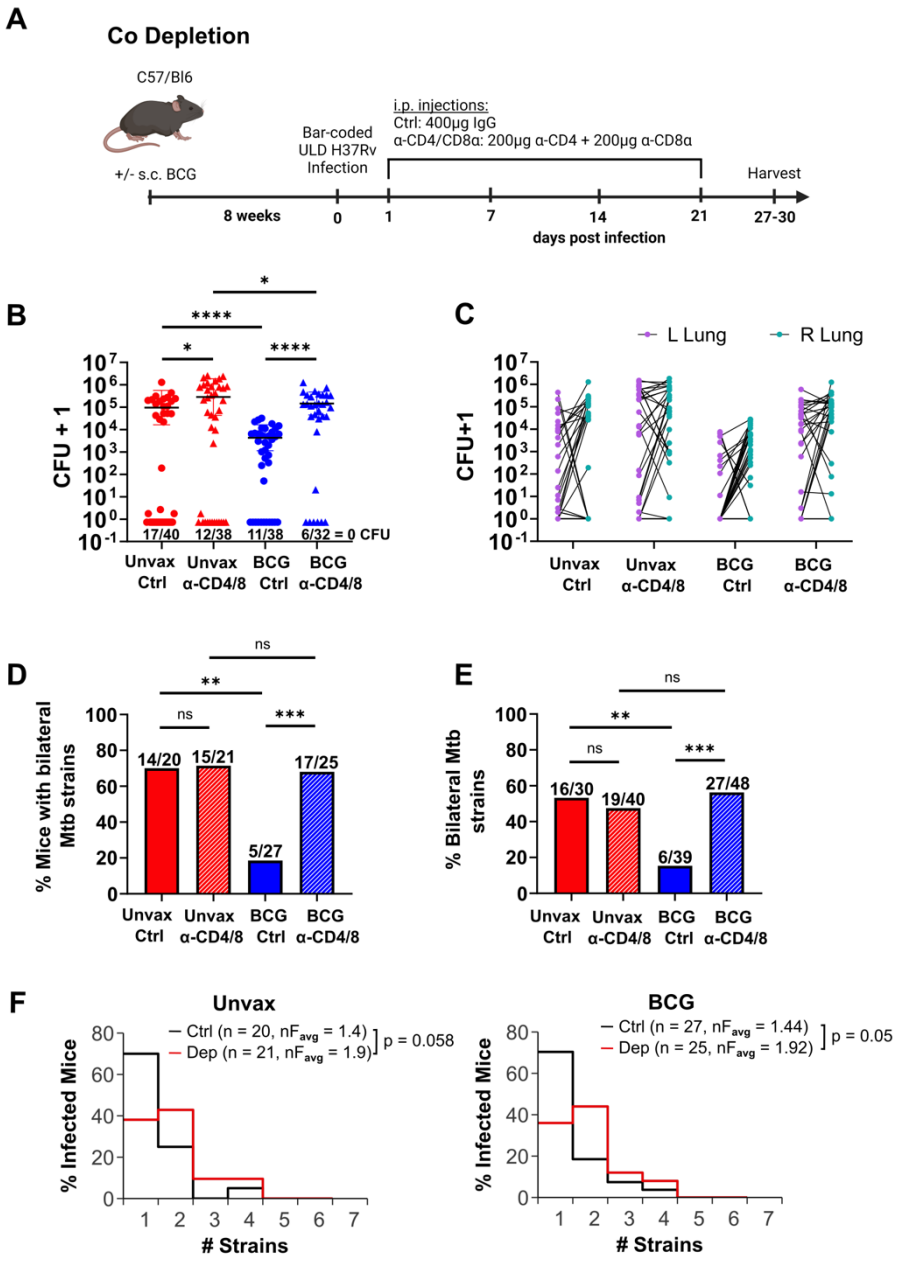

Figure 3. 8. T cells are required for all metrics of protection in the ULD model. (A) Schematic of experimental timeline. C57Bl/6 (B6) mice were infected with ULD (1-3 CFU) of bar-coded H37Rv Mtb 8 weeks post vaccination with s.c. 10^6 BCG-Aeras Pasteur or no vaccination. Mice were injected i.p. with 400µg IgG or 200µg anti-CD4 and 200µg anti-CD8a antibody on days 1, 7, 14, and 21 post-infection (p.i.). At days 27-31p.i. half of the right lung was prepared for flow cytometry and the other half of the right lung and whole left lung and spleen were plated for CFU. Genomic DNA was extracted and sequenced from bacterial colonies of infected mice. **(B)** Combined lung CFU of unvaccinated (red) and BCG vaccinated (blue) mice that were non-depleted (circles) or CD4 and CD8 T cell depleted (triangles) are graphed with mean +/- SD. Proportions of mice with undetectable CFU are shown above the X axis. Significance was analyzed on log-transformed values excluding mice with 0 CFU by Mann-Whitney test on GraphPad Prism 9. ****p<0.0001 **(C)** Left versus right lung CFU. **(D)** Proportion of mice with at least one bilateral Mtb strain and **(E)** Proportion of bilateral strains. Vaccine efficacy for preventing dissemination to the contralateral lung was calculated as 1-(% BCG)/(% Unimmunized). Significance was determined by chi-square test on GraphPad Prism 9. *p<0.05, **p<0.01. **(G)** Distribution curves of infection. n = number of mice, nF$_{avg}$ = average number of bar-coded strains per mouse. Significance determined by likelihood ratio test. Data are compiled across two independent experiments.

Lastly, we sought to determine the role of T cells in preventing infection. Shown in **Figure 3.8B**, the BCG T cell depleted group had the fewest mice with 0 CFU (6/32 = 0 CFU) compared to the other groups, however, this was not statistically significant compared to the BCG control group (11/38 = 0 CFU) in these two compiled experiments (**Figure 3.8B and Figure S3.16E**). Our previous work demonstrated that BCG only has 13% efficacy in preventing detectable infection when looking at 31 experiments that include over 500 mice per group (154). Thus, we are underpowered in these CD4 and CD8 depletion studies to assess prevention of detectable infection in individual ULD experiments at the whole mouse level, and therefore sought to use the bar-coded strains to measure prevention of infection at the individual strain level. We grouped the mice by the number of founding Mtb strains to create distribution curves of infection. As expected, most infected mice from the control groups were infected with one strain of Mtb and fewer mice were infected with two or more strains (**Figure 3.8F**), consistent with our Poisson distribution of the ULD model previously described (154). For unvaccinated mice, the T cell depleted distribution curve trended towards more Mtb strains with a higher average number of founding strains (nF_{avg}) of 1.9 compared to the control curve which had nF_{avg} of 1.4 ($p = 0.058$). For BCG vaccinated mice, T cell depletion significantly shifted the distribution curve towards more Mtb strains, and the nF_{avg} increased from 1.44 in control mice to 1.92 in the T cell depleted mice ($p = 0.05$) (**Figure 3.8F and S3.16F**). This suggests that T cells are important in preventing infection of Mtb strains particularly in BCG vaccinated mice. Taken together, our data demonstrate the crucial role of T cells in Mtb immunity and vaccine-mediated immunity.

3.2.4 B cells are not required for vaccine-mediated immunity in the ULD model.

We next assessed the role of B cells in vaccine-mediated immunity. Because of a lack of established B cell antibody depletion methods in B6 mice, we decided to use $\mu MT^{-/-}$ mice

deficient in B cells, consistent with previous studies (105, 106). Unvaccinated or BCG vaccinated wild-type C57/Bl6 (WT) or $\mu MT^{-/-}$ mice were infected with bar-coded ULD H37Rv and were harvested between days 35-37 p.i. (**Figure 3.9A**). Data were compiled across two independent experiments. B cells were not required for control of lung burden (**Figure 3.9B**). B cells also did not contribute toward preventing dissemination to the contralateral lung or spleen (**Figure 3.9C-E**). Lastly, B cells were not required for preventing infection of Mtb strains (**Figure 3.9F**). Overall, B cells were not required for any of these three metrics of vaccine-mediated protection that can be measured in the ULD model.

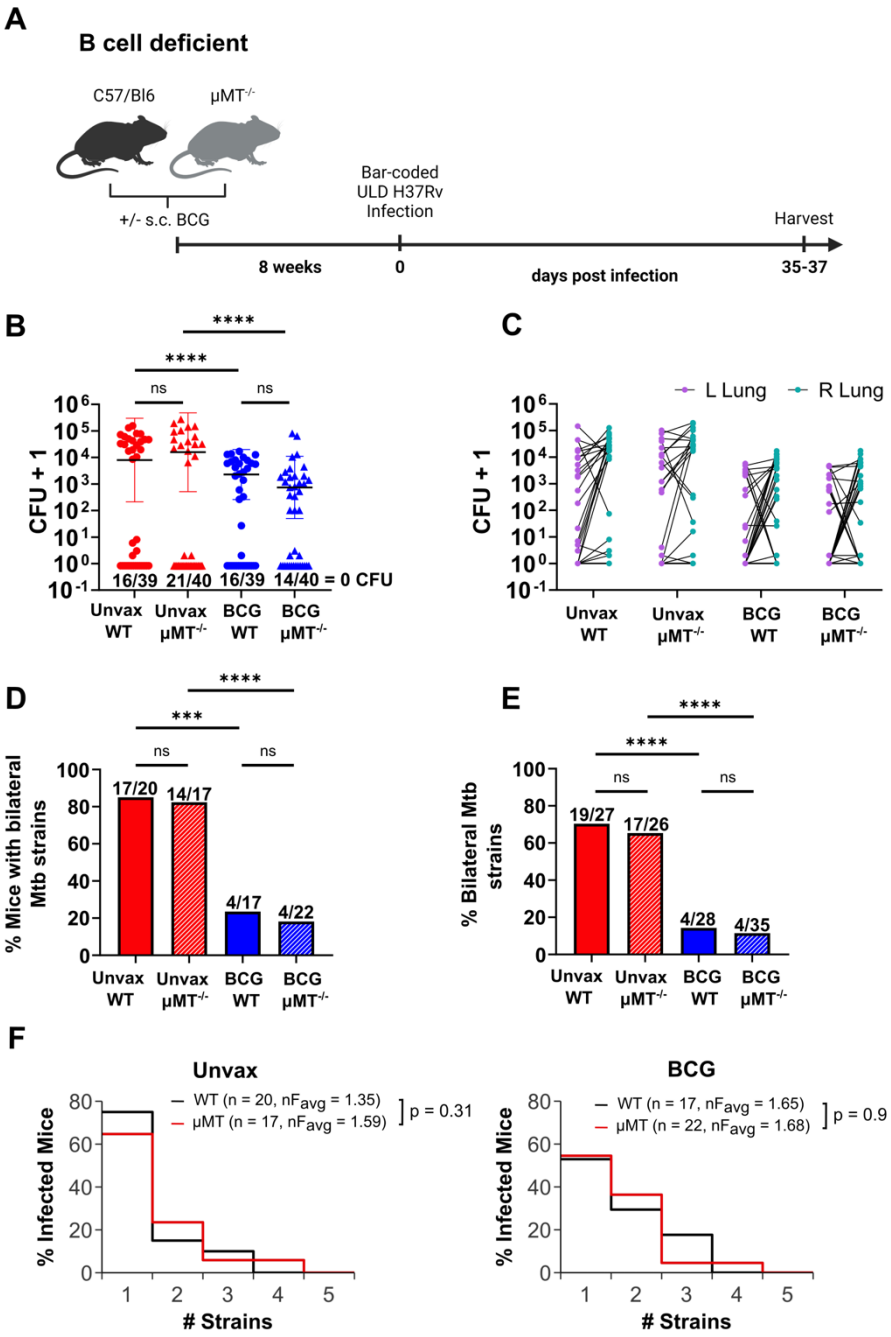

Figure 3. 9. B cells are not required for any metric of protection in the ULD model. (A) Schematic of experimental timeline. C57Bl/6 wild-type (WT) or μMT$^{-/-}$ B cell deficient mice were infected with ULD bar-coded H37Rv Mtb 8 weeks post BCG vaccination or no vaccination. At days 35-37p.i. half of the right lung was prepared for flow cytometry and the other half of the right lung and whole left lung and spleen were plated for CFU. Genomic DNA was extracted and sequenced from bacterial colonies of infected mice. **(B)** Combined lung CFU of unvaccinated (red) and BCG vaccinated (blue) mice that were WT (circles) or μMT$^{-/-}$ (triangles) are graphed with mean +/- SD. Significance was analyzed on log-transformed values excluding mice with 0 CFU by Mann-Whitney test on GraphPad Prism 9. ns = not significant, ****p<0.0001. **(C)** Left versus right lung CFU. **(D)** Proportion of mice with at least one bilateral Mtb strain and **(E)** proportion of bilateral strains. Significance was determined by chi-square test on GraphPad Prism 9. **(F)** Distribution curves of infection. nF_{avg} = average number of bar-coded strains per mouse. Significance determined by likelihood ratio test. Data are compiled across two independent experiments.

3.2.5 Transfer of Mtb-specific CD4 T cells is sufficient for control of lung burden.

Our results so far have been consistent with conventional dose murine studies that T cells are required, and B cells are not required for immunity against Mtb (37, 38, 105, 106). The T cell depletion studies in CD-infected mice also demonstrated that it was CD4 T cells and not CD8 T cells that were important for survival (38). We therefore wanted to determine if CD4 T cells were sufficient for the protection in the ULD model (**Figure 3.8**) regardless of vaccination status. To test this possibility, we adoptively transferred transgenic Mtb ESAT-6-specific CD4 T cells (C7) or OVA-specific CD4 T cells (OTII) into ULD-infected recipient mice (5×10^6 cells intravenously) at day 10 and day 19 p.i. Recipient mice, or no transfer (NT) controls were harvested at day 28p.i. and assessed for bacterial burdens (**Figure 3.10A**). ESAT-6-specific Th1 CD4 T cells were sufficient for controlling lung bacterial burden and reduced lung burden by 22-fold ($p = 0.0001$) while OVA-specific Th1 CD4 T cells were not sufficient for controlling lung burden and only reduced lung burden by 1.4-fold ($p = 0.33$) (**Figure 3.10B**). OVA-specific and ESAT-6-specific T cells trended towards reducing the proportion of mice with bilateral Mtb strains and the proportion of bilateral Mtb strains compared to the no transfer control group, but these differences did not reach statistical significance (NT vs OTII: $p = 0.475$; NT vs C7: $p = 0.213$) (**Figure 3.10C-E**). Finally, the nF_{avg} was not significantly different for any group with this sample size (NT $nF_{avg} = 1.23$, OTII $nF_{avg} = 1.56$, C7 $nF_{avg} = 1.44$) (**Figure 3.10F**). We repeated this experiment twice with adoptive transfer of 1 million CD4 T cells (instead of 5 million) and obtained similar findings. These data suggest that Mtb-specific Th1 cells, but not Th1 cells with an irrelevant specificity, are sufficient for controlling lung burden even without BCG vaccination but are not sufficient for prevention of dissemination or prevention of infection, at least using the number of T cells we transferred.

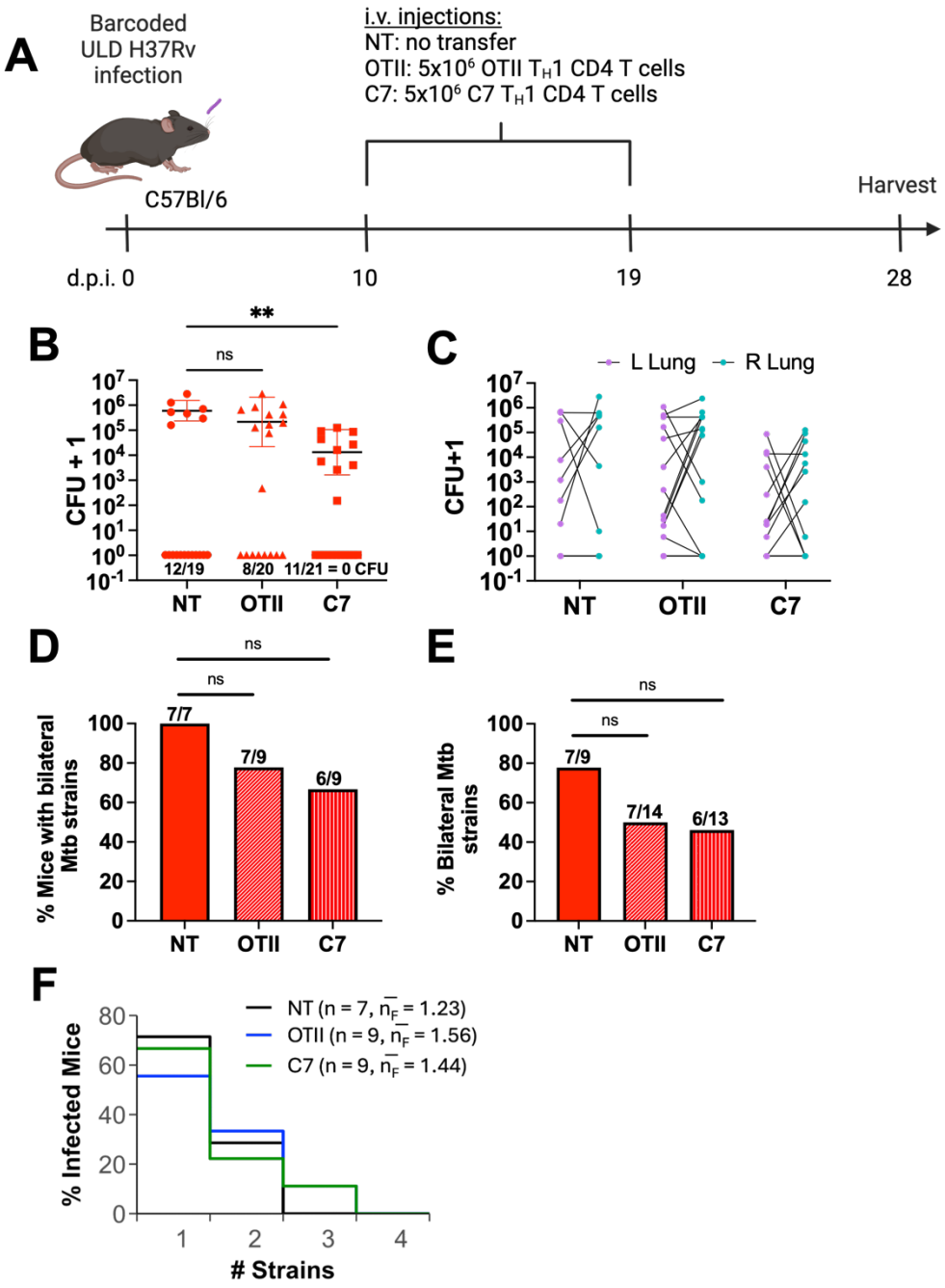

Figure 3. 10. Mtb-specific CD4 T cells are sufficient for controlling bacterial burden but may not be sufficient for prevention of dissemination or prevention of infection. (A) Schematic of adoptive transfer experimental timeline. B6 mice were infected with bar-coded ULD H27Rv and were injected intravenously (i.v.) with 5 million OTII-specific Th1 CD4 T cells, C7-specific Th1 CD4 T cells, or nothing at days 10 and 19 p.i. At day 28 p.i. lungs were plated for CFU and gDNA was extracted and sequenced from bacterial colonies of infected mice. (**B)** Combined lung CFU of mice with no transfer (NT) (circles), OTII-transfer (OTII) (triangles), or C7-transfer (C7) (squares) are graphed with mean +/- SD. Significance was analyzed on log-transformed values excluding mice with 0 CFU by Mann-Whitney test on GraphPad Prism 9. ns = not significant, **p<0.01. **(C)** Left versus right lung CFU. **(D)** Proportion of mice with at least one bilateral Mtb strain and **(E)** proportion of bilateral strains. Significance was determined by chi-square test on GraphPad Prism 9. **(F)** Distribution curves of infection. nF_{avg} = average number of bar-coded strains per mouse. Data shown are from one independent experiment.

3.2.6 CD4 T cells play larger role than CD8 T cells in BCG-mediated control of lung bacterial burden.

Our findings that T cells are required for vaccine-mediated immunity in the ULD model (**Figure 3.8**) but that CD4 T cells may not be sufficient for all parameters of protection (**Figure 3.10**), led us to further dissect the relative roles of CD4 T cells and CD8 T cells in vaccine-mediated immunity with CD4 or CD8 single depletion experiments. Unvaccinated or BCG vaccinated B6 mice were infected with bar-coded ULD Mtb and injected i.p. with IgG isotype (Ctrl) or either α-CD4 or α-CD8α weekly, starting D1p.i. and were harvested approximately after 4 weeks (CD8 depletion) or 5 weeks (CD4 depletion) post infection (**Figure 3.11A**). We confirmed appropriate CD4 or CD8 T cell depletion in the lung tissue (**Figure S3.17A and C**). Depletion of CD4 T cells did not deplete effector $CD62L^{-}$ $CD44^{hi}$ CD8 T cells (**Figure S3.17B**). Depletion of CD8α T cells did not deplete effector $CD62L^{-}$ $CD44^{hi}$ CD4 T cells or CD8α+ conventional dendritic cells (**Figure S3.17D-F**). Data in **Figure 3.11-3.13** were compiled across 3 (CD4 depletion) or 4 (CD8 depletion) independent experiments.

CD4 T cells contributed to the control of lung burden regardless of vaccination status, as CD4 depletion increased lung burden 5.5-fold in unvaccinated mice ($p<0.0001$) and 18-fold in BCG vaccinated mice ($p<0.0001$) (**Figure 3.11B**). However, unvaccinated CD4 depleted mice still had 4.75-fold increase in lung burden compared to the BCG CD4 depleted group ($p<0.0001$), suggesting that other factors could be involved in control of lung burden (**Figure 3.11B**). Unvaccinated CD8 depleted mice had a 1.37-fold decrease in lung burden compared to unvaccinated control mice ($p = 0.488$), suggesting that CD8 T cells were not required for control of lung burden in unvaccinated mice (**Figure 3.11C**). BCG CD8 depleted mice had a modest but significant 2.4-fold increase ($p = 0.0025$) in lung burden compared to BCG control mice, suggesting that CD8 T cells contribute towards control of lung burden in BCG vaccinated mice, although to a lesser extent than CD4 T cells (**Figure 3.11C**). Overall, CD4 T cells play the

largest role in controlling lung burden regardless of vaccination status while CD8 T cells also play a minor but still significant role in BCG-mediated control of lung burden.

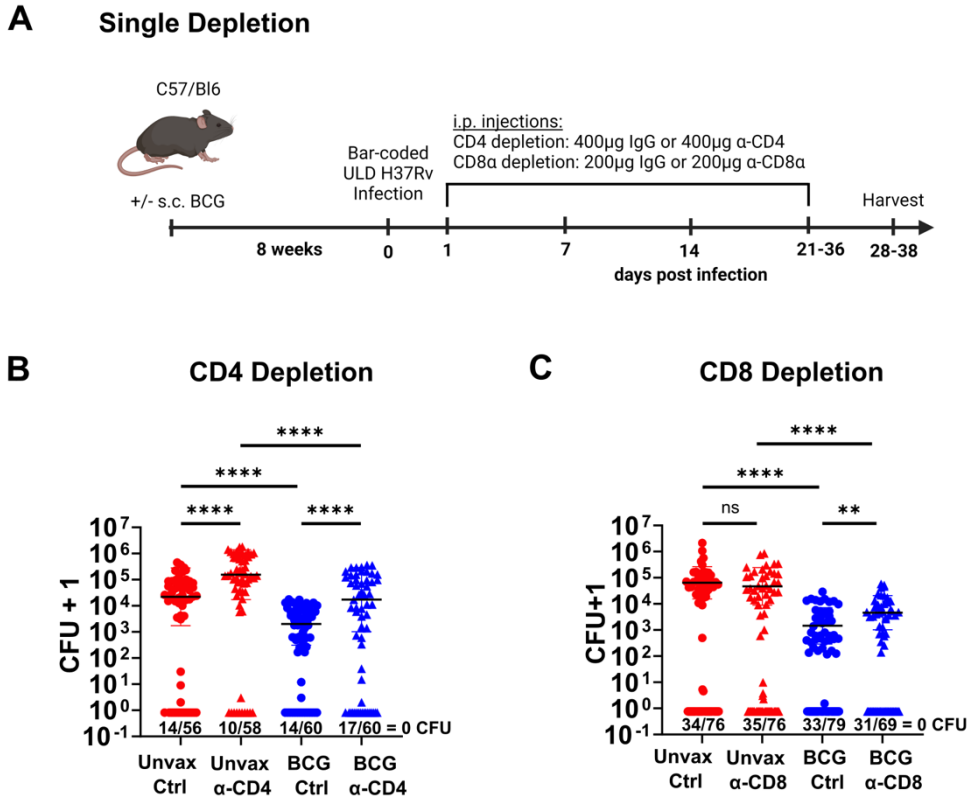

Figure 3. 11. CD4 T cells play a larger role than CD8 T cells in control of bacterial burden. (A) Schematic of CD4 and CD8 T cell single depletion experiments. C57/BL6 mice were infected with ULD bar-coded H37Rv Mtb 8 weeks post BCG vaccination or no vaccination. CD4 depletion: mice were injected i.p. with 400µg IgG or 400µg anti-CD4 antibody on days 1,7, 14, 21, 28p.i. and the day before harvest, and mice were harvested between day 35-38p.i. (3 independent experiments). CD8 depletion: mice were injected i.p. with 200µg IgG or 200µg anti-CD8a antibody on days 1, 7, 14, and 21p.i. and were harvested between day 28-38p.i. (4 independent experiments). At the time of harvest, half of the right lung was prepared for flow cytometry and the other half of the right lung and whole left lung and spleen were plated for CFU. Genomic DNA was extracted and sequenced from bacterial colonies of infected mice. Data are compiled across 3 (CD4) or 4 (CD8) independent experiments. Combined lung CFU with mean +/- SD of unvaccinated (red) or BCG vaccinated (blue) mice that were non-depleted (circles) or depleted (triangles) of CD4 T cells **(B)** and CD8 T cells **(C)**. Significance was analyzed on log-transformed values excluding mice with 0 CFU by Mann-Whitney test on GraphPad Prism 9. **p<0.01, ****p<0.0001.

3.2.7 CD4 T cells play the predominant role in BCG-mediated prevention of dissemination to the contralateral lung.

Next, we combined CFU and bar-coded sequencing data to determine the relative roles of CD4 and CD8 T cells in prevention of dissemination. CD4 T cells played a major role in preventing BCG-mediated dissemination to the contralateral lung as the BCG CD4 depleted

group had 60% of mice with bilateral Mtb strains compared to 19% of the BCG control mice ($p = 0.0005$) and 45% of bilateral strains compared to 11.4% of the BCG control group ($p<0.0001$) (**Figure 3.12A-C, Figure S3.18A**). CD8 T cells did not play a significant role in BCG-mediated prevention of dissemination to the contralateral lung (Bilateral mice: BCG control = 19% vs BCG CD8 depleted = 25.7%, $p = 0.67$; Bilateral strains: BCG control = 13.3% vs BCG CD8 depleted = 19.1%, $p = 0.52$) but this varied by experiment (**Figure 3.12D-F, Figure S3.148D**). However, the BCG CD4 depleted group had significantly less dissemination than the unvaccinated CD4 depleted group (Bilateral mice: BCG CD4 depleted = 60% vs Unvax CD4 depleted = 85%, $p = 0.0189$; Bilateral strains: BCG CD4 depleted = 45.1% vs Unvax CD4 depleted = 68.4%, $p = 0.0049$), and there was no significant difference in dissemination between unvaccinated or BCG vaccinated mice depleted of all T cells, suggesting that CD8 T cells could play a minor role in preventing dissemination to the contralateral lung (**Figure 3.12A-C and Figure 3.8C-E**).

We also measured prevention of dissemination to the spleen by comparing overall spleen CFU and looking at the percent of mice with CFU in the spleen (**Figure S3.18B-C and E-F**). CD4 T cells contributed towards controlling spleen burden regardless of vaccination status (Unvaccinated control vs depleted: 11.7-fold increase, $p<0.0001$; BCG vaccinated control vs depleted: 62.7-fold increase, $p<0.0001$) (**Figure S3.18B**). BCG CD4 depleted mice trended towards having increased dissemination to the spleen compared to BCG control mice that was consistent in all experiments but wasn't statistically significant when compiled (BCG Control: 74% vs BCG CD4 depleted: 88% of mice with dissemination to spleen, $p = 0.108$) (**Figure S3.18C**). CD8 T cells did not contribute towards controlling spleen burden (Unvaccinated control vs depleted: 2.08-fold increase, $p = 0.717$; BCG vaccinated control vs depleted: 1.01-fold increase, $p = 0.372$) but BCG CD4 depleted mice did trend towards increased dissemination to the spleen compared to BCG control mice (BCG Control: 56.5% vs BCG CD4 depleted: 76% of mice with dissemination to spleen, $p = 0.095$), an observation consistent in 2 out of 4

experiments (**Figure S3.18E-F**). Together, this data supports a major role for CD4 T cells in prevention of dissemination with a minor to no role of CD8 T cells.

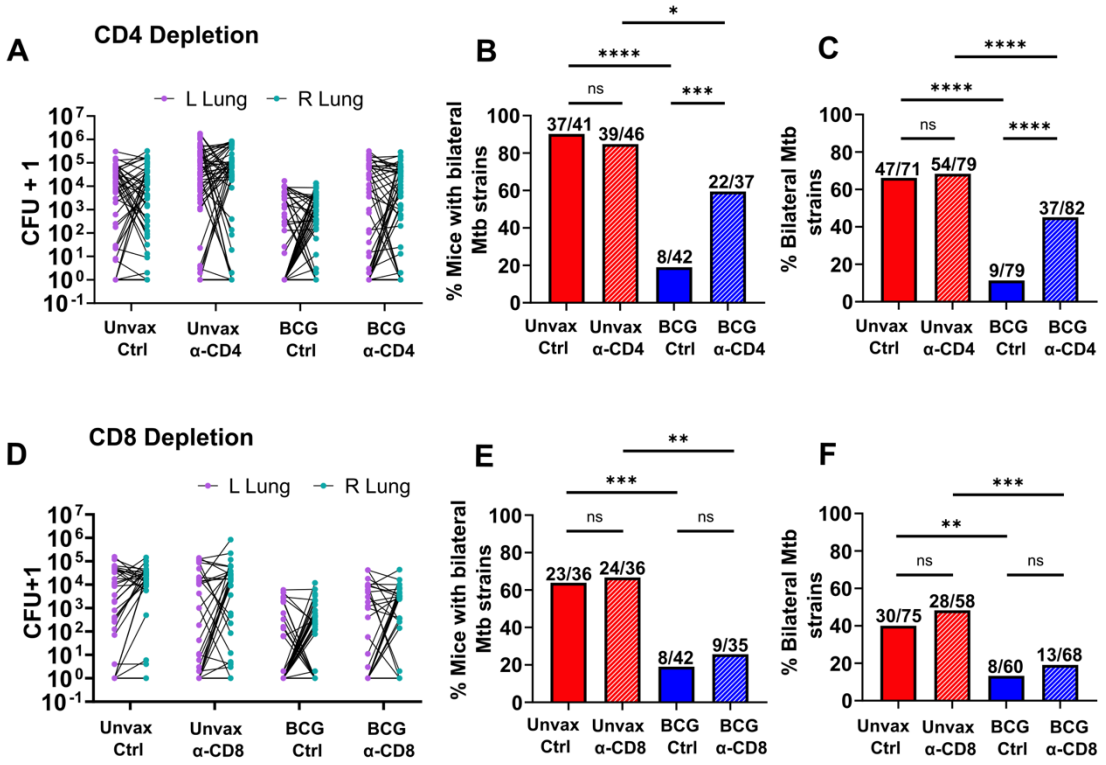

Figure 3. 12. CD4 T cells play a larger role than CD8 T cells in BCG-mediated prevention of dissemination to the contralateral lung. Left versus right lung CFU for **(A)** CD4 depletion and **(D)** CD8 depletion. Proportion of mice with bilateral Mtb strains for **(B)** CD4 depletion and **(E)** CD8 depletion. Proportion of bilateral Mtb strains for **(C)** CD4 depletion and **(F)** CD8 depletion. Data are compiled across 3 **(A-C)** or 4 **(D-F)** independent experiments and were analyzed using Chi-square test on GraphPad Prism 9. ***p<0.001, ***p<0.0001.

3.2.8 CD8 T cells play larger role than CD4 T cells in BCG-mediated prevention of detectable infection.

Finally, we investigated the relative roles of CD4 and CD8 T cells in prevention of infection. When we compared the percentage of infected mice across each group, there were no significant differences in the proportion of mice infected in each group, which as expected, indicates that these depletion experiments were not powered sufficiently to measure prevention of infection in this manner (**Figure S3.19A and C**). The estimated infectious dose varied by experiment, and as a result, CD8-depleted mice had fewer infected mice across all groups

compared to CD4 depleted mice (**Figure S3.19A and C**). We therefore again used the bar-coded strains to measure prevention of infection at the individual strain level (**Figure 3.13**).

For CD4 depletion, the unvaccinated CD4 depleted mice had a slightly lower nF_{avg} of 1.72 compared to the control group which had a nF_{avg} of 1.82 but there was no statistically significant difference in number of founders ($p = 0.9$) (**Figure 3.13A and S3.19B**). For BCG vaccinated mice, the BCG CD4 depleted curve trended towards more infection with a nF_{avg} of 2.22 compared to a nF_{avg} of 1.76 in BCG control mice, however, again there was no statistically significant difference in number of founders between groups ($p = 0.24$). For CD8 depletion, the unvaccinated CD8 depleted mice had a lower nF_{avg} of 1.61 compared to a nF_{avg} of 2.14 for the unvaccinated control group and had a significantly lower number of founders than the control group ($p = 0.02$) (**Figure 3.13B and S3.19D**). Surprisingly, for the BCG vaccinated mice, the BCG CD8 depletion curve shifted towards more infection with an increase in nF_{avg} of 1.41 for BCG control mice to a nF_{avg} of 2.0 for BCG CD8 depleted mice. There was also a statistically significant increase in number of founders than the control group ($p = 0.005$) (**Figure 3.13B and S3.19D**). This suggests that CD8 T cells play a major role in prevention of infection while CD4 T cells play a more minor role. The impact of CD8 T cells on prevention of infection only occurs in BCG vaccinated mice, suggesting that BCG may induce a subset of CD8 T cells capable of controlling bacterial burden. Our results from **Figures 3.1-3.7** may suggest that these BCG induced CD8 T cells could be an activated, proliferative, antigen-specific, and/or cytotoxic subset.

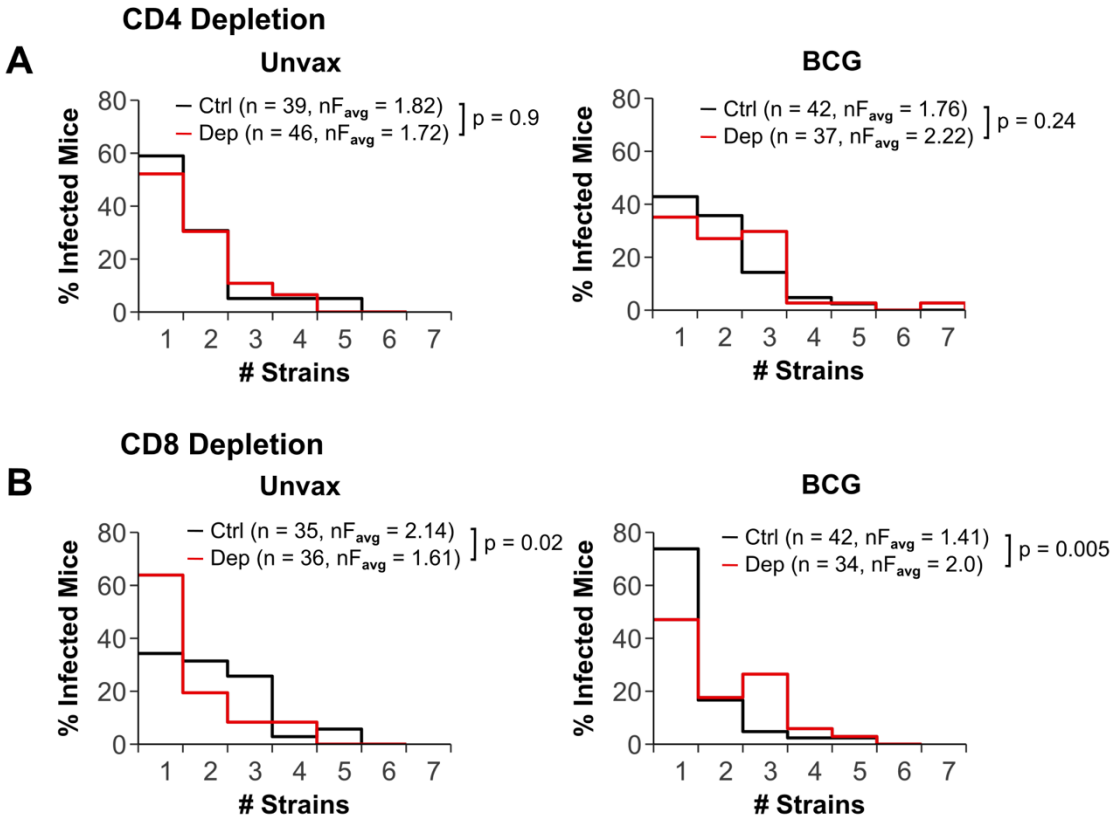

Figure 3. 13. CD8 T cells play a larger role than CD4 T cells in BCG-mediated prevention of infection. Distribution curves of infection for **(A)** CD4 depletion and **(B)** CD8 depletion. Data are compiled across 3 **(A)** or 4 independent experiments **(B)**. nF_{avg} = average number of bar-coded strains per mouse. Significance determined by likelihood ratio test.

We were surprised to determine any role for CD8 T cells in BCG-mediated immunity because CD8 T cells do not play a significant role in BCG-mediated control of lung burden in the CD model (190, 191). Because the prior literature used earlier timepoints than in our experiments, we performed parallel CD8 depletion experiments (n = 2) in CD Mtb-infected mice. We found no significant difference in lung burden for unvaccinated or BCG vaccinated mice depleted of CD8 T cells (p = 0.9 for unvaccinated control vs depleted, p = 0.6 for BCG vaccinated control vs depleted) (**Figure S3.19E**). The ULD model is therefore important to use for investigating mechanisms of vaccine-mediated protection, as the role of CD8 T cells in vaccine-mediated protective immunity was masked by using an artificially high infectious dose.

3.3 Discussion

In this study, we investigated mechanisms of vaccine-induced protection against Mtb infection. We first examined BCG-induced adaptive immune responses to early Mtb infection and found that BCG vaccination increased the number of antigen-specific CD4 T cells and CD8 T cells in the lung tissue. This is consistent with prior work from our lab that found an increase in Ag85B-specific CD4 T cells and TB10.4-specific CD8 T cells in BCG vaccination as early as day 10p.i. (134). Notably, while studies have investigated vaccine-induced T cell responses pre-challenge, few studies investigate BCG-induced T cells responding after Mtb infection. One study used Mtb whole-cell lysate to stimulate lung and spleen cells from BCG vaccinated mice to look at BCG-induced T cell responses to Mtb *in vitro* (192). Other studies have compared T cell responses of unvaccinated versus BCG vaccinated mice but only at timepoints after divergence in lung bacterial burdens (46, 193). Therefore, to our knowledge, the work in our lab is the first to examine BCG-induced T cells responding early after Mtb infection, which could be more useful in determining which vaccine-induced responses are relevant to protection.

We extended our previously published work to further characterize BCG-induced T cells after Mtb infection. The confocal microscopy images suggested that BCG induces an influx of both CD4 and CD8 T cells into the lesion compared to lesions from unvaccinated mice. The flow cytometry and scRNAseq data suggested that these T cells are activated and proliferative. This is consistent with our previously published confocal microscopy work, where we used phospho-S6 (pS6) as a marker of recent T cell activation via TCR engagement to determine that BCG induces more pS6+ CD4 T cells in the lung tissue early after Mtb infection compared to unvaccinated mice, however, the pS6+ CD4 T cells were located distal to the site of Mtb infection (134). Here, we focused on both CD4 and CD8 T cell responses and used IRF4 as a marker for recent antigen sensing. IRF4 is upregulated more slowly than pS6, however its expression is linked to the strength and duration of antigenic signals and remains high in

responding T cells (194). To our knowledge, our confocal microscopy images are the first to show IRF4+ T cells only in lesions of BCG vaccinated mice and not unvaccinated mice. We observed many IRF4+ CD4 T cells in the lesion, consistent with the BCG-induced pS6+ CD4 T cells previously published (134), however, their distance to Mtb infected cells still need to be quantified.

Given the role of CD8 T cells in BCG-mediated prevention of infection, we were surprised that only a few IRF4+ CD8 T cells could be detected. Whether there is an increase in BCG-induced IRF4+ CD8 T cells in a different location of the tissue distal to the lesion or at a different timepoint post-infection remains to be determined. Our flow cytometry data also suggests that BCG induces more Ki67+ CD8 T cells than unvaccinated mice. The discrepancy of IRF4+ versus Ki67+ CD8 T cells might have to do with the kinetics of BCG induced CD8 T cell activation and proliferation at this timepoint. It is also possible that the large number of Ki67+ CD8 T cells but small number of IRF4+ CD8 T cells reflects bystander CD8 T cell activation independent of TCR signaling. Alternatively, perhaps the rare BCG-induced IRF4+ CD8 T cells are sufficient for mediating protection, or the protective effect is not dependent on antigen sensing. Further quantitative analysis is needed to measure these differences and compare with pS6+ CD8 T cell expression to get a fuller picture of BCG-induced CD4 and CD8 T cell antigen sensing and activation.

The scRNAseq data further demonstrated that BCG-induced effector CD4 and CD8 T cells are also transcriptionally distinct. The distribution of cells among the lymphocyte clusters suggested that BCG could induce unique populations of CD4 T cells and CD8 T cells not present in unvaccinated mice. Our results analyzing functional signatures of the cell clusters showed that BCG increases glycolysis signatures in specific sub-regions of the activated CD4 and activated CD8 clusters. A metabolic shift towards glycolysis is important for activation, proliferation, and differentiation of both CD4 and CD8 T cells and increased glycolysis is important for boosting effector functions such as IFNγ- production and cytotoxicity as well as

differentiation of T cells (195, 196). There is also some evidence that BCG can induce glycolysis in T cells. A study in patients with type 1 diabetes showed that BCG treatment induces a metabolic switch towards aerobic glycolysis, and a follow-up study showed that BCG is associated with increased transcription of genes affecting glycolysis pathways in CD4 T cells (197, 198). Here, it is possible that BCG induces a metabolic shift towards increased glycolysis in a subset of CD4 T cells early after Mtb infection. The specific sub-regions where BCG increased the glycolysis signatures also overlaps with increased T and NK activation signature for both activated CD4 and activated CD8 clusters. This suggests that these cells could indeed be more activated and have more effector properties.

For the activated CD4 cluster, one sub-region of increased glycolysis signature also overlaps with the exhaustion or inhibitory signature. It is possible that these cells could be terminally differentiated effector CD4 T cells that are induced by BCG but might not be the most protective against Mtb. There are also BCG-induced activated CD4 cells with a strong interferon response signature that do not overlap with the exhaustion or inhibitory signature. These could be activated CD4 T cells responding to IFN-γ but not yet terminally differentiated. It is possible that BCG-induced less terminally differentiated CD4 T cells could be more protective by preferentially localizing to the lung parenchyma while the terminally differentiated effector CD4 T cells may be more localized to the lung vasculature. This could make these CD4 T cells best positioned close to the lesions to have their effector functions such as producing IFN-γ and other Th1 cytokines to equip the macrophage to respond against the Mtb, overall resulting in reduced lung burdens and prevention of dissemination to the contralateral lung.

Lastly, BCG increases cytotoxicity in the sub-regions of the activated CD8 cluster that are absent in unvaccinated samples. In addition, this sub-region of increased cytotoxicity signature does not fully overlap with the exhaustion or inhibition signature for this activated CD8 T cluster. The sub-region with strong cytotoxic signature also had a strong interferon response signature. This could suggest that the BCG-induced CD8 T cells with effector properties

including cytotoxicity could be important for mediating protection. Since we found that CD8 T cells play a major role in preventing infection, it is possible that the BCG-induced effector CD8 T cells could directly or indirectly interact with and kill Mtb-infected cells very early after infection, before lots of bacterial replication can occur. This would result in less founding strains able to establish infection and would indirectly reduce BCG-mediated lung burdens.

Using this scRNAseq method, we were also able to extract myeloid cells. Current work is ongoing to determine if BCG induces any of these myeloid cell populations that are responding early after Mtb infection. One caveat of our scRNAseq protocol is that we are not able to capture a significant amount of lung epithelial cells by our extraction technique to make definitive conclusions about differences of this population in unvaccinated versus BCG vaccinated.

The CD model is useful for investigating phenotypes of BCG-induced T cells after Mtb infection by reducing noise and synchronizing the stage of mouse infection. As shown in the literature, reduction in bacterial burden and survival are the only current measures of protection in mice (37, 38), and the differences in these measurements conferred by different vaccines is

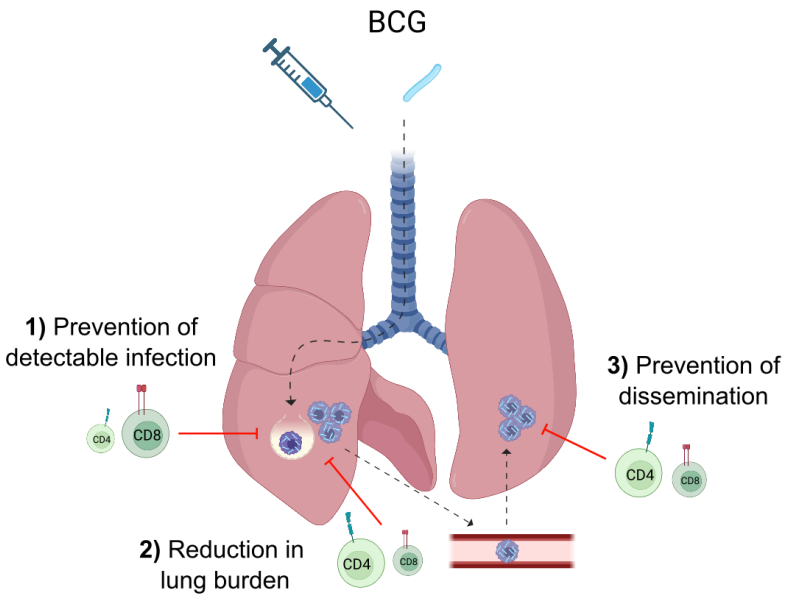

Figure 3. 14. Distinct roles of CD4 T cells and CD8 T cells in BCG-mediated immunity within the ULD mouse model. In BCG vaccinated mice, BCG induced CD8 T cells play a larger role than CD4 T cells in preventing infection. CD4 T cells play a larger role than CD8 T cells for BCG-mediated control of lung bacterial burden and prevention of dissemination to the contralateral lung. Created with BioRender.

usually quite modest. However, the immune responses optimal for reducing lung burden after infection with 1-3 CFU may be different than those required for 50-100 CFU. Additionally, little is known about the roles of CD4 and CD8 T cells in the context of BCG vaccination. We therefore turned to the ULD model to dissect the relative contributions of CD4 and CD8 T cells in BCG-mediated immunity against Mtb and discovered that CD4 and CD8 T cells mediate distinct aspects of protective vaccine-induced immunity (**Figure 3.14**). In ULD-infected, BCG vaccinated mice, where vaccination expands the T cell repertoire prior to Mtb infection, mice inhale ~1-3 Mtb bacilli into one lung and CD8 T cells play a larger role than CD4 T cells in preventing infection of Mtb strains. For Mtb that establishes infection, CD4 T cells play a major role and CD8 T cells play a minor role in BCG-mediated control of bacterial replication. Finally, CD4 T cells play the predominant role in preventing dissemination to the contralateral lung.

Our data provides new insight on the mechanism of prevention of infection with CD8 T cells playing a major role and CD4 T cells playing a minor role. This role for CD8 T cells only occurs in a vaccinated setting, suggesting that BCG induces a specific population of CD8 T cells capable of preventing infection. Our flow cytometry and scRNAseq data leads us to hypothesize that the BCG-induced CD8 T cells able to prevent infection could have an activated and cytotoxic phenotype, however, further testing is required to confirm this. It was surprising that co-depletion of all T cells, but not single depletion of CD4 nor CD8 T cells, resulted in a trend towards increased Mtb strains in unvaccinated mice. One possible explanation is that the mechanism of prevention of infection could be different in a vaccinated versus unvaccinated setting. In a vaccinated setting, BCG induces CD8 T cells capable of clearing Mtb strains so single depletion of CD8 T cells or co-depletion of both CD4 and CD8 T cells leads to an increase in founding strains. BCG-induced CD4 T cells play a minor role so there is not significant impact of single depletion of CD4 T cells. In unvaccinated mice, perhaps CD8 T cells naturally responding to Mtb infection play a role in clearing Mtb but may require CD4 T cell help

to perform this function. Therefore, each cell type could compensate for the lack of the other during single depletion and only co-depletion results in a trend towards more infection.

In a recent non-human primate (NHP) study, CD8+ lymphocytes played roles in controlling bacterial burden and limiting establishment of infection and dissemination in unvaccinated NHPs (99). A follow up study showed in IV BCG vaccinated NHPs that CD4+ and CD8+ lymphocytes played roles in controlling bacterial burden and limiting dissemination and CD4+ but not CD8+ lymphocytes had a modest but significant role in limiting establishment of infection (101). These results deviate from our findings since we could not detect a role for CD8 T cells in an unvaccinated setting and CD8 T cells played a major role in prevention of infection but a minimal role in prevention of dissemination. One consideration is that in NHPs, some CD4 T cells also express CD8α, particularly activated CD4 T cells, so effects of CD8α depletion could be due to unintentional depletion of CD4 T cells, restricted by MHCII, that upregulate CD8α (99, 199). An advantage to our model is that mice are less prone to this upregulation of CD8α in CD4 T cells, resulting in more targeted CD8 T cell depletion.

It is also possible that depletion of CD8+ NK cells in NHPs could explain the discrepancies between our results in mice and data in NHPs. In our scRNAseq experiment, BCG did significantly increase the proportion of NK cells responding early after Mtb infection. However, by flow cytometry, CD8+ NK cells make up a minor proportion of the NK cells in lung tissue and 80-90% are CD4- CD8- (data not shown). Therefore, although we did not directly measure the numbers of NK subsets in these experiments, depletion of CD8+ NK cells are unlikely to be responsible for our observed phenotypes, although we cannot rule out the potential contribution of this cell type. In NHPs, data from Simonson, A.W., et al., show that CD8α depletion did partially deplete total NK cells in BAL (101). Further analysis showed that CD8α depletion resulted in a shift from CD8α NK cells to NKG2A+ NK cells and a shift in NK functionality after CD8α depletion with a major reduction in IL-17 and TNF expressing NK cells

(101). Therefore, depletion of CD8+ NK cells could be at least partially responsible for the CD8-mediated protection in unvaccinated NHPs.

There are some differences in cellular expression of CD8α in mice compared to NHPs and humans. Mice express CD8α on only a minor population of conventional dendritic cells (cDCs), NK cells, NKT cells, and $\gamma\delta$ T cells. A recent paper by Sutton, M.S., et al. looked at the effect of *in vivo* antibody mediated depletion of leukocyte populations in NHPs. They showed that at baseline in the BAL, the majority of MAIT cells, $\gamma\delta$ T cells, and NK cells express CD8α and only a minority of each cell type is CD4-CD8- (199). In humans, CD8α is expressed on ~40% of NK cells and 30% of $\gamma\delta$ T cells express CD8α in the blood, however, it is unclear what proportion of these cells express CD8α in the lung (200, 201). Circulating human MAIT cells are mainly CD8α+, although MAIT cells in mucosal tissues have a higher frequency (40-50%) of CD4-CD8- double negative MAIT cells (202).

Because conventional dendritic cells (cDCs) can express CD8α in mice, we compared CD8-expressing cDCs in the lung with or without CD8 depletion. cDCs are not a significantly infected cell population in the lung so we wouldn't expect cDCs to be responsible for early killing of Mtb. However, it is possible that CD8+ cDCs could help expand and activate CD4 T cells important for control and therefore depletion of this population could result in depletion in activated CD4 T cells. When looking all subsets of cDCs by flow cytometry, we found that CD8+ cDCs were not depleted by α-CD8 and we found similar numbers of CD4 T cells and activated $CD44^{hi}$ CD4 T cells in control versus depleted groups. This suggests that the BCG-mediated roles of CD8 T cells were not directly or indirectly due to CD8+ cDCs.

One outstanding question is when does BCG-mediated prevention of infection occur? We have previously hypothesized that BCG does not block initial infection but can clear infection after days 14-15 p.i. because the reduction in lung burden in BCG vaccinated mice doesn't occur until after this timepoint (154). However, our CD8 depletion data suggests that

BCG-induced CD8 T cells might function earlier than expected by preventing founding Mtb strains from establishing infection. We hypothesize that the modest role of BCG-induced CD8 T cells in controlling lung burden is an indirect result of fewer founding strains able to replicate and contribute towards lung burden. Therefore, it is possible that BCG-induced CD8 T cells act very early after inhalation of Mtb, perhaps by directly killing the Mtb-infected cells. Furthermore, because 1-3 CFU is a more physiologic dose challenge, the ability of CD8 T cells to prevent establishment of infection on the individual strain level suggests a more profound role of CD8 T cells in preventing infection, and vaccines that target the appropriate CD8 T cells could be key to preventing infection.

The newfound role of CD8 T cells in BCG-mediated immunity in mice also leads us to wonder what types of CD8 T cells are important. The NHP studies raised the possibility that innate-like CD8+ lymphocytes could be responsible for the IV BCG-induced protection. Concordantly, we hypothesize that non-classical CD8 T cells could be responsible for this early protective phenotype because many non-classical CD8 T cells recognize conserved microbial products and could therefore be activated faster after Mtb infection than classical CD8 T cells. Additionally, non-classical CD8 T cells can home to mucosal surfaces and other studies have shown that BCG induces non-classical CD8 T cells such as MAIT cells and $\gamma\delta$ T cells (177, 203, 204). In our studies, we depleted both classical MHC Ia and non-classical MHC Ib CD8 T cells. Future studies could make use of H-2 K^bD^b double knockout mice to further dissect the contributions of non-classical CD8 T cells in BCG-mediated protection. Additionally, mice are a great model system for dissecting the contribution of specific types of non-classical CD8 T cell subsets (i.e. Qa-1, the functional homolog of HLA-E in humans) in BCG-mediated protection.

CD4 T cells played a major role in control of lung burden regardless of vaccination status. This role of CD4 T cells in unvaccinated mice is consistent with prior literature using the CD infection model (37, 38). Very few mouse studies to date have successfully investigated the BCG-mediated role of CD4 T cells against Mtb infection (205). Here we confirm that CD4 T cells

do indeed play a major role in BCG-mediated control of lung burden. It was interesting that co-depletion resulted in a more moderate increase of bacterial burden for unvaccinated mice compared to BCG vaccinated mice given the larger increase in lung burden in unvaccinated mice of the single CD4 depletion experiments. The experimental endpoints of the co-depletion experiments were 1-1.5 weeks earlier than the CD4 single depletion experiments. It is possible that there would be a larger increase in bacterial burden for unvaccinated T cell depleted mice if harvested a week later.

We have shown for the first time a role for CD8 T cells in BCG-mediated control of bacterial burden in mice. Again, this only occurred in the BCG vaccinated group, suggesting that BCG induces CD8 T cells that can contribute to the control of bacterial burden. When performing parallel ULD and CD CD8 depletion experiments, we saw a significant reduction in lung burdens of BCG vaccinated CD8 depleted mice only with the ULD model. The CD lung burden data is consistent with other mouse studies that used a similar infectious dose but an earlier day 14p.i. timepoint (190, 191). If the immune mechanisms of protection were the same using the CD and ULD models, then it would not be necessary to use the ULD model for these studies. However, our study provides evidence that the role of CD8 T cells in BCG-mediated control of lung bacterial burden was masked by using a supraphysiologic challenge dose.

To measure prevention of dissemination to the contralateral lung, we previously described how CFU of the left versus right lung underestimates containment, so we infect mice with a pool of bar-coded strains to distinguish between lungs with disseminated infection versus separate infections by different Mtb strains (154). Using this approach, we measured the proportion of mice with at least one bilateral Mtb strain and determined that CD4 T cells play the predominant role in BCG-mediated prevention of dissemination to the contralateral lung. We also used this approach to measure the proportion of overall Mtb strains that were bilateral for each mouse group. This is to account for mice infected with a mix of unilateral and bilateral Mtb

strains. The results were consistent with the proportion of mice with bilateral strains, supporting our conclusions that CD4 T cells play the predominant role in prevention of dissemination.

Depletion of CD8 T cells in BCG vaccinated mice did not result in a significant increase in dissemination to the contralateral lung which would suggest that CD8 T cells play a minimal role in BCG-mediated prevention of dissemination to the contralateral lung. However, depletion of all T cells in BCG vaccinated mice fully reversed the prevention of dissemination to the contralateral lung phenotype compared to BCG vaccinated non-depleted mice, back to the same levels as unvaccinated T cell depleted mice. This suggests that CD8 T cells still play a minor role, perhaps dependent on CD4 T cells, in BCG-mediated prevention of dissemination to the contralateral lung.

Because most unvaccinated mice already have dissemination to the contralateral lung by the time of harvest, it is difficult to assess the roles of T and B cells in an unvaccinated setting. It is likely that CD4 T cells are important for preventing dissemination in an unvaccinated setting because humans infected with HIV and depleted of CD4 T cells have difficulty containing TB infection (39). Our supplemental spleen CFU data suggests that CD4 T cells but not CD8 T cells could play a role in controlling spleen burden in both unvaccinated and BCG vaccinated mice. There is already a high proportion of unvaccinated non-depleted mice with dissemination to the spleen, so it is difficult to say if CD4 T cells help block dissemination to the spleen or are involved in reducing Mtb replication once in the spleen.

There are several limitations of this study. The experiments were performed using a single Mtb strain (H37Rv) and a single mouse strain (C57/BL6). It is possible that different strain combinations of bacteria and host could impact the host immune response. For example, recent work demonstrates that unvaccinated C3HeB/FeJ (C3H) mice infected with the hypervirulent clinical Mtb isolate SA161 develop large necrotizing granulomas while BCG vaccination blocks the necrotizing granuloma formation and induces the formation of smaller, less organized lesions (25). The parameters of BCG-mediated protection in this model using ULD challenge

could be more dramatic, and it would be interesting to investigate the relative contributions of BCG-induced CD4 and CD8 T cells that could be involved in protection including abrogating the formation of necrotic granulomas. Another limitation is the variability in protective phenotypes between repeat experiments. Some of this variability is due to the inherent mouse-to-mouse variability in the ULD model and the large number of mice required to perform each experiment. Additionally, BCG only has a 13% efficacy in preventing detectable infection in the ULD model (154), so it is possible that the protective role of CD4 and CD8 T cells could be enhanced if using a model of pre-existing or concomitant immunity with a larger prevention of infection efficacy.

In the scRNAseq experiment, we found that proportions of B cell but not activated B cell clusters were also significantly increased in BCG vaccinated samples, and pathway analysis suggested that the BCG-induced B cells were responding to the boost in interferon within the environment rather than having unique effector functions. This led us to further investigate the role of B cells in BCG-mediated immunity. We did not observe any effect of B cells on BCG-mediated immunity against Mtb, however, there are caveats to the $\mu MT^{-/-}$ mice. Since $\mu MT^{-/-}$ mice are a genetically modified strain with target deletion of the IgM heavy chain gene, the mice have altered immune system development that could lead to compensatory changes in other immune cell populations such as altered development and function of T cells. Additionally, the absence of B cells affects the development and architecture of lymphoid organs such as the spleen and lymph nodes which could impact the function of these organs during the immune responses to BCG vaccination and Mtb infection. Since we did not see any interesting phenotypes with the $\mu MT^{-/-}$ mice, we did not further investigate roles of B cells or antibodies using alternative experimental approaches such as BCR transgenic mice, antibody-mediated depletion, or conditional knockout systems.

The adoptive transfer approach also has caveats to consider. The purpose of the adoptive transfer experiment was to determine if the addition of functional Th1 CD4 T cells to

mice with an intact immune system could reveal similar protective phenotypes as BCG vaccination, which would suggest that CD4 T cells are sufficient for the protective effects afforded by BCG. Our data showed that ESAT-6 specific CD4 T cells, but not OTII-specific CD4 T cells, are sufficient for controlling lung burden but are not sufficient for preventing dissemination or infection. This experiment used a slightly earlier timepoint compared to the CD4 single depletion experiments (29 d.p.i. vs 35-38 d.p.i.) and there are too few infected mice to robustly assess significant differences in dissemination or infection. Therefore, it is possible that there could be an impact of transferring ESAT-6 specific CD4 T cells on the other protective parameters if we used a later timepoint and had larger sample sizes. Additionally, ESAT-6 is Mtb-specific, not BCG-specific. Use of Ag85B-specific CD4 T cells instead of or in addition to ESAT-6 specific CD4 T cells may better reflect the protective BCG-induced CD4 T cell response. Finally, we do not have equivalent transgenic strains to look at antigen-specific CD8 T cells. While the adoptive transfer data suggests that BCG induces other immune responses independent of Th1 CD4 T cells that are important for preventing dissemination and infection, we could not be certain without using alternative approaches including CD8 depletion.

In conclusion, our results demonstrate that CD4 and CD8 T cells mediate distinct aspects of vaccine-induced immunity against Mtb infection. Using our ULD challenge model, we were able to discern these different mechanisms relevant to clinical TB outcomes. This work may provide new insights on the optimal CD4 and CD8 T cell responses to target with vaccine candidates. For example, a vaccine candidate that more strongly induces cytotoxic CD8 T cells early after Mtb infection might be better equipped than BCG at preventing initial infection or preventing sustained Mtb infection. Further work is needed to identify if a single type of CD8 T cell is sufficient for this early protection. It would be important to evaluate CD4 and CD8 T cell responses in current vaccine candidates using the ULD model to determine if specific vaccine-induced CD4 and CD8 T cell responses correlate with better outcomes for each parameter of protection.

3.4 Materials and Methods

3.4.1 Mice

C57BL/6J and B6.129S2-Ighm^{tm1Cgn}/J (μMT$^{-/-}$) mice between the ages of 9-12 weeks were purchased from Jackson Laboratories (Bar Harbor, ME). All animals were housed and maintained in specific-pathogen-free conditions at Seattle Children's Research Institute (SCRI). All animal studies were performed in compliance with the SCRI Animal Care Use Committee.

3.4.2 BCG Immunizations

BCG-Pasteur (Urdahl lab) or BCG Aeras Pasteur provided by Rhea Coler (SCRI) were used for all studies. BCG was cultured in Middlebrook 7H9 with OADC supplement plus 0.05% Tween-80 at 37˚C with constant agitation for five days. BCG was back diluted in 7H9 for two days and grown to an OD of 0.2-0.5. Bacteria were diluted in PBS and mice were injected subcutaneously with 10^6 CFU in 200μL. BCG was diluted and plated on 7H10 plates and plates were counted for CFU after 21 days to confirm dose of immunization. After immunization, mice were rested for 8 weeks prior to Mtb infection.

3.4.3 Conventional dose Mtb Aerosol Infections

H37Rv Mtb or H37Rv transformed with mCherry reporter plasmid were used for infections. Mice were placed in a Glas-Col aerosol infection chamber and 5mL of diluted Mtb was injected into the nebulizer of the infection chamber. The nebulization cycle was set to 45 minutes followed by 45 minutes of cloud decay.

3.4.4 Ultra-low dose Mtb Aerosol Infections

Bar-coded H37Rv Mtb was used for all infections (source). Mtb stocks were grown in Middlebrook 7H9 with OADC supplement and 0.05% Tween-80 at 37˚C with constant agitation to an OD = 1. Cultures were filtered through a 5μm filter to remove clumps and aliquots were frozen at -80˚C. Frozen filtered stocks were thawed and titered side by side with stocks used for conventional dose infection to determine how to dilute the ULD stocks with the goal of leaving 37% of mice uninfected. Mice were placed in a Glas-Col aerosol infection chamber and 5mL of diluted Mtb was injected into the nebulizer of the infection chamber. The nebulization cycle was set to 45 minutes followed by 45 minutes of cloud decay.

3.4.5 T cell depletion

For CD4 T cell depletion, mice were injected intraperitoneally (i.p.) with 400μg anti-CD4 GK1.5 (BioXcell) in PBS at D1, D7, D14, D21, D28, D35 post-infection. For CD8a T cell depletion, mice were injected i.p. with 200μg anti-CD8a 2.43 or YTS 169.4 (BioXcell) in PBS at D1, D7, D14, and D21 post-infection. To deplete all T cells, mice were injected intraperitoneally (i.p.) with 200μg anti-CD4 GK1.5 and 200μg anti-CD8a 2.43 or YTS 169.4 (BioXcell) in PBS at D1, D7, D14, and D21 post-infection. Non-depleted mice were injected i.p. with 200μg rat IgG2b LTF-2 isotype control in PBS at the same timepoints.

3.4.6 CFU Plating

Right lung, left lung, or spleen were homogenized in 1mL PBS+0.05% Tween-80 (PBS-T) either in M tubes using a Miltenyi GentleMACS machine (Miltenyi) or in 15mL conicals using a sonicator. Tissue homogenates were diluted in PBS-T and plates onto 7H10 plates. For ULD

infections, undiluted homogenates were also plated between two 7H10 plates. Plates were incubated at 37˚C for approximately 21 days and then were quantified for CFU.

3.4.7 Single cell preparation and antibody staining

Right lungs of mice were homogenized in HEPES buffer with Liberase Blendzyme 3 (70µg/mL; Roche) and DNaseI (30µl/mL; Sigma-Aldrich) using a Miltenyi GentleMACS machine lung cycle 1 (Miltenyi). Samples were incubated at 37˚C for 30 minutes and then were further homogenized using lung cycle 2. For T cell depletion studies, 800µL of right lung was taken for CFU analysis and the rest was used for flow cytometry analysis. Samples were filtered through 100µm cell strainers, spun at 1500RPM for 5 minutes at 4˚C, resuspended in RBC lysis buffer, spun, and resuspended in PBS. 10µl of cells were added to 190µL 4% paraformaldehyde for cell counts. Cells were first stained with 50µL Zombie UV viability dye (BioLegend) for 10min at room temperature (RT). The viability dye was quenched with 100µL of antibody cocktail made in 50% FACs buffer (2.5% FBS, 0.1% NaN_3, PBS) and 50% Fc block buffer. Samples were stained with antibody for 20min at 4˚C if no tetramer or 1hr at RT with tetramer. Cells were washed with FACs buffer and were fixed in 3:1 Ebio Fix perm (Thermo Fisher) overnight. If antibody panel included intracellular (IC) antibodies, cells were washed with 1x permwash, incubated with IC antibodies made in 1x permwash, washed in permwash, and fixed in FACs fix (2% paraformaldehyde). Ag85B (I-A(b) 280-294) and TB10.4 (K(b) 4-11) tetramers were obtained from the NIH Tetramer Core Facility. Flow cytometry was performed using the Cytek Aurora spectral flow cytometer (UW flow core, Cytek) and analyzed using FlowJo.

3.4.8 10x single cell RNA sequencing

After 12 or 13 days post-infection, 4 unvaccinated and 12 BCG vaccinated C57Bl/6 mice were i.v. labeled with CD45.2 APC 10 minutes prior to sacrifice and right lungs of mice were prepared

as single cell suspensions as described above. Cells were resuspended in 200 μl MACS buffer (PBS containing 2.5% FBS plus 1 mM EDTA) and then stained with 50μL Zombie Aqua viability dye (BioLegend) for 10min at RT. The viability dye was quenched with 100μL antibody cocktail (BV421 SiglecF, PE Ter119, and BV650 CD11c). The cells were run on a FACS AriaII (BD) sorter and parenchymal cells were collected by sorting alveolar macrophages (AM, SiglecF+CD11c+) into one tube to account for autofluorescence in the IV label channel, and IV negative cells were sorted into a different tube. The AM and IV- cells were combined after sorting and were counted on a hemocytometer. The cells were washed once with ice-cold DPBS and were resuspended to 1000 cells/μl in DPBS. 8000 cells were inputted into the 10x Genomics pipeline following the manufacturer's guidelines and cDNA was generated. Samples were centrigued twice through 0.2 μm SpinX (Costar) columns and then were transferred out of the BSL3 facility for subsequent library generation. Libraries were submitted to Psomagen (Rockville, MD) for NovaSeq sequencing with 300M reads per sample.

10X Chromium 3' derived single-cell RNAseq sequence reads were aligned to the 10X Genomics pre-built mouse reference genome mm10-2020-A, assigned to cells by barcodes, and UMI summarized using the 10X Cell Ranger 7.1.0 software package. T cells were identified using the Celltypist [PMID: 35549406] python package to map our scRNAseq data to two previously published mouse immune cell atlases, Tabula Muris [PMID: 30283141] and scMCA [PMID: 29474909]. Celltypist-identified T cells were re-clustered using the R Seurat package[PMID: 34062119] to identify T cell subsets with distinct gene expression profiles. Within-subset BCG vs unvaccinated differentially expressed genes were identified using the Seurat FindMarkers() function using the "roc" test, where the log2 fold change > 1 and AUC>0.6. Pathway enrichment was determined by assessing significant overlap with defined blood transcriptional module sets [LI: PMID 24336226:, DC: PMID 23601689, HALLMARK: PMID: 26771021] where hypergeometric FDR<0.05.

3.4.9 Confocal Microscopy

Mice were infected with H37Rv Mtb-mCherry and were euthanized at D12 post-infection. Right inferior lung lobes were dissected into BD Cytofix solution diluted 1:3 in PBS for 22-24 hours at 4˚c. Tissues were washed twice in PBS and dehydrated in 30% sucrose overnight. Tissues were then embedded in OCT and stored at -80˚C. Tissue blocks were sectioned to create 20µm sections. Sections were hydrated with 0.1M TRIS buffer, blocked in blocking buffer (0.1M TRIS with 1% normal mouse serum, 1% bovine serum albumin, and 0.3% Triton X100), and were stained with 100uL of antibody cocktail made in blocking buffer at room temperature overnight. Slides were washed twice with 0.1M TRIS buffer and were cover-slipped with Fluoromount-G mounting media. Images were acquired on a Leica Stellaris8 confocal microscope. For visual clarity, thresholds were applied to the displayed channel intensities in Imaris with identical settings applied across experimental groups.

3.4.10 Genomic DNA Extraction

Genomic DNA from bacterial colonies grown from infected tissues were extracted as previously described (154). Briefly, colonies were scraped into resuspension buffer (25mM Tris-HCl pH 7.9, 10mM EDTA, 50mM glucose, water) + 10mg/mL lysozyme and were incubated at 37˚C overnight. Samples were resuspended with 10% sodium dodecyl sulfate and 10mg/mL Proteinase K and were heated at 55˚C for 30 minutes. Samples were then resuspended in 5M NaCl followed by Cetrimide saline solution and heated at 65˚C for 10 minutes. Genomic DNA was extracted twice with 24:1 chloroform:isoamyl alcohol. DNA was precipitated with 0.7x volume of isopropanol and washed with 70% ethanol. Finally, DNA was eluted with DEPC water.

3.4.11 Barcoded Sequencing

Mice were infected with a pool of 50 bar-coded strains. Sequencing of bacterial bar-codes has been previously described (29, 206). Briefly, genomic DNA was pre-amplified with pooled barcoded primers before libraries were prepared with NEBNext Ultra DNA Library Prep Kit for Illumina (New England Biolabs) using the AMPure XP reagent (AgenCourt Bioscience) for size selection and cleanup. The NEBNext Multiplex Oligos for Illumina (New England Biosciences) were used to barcode DNA libraries and enabled multiplexing of 96 libraries per sequencings run. Samples were sequenced using the NextSeq 500 Mid Output v2 kit (Illumina) at the University of Washington Northwest Genomics Center. Read alignment was carried out using a custom processing pipeline that has been previously described (189).

3.4.12 Distribution Curves with barcoded data

Fitting Distribution Curves to barcoded data.

To estimate an effective dose of Mtb acquired by mice in the exposed population we fit a Poisson distribution P to the data on the number of founding/barcoded strains in each dataset using a likelihood approach [3]. Poisson distribution for a homogeneous population is defined as

$$P(i|D) = \frac{D^i}{i!}e^{-D},\ i = 0, 1, \cdots \infty, \quad (1)$$

where $D = \bar{n}_F = \lambda$ is the effective dose. Note that this model also includes uninfected mice (that have 0 barcodes). Specifically, when observing i_k barcodes in k^{th} mouse for n mice, the likelihood of the model is

$$L(D) = \prod_{k=1}^{n} P(i_k|D), \quad (2)$$

where $P(i_k|D)$ is given in eqn. (1) or its extensions. To investigate if the effective dose D is different between two sets of data (e.g., between control/BCG-vaccinated mice and CD8-depleted/BCG-vaccinated mice), we fit the model (e.g., eqn. (1)) to each of two datasets independently (resulting in two different estimates of the dose D for each of the datasets) or to the data pooled together from the two experiments (resulting in one estimate of D). Then we compare the difference in the quality of the model (i.e., likelihood) fit using a likelihood ratio test (**LRT**) [4]. If treatment does impact the dose, the model will fit pooled data with significantly lower quality than the model fitted to each dataset independently.

Fitting truncated Poisson distribution to barcode distribution data.

While the Poisson distribution (eqn. (1)) is typically fitted to barcode distribution data from both uninfected (i = 0) and infected (i > 0) mice, it is also possible to analyze a subset of barcode distribution data by focusing only on data from infected mice. In this case, we use the truncated Poisson distribution conditioned on infection

$$P\ (i|D) = \frac{D^i}{i!(1-e^{-D})} e^{-D},\ i = 1, \cdots \infty, \tag{3}$$

where $\sum_{i=1}^{\infty} P(i) = 1$. We also used this model to test if the estimated dose D varies with treatment also using LRT as described above.

Detecting deviations from Poisson in pooled barcode distribution data.

In some cases, for example, when pooling the data from several independent experiments, a single Poisson distribution may not accurately fit the data suggesting heterogeneity. One extension of the homogeneous Poisson model (eqn. (1)) is to assume two (or more) sub-populations that have different effective Mtb doses D_1 and D_2:

$$P(i|D_1, D_2) = f_1 P(i|D_1) + f_2 P(i|D_2), \tag{4}$$

where $f_1 + f_1 = 1$ are the fractions of mice with effective doses D_1 and D_2, respectively. We determined whether the inhomogeneous Poisson distribution (eqn. (4)) fits the pooled data better than a homogeneous Poisson distribution (eqn. (1)) using LRT.

3.4.14 Statistics

For comparing differences in bacterial burdens or CFU per founder, we used Mann-Whitney test on log-transformed, non-0 values (defined as CFU greater than 2.0 after log transformation). For comparing differences in proportions, we used Chi squared test if all cells were greater than 5 and Fisher's Exact test if at least one cell was less than 5. All tests were performed using GraphPad Prism 10.

3.5 Acknowledgements

Thank you to Fergal Duffy, Alan Diercks, and John Aitchison for their contributions to the bioinformatic processing, analysis, and visualization of the scRNAseq data. Thank you to Ben Gern for his support and guidance in the study design, data collection, and visualization of the confocal microscopy experiment. Thank you to Danica Shao and Paul Edlefsen for their contributions to formal analysis of the ULD CFU and dissemination data. Thank you to Vitaly Ganusov for his contribution to modeling, formal analysis, and visualization of the barcode data and distribution curves. Thank you to Courtney Plumlee and Kevin Urdahl who contributed to conceptualization, methodology, investigation, visualization, validation, formal analysis, writing – review & editing, funding acquisition, and supervision throughout the work in this chapter. This work was supported by NIH contract 75N93019C00070 (K.B.U) and the Bill and Melinda Gates Foundation, INV-026296 (K.B.U).

The authors would like to thank Lindsay Engels, Kaitlin Durga, Sonia Chen, Daniel Kim, and the Seattle Children's OAC staff for technical support. Thank you to the staff at the UW Cell Analysis Facility for support with the Cytek Aurora spectral cytometer. Thank you to Michael Gerner for providing OTII mice used in the adoptive transfer experiment.

3.6 Supplemental Figures

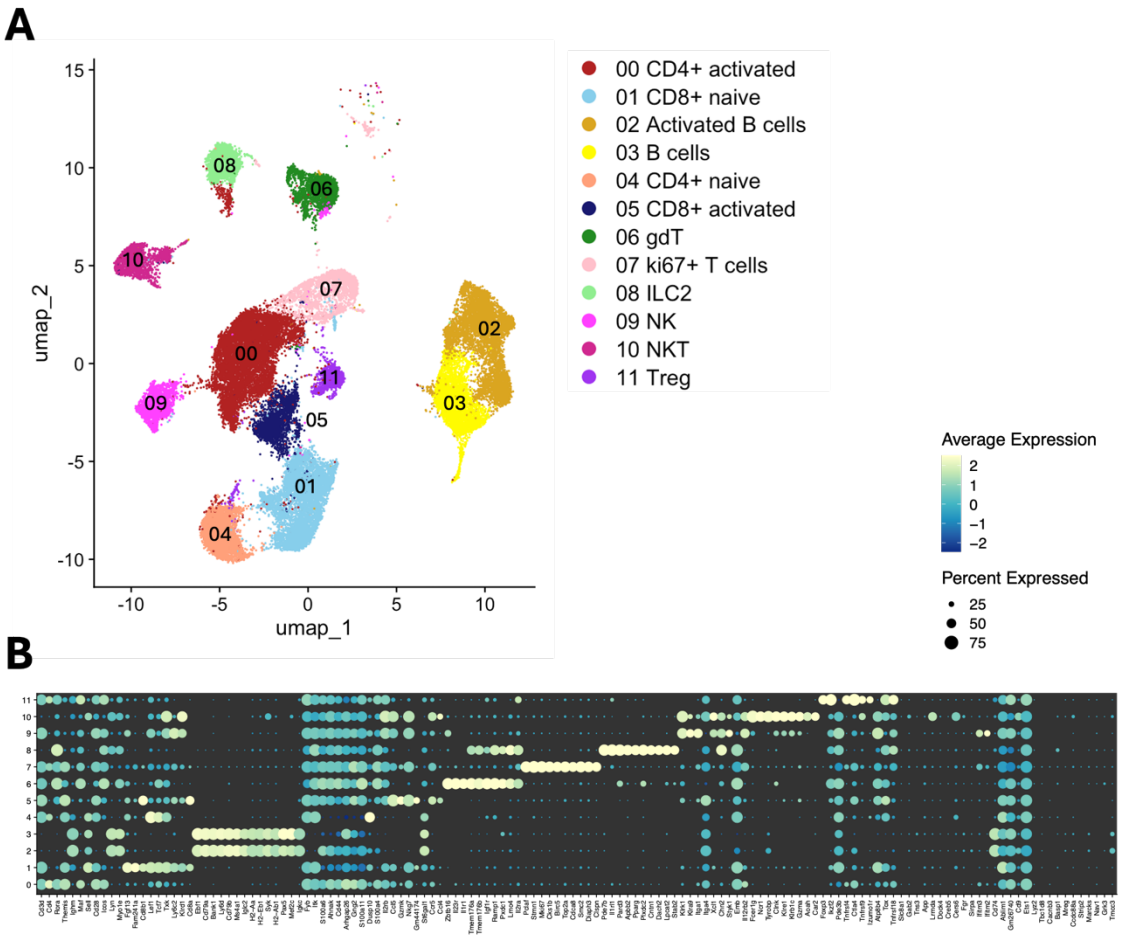

Figure 3. 15. Lymphocyte clusters of unvaccinated and BCG vaccinated mice identified via scRNAseq. **(A)** Lymphocyte subclusters compiled for all cells using the R Seurat package. **(B)** Heatmap showing average gene expression of marker genes used to guide annotation of cell clusters.

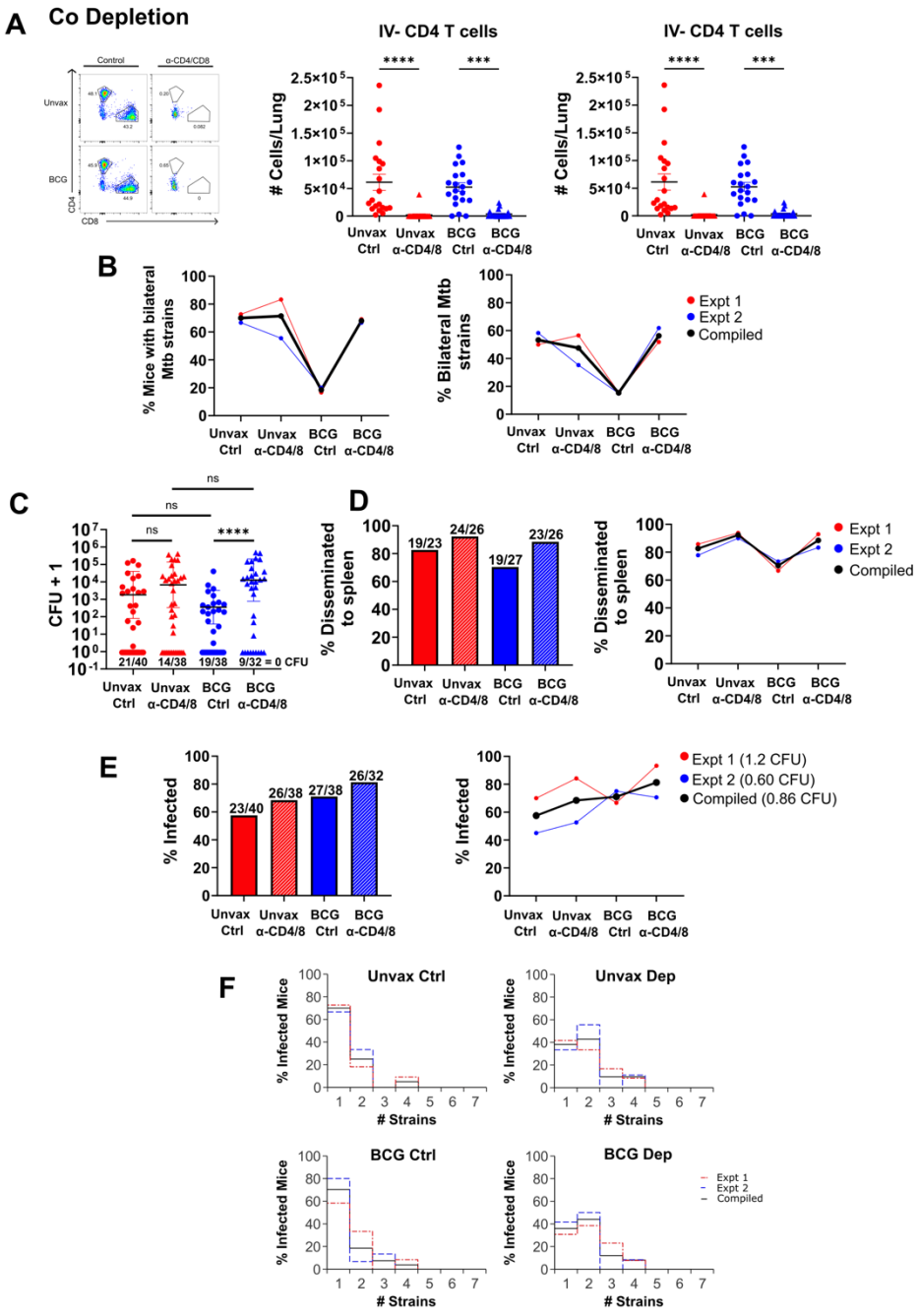

Figure 3. 16. Co-depletion of CD4 and CD8 T cells leads to worse protection for all metrics of BCG-mediated immunity. (A) Flow cytometry plots of CD4 and CD8 T cells from one mouse per group and gated on lymphocytes, single cells, live cells, CD11b- CD11c-, CD3+, and TCRb+ (left). Numbers of IV- CD4 T cells per lung (middle) and numbers of IV- CD8 T cells per lung (right) from one representative experiment. Significance was analyzed by unpaired t-test on GraphPad Prism 9. ****p<0.0001. **(B)** Proportion of mice with at least one bilateral Mtb strain (left) and proportion of bilateral strains (right) separated by experiment. **(C)** Spleen CFU with mean +/ SD. Proportions of mice with undetectable CFU are shown above the X axis. Significance was analyzed on log-transformed values excluding mice with 0 CFU by Mann-Whitney test on GraphPad Prism 9. ns = not significant, ***p<0.001. **(D)** Proportion of mice with Mtb CFU that disseminated from the lung to the spleen for compiled data (left) or data separated by experiment (right). **(E)** Proportion of infected mice defined as mice with CFU >0 for compiled data (left) or data separated by experiment (right). **(F)** Distribution curves of infection separated by experiment.

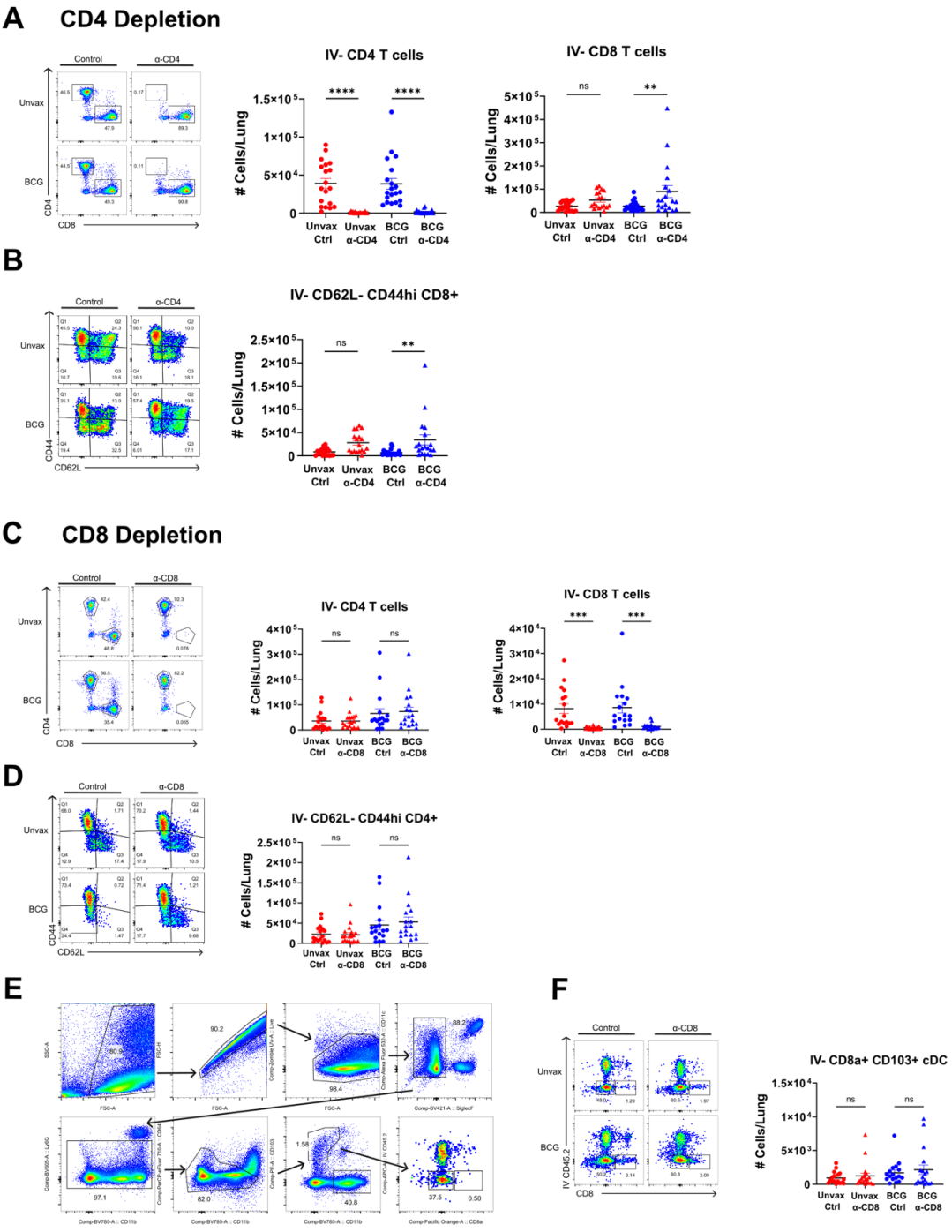

Figure 3. 17. Targeted depletion of CD4 T cells or CD8 T cells by antibodies. Flow cytometry plots of CD4 and CD8 T cells from one mouse per group and gated on lymphocytes, single cells, live cells, CD11b- CD11c-, CD3+, and TCRb+ (left). Numbers of IV- CD4 T cells per lung (middle) and numbers of IV- CD8 T cells per lung (right) from one representative experiment for CD4 depletion **(A)** and CD8 depletion **(C)**. Flow cytometry plots from one mouse per group, gated on lymphocytes, single cells, live cells, CD11b- CD11c-, CD3+, TCRb+, and CD4 or CD8a+ (left), and numbers of IV- CD62L- CD44hi CD8 T cells per lung **(B)** or IV- CD62L CD44hi CD4 T cells per lung **(D)** from one representative experiment. **(E)** Gating strategy for IV- CD8+ CD103+ conventional dendritic cells (cDC). **(F)** Flow cytometry plots of IV- CD8+ cDCs from one mouse per group (left) and numbers of IV- CD8+ cDCs per lung (right) from one representative experiment. Significance was analyzed by unpaired t-test on GraphPad Prism 9. ns = not significant, **p<0.01, ***p<0.001, ****p<0.0001.

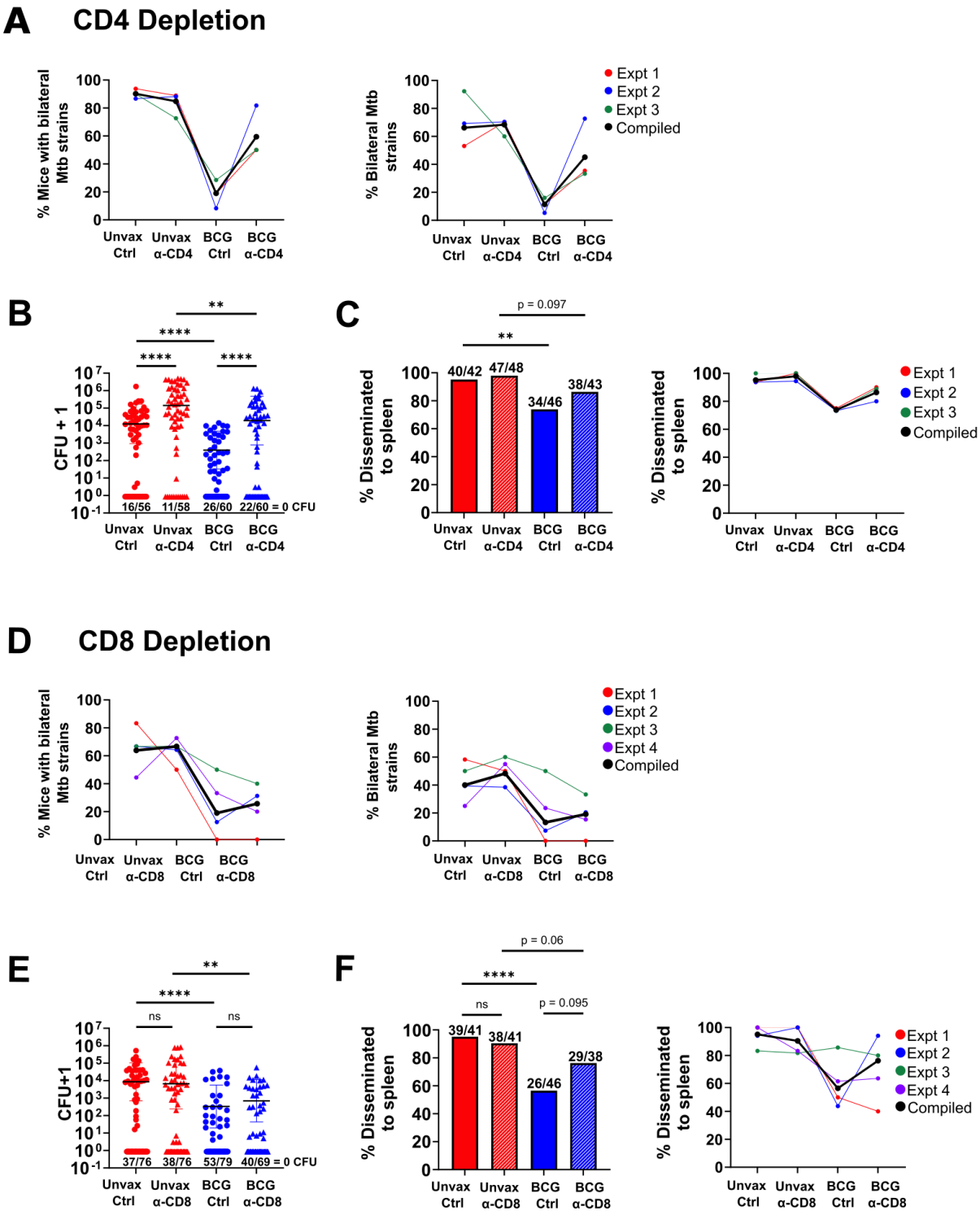

Figure 3. 18. Roles of CD4 and CD8 T cells in prevention of dissemination by experiment. Proportion of mice with at least one bilateral Mtb strain (left) and proportion of bilateral strains (right) separated by experiment for CD4 depletion **(A)** or Cd8 depletion **(D)**. Spleen CFU with mean +/ SD for CD4 depletion **(B)** or CD8 depletion **(E)**. Proportions of mice with undetectable CFU are shown above the X axis. Significance was analyzed on log-transformed values excluding mice with 0 CFU by Mann-Whitney test on GraphPad Prism 9. **p<0.01, ****p<0.0001. Proportion of mice with Mtb CFU that disseminated from the lung to the spleen for compiled data (left) or data separated by experiment (right) for CD4 depletion **(C)** or CD8 depletion **(F)**.

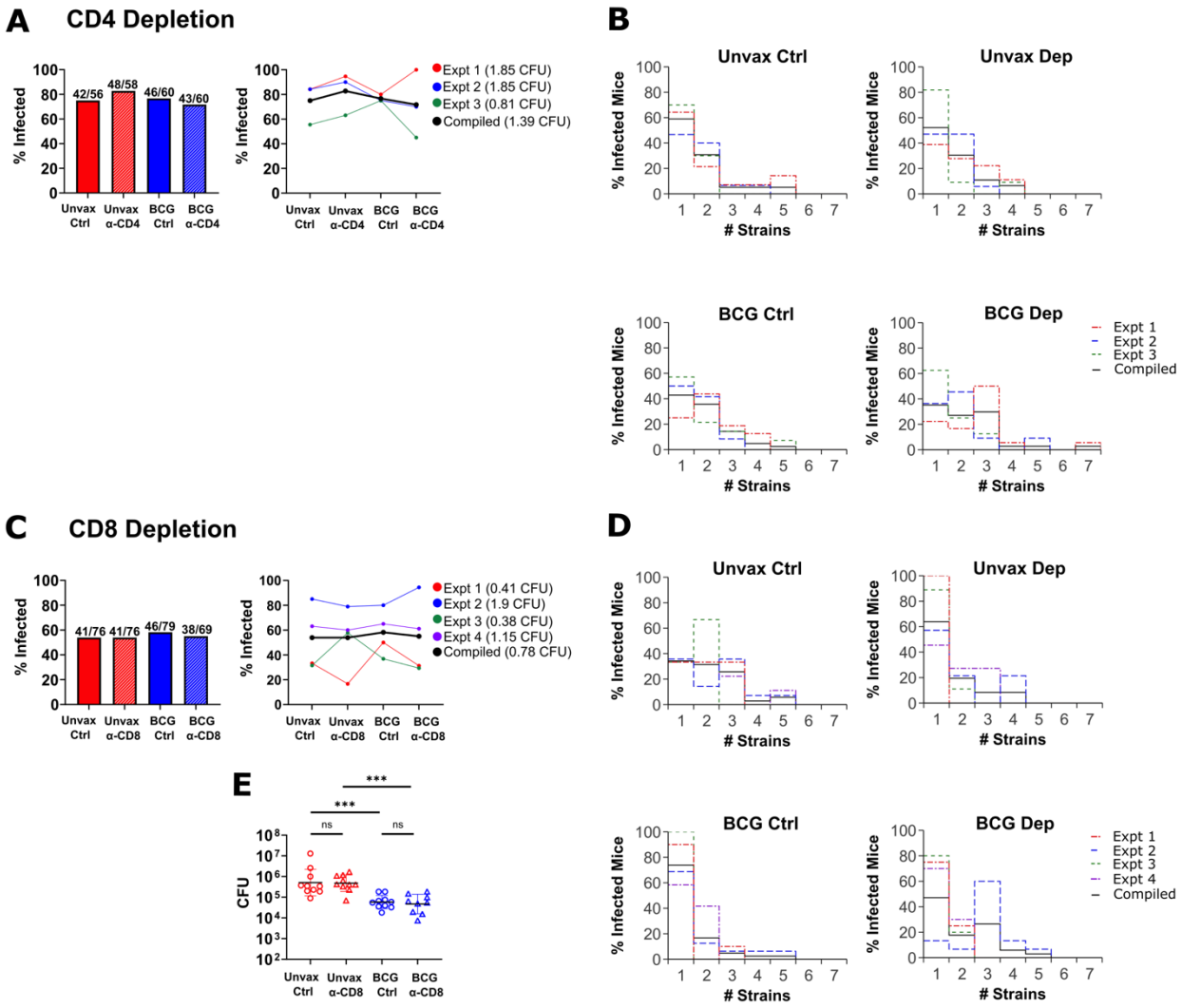

Figure 3. 19. Roles of CD4 and CD8 T cells in prevention of infection by experiment. Proportion of infected mice defined as mice with CFU >0 for compiled data (left) or data separated by experiment (right) for CD4 depletion **(A)** or CD8 depletion **(C)**. Distribution curves of infection separated by experiment for CD4 depletion **(B)** or CD8 Depletion **(D)**. **(E)** Lung CFU of conventional dose (CD), H37Rv infected unvaccinated or BCG vaccinated B6 mice, depleted or not depleted of CD8 T cells. Mice were injected i.p. with 200µg IgG or 200µg anti-CD8a antibody on days 1, 7, 14, and 21p.i. and were harvested between day 28-30p.i. Significance was analyzed by unpaired t-test on GraphPad Prism 9. ns = not significant, ***p <0.001. Data are graphed with mean +/- SD and are compiled across two independent experiments.

Chapter 4. Conclusion

4.1 Summary

The studies in this dissertation investigated vaccine-mediated protection in mice. Using the ULD challenge model, which represents a more physiologic infectious dose than used in the standard mouse model, we assessed parameters of BCG-mediated protection against Mtb infection **(Chapter 2)** and then dissected the relative roles of CD4 and CD8 T cells in BCG-mediated protection **(Chapter 3)**. We discovered that that the ULD model enables measurements of protection and reveals mechanisms of immunity that were not possible to elucidate in the conventional mouse model. Here, I present current approaches and future directions to answer outstanding questions that have arisen from this work.

4.2 Future directions

4.2.1 Distinguishing uninfected mice from mice that prevented infection in the ULD model

To administer an aerosolized physiologic dose of 1-3 infectious bacilli, the Mtb dose loaded into the nebulizer is intentional reduced such that only 60-70% of the mice in the infection chamber become infected (152). Because we currently don't have a means of differentiating mice that were never infected from mice that were initially infected and subsequently cleared infection, vaccine efficacy studies must include large numbers of mice to be able to assess prevention of infection. For example, in **Chapter 2**, we pooled data from many experiments with a total of over 500 mice in each group to conclude that BCG had a 13% efficacy in preventing infection; this was a statistical argument based on the number of mice with undetectable CFU in each group. During my PhD thesis work I unsuccessfully tried many immunologic and molecular methods to distinguish mice never infected from those that cleared

infection, including tetramer pulldown of Mtb-specific CD4 T cell responses and amplification of Mtb DNA from lung homogenate, but no method has been sensitive enough for this purpose.

Currently, in collaboration with Nick Walter at University of Colorado, and Brendan Podell and Greg Robertson at Colorado State University, we have been adopting a new method to sensitively detect very small amounts of bacteria. Our normal method of quantifying bacterial burden requires viable bacteria that grow as colonies on a plate. However, in mice with cleared Mtb infection, it is possible that traces of non-viable Mtb in the form of stable ribosomal RNA remain in the lung tissue. The recently described RS ratio is linked to bacterial replication and quantifies ongoing bacterial rRNA synthesis. Our collaborators take advantage of a digital PCR method (CAMM assay) to measure the ratio of rapidly degraded, unstable pre-rRNA (ETS1) over stable rRNA (23S rRNA). In preliminary experiments, we tested the sensitivity of the CAMM assay compared to conventional CFU analysis in unvaccinated or BCG vaccinated C3H mice at days 7 or 28 post-ULD Mtb infection (**Figure 4.1**). One caveat of this experiment is that because of the nature of the ULD infection, mouse lungs can be processed either for CFU analysis or for the CAMM assay but not both. Thus, the CFU analysis and CAMM assay were performed in different mice (albeit mice that were in the infection chamber at the same time and thus exposed to similar levels of aerosolized Mtb), limiting direct comparisons. At day 28 p.i., both ETS1 and 23S rRNA aligned with CFU data in unvaccinated mice, measured as the percent lobe positivity in neither lobe, right lobe, left lobe, or both lung lobes. In BCG vaccinated mice ETS1 continued to give similar results as CFU determinations, however, Mtb 23S was detected in a higher proportion of lung lobes than either ETS1 or CFU (**Figure 4.1**). BCG DNA was also distinguished from Mtb DNA in the CAMM assay, so the assay was not simply detecting BCG rRNA (data not shown). The half-life of Mtb 23S in the lung is not currently known, and therefore it is not known whether the difference in proportion of lungs with detectable CFU vs detectable 23S rRNA represents residual 23S rRNA remaining from dead Mtb or whether the Mtb could be alive, but non-culturable. Future experiments are being

designed to determine the Mtb 23S half-life in the lung and to discriminate between these possibilities. However, the data is promising that the CAMM assay and 23S rRNA measurement may be sufficiently sensitive to accurately distinguish uninfected from cleared mice. This would especially be helpful for measuring parameters of protection for other promising vaccine candidates in a sensitive and robust way using less mice than we needed for the BCG study (154) (see section 4.2.2).

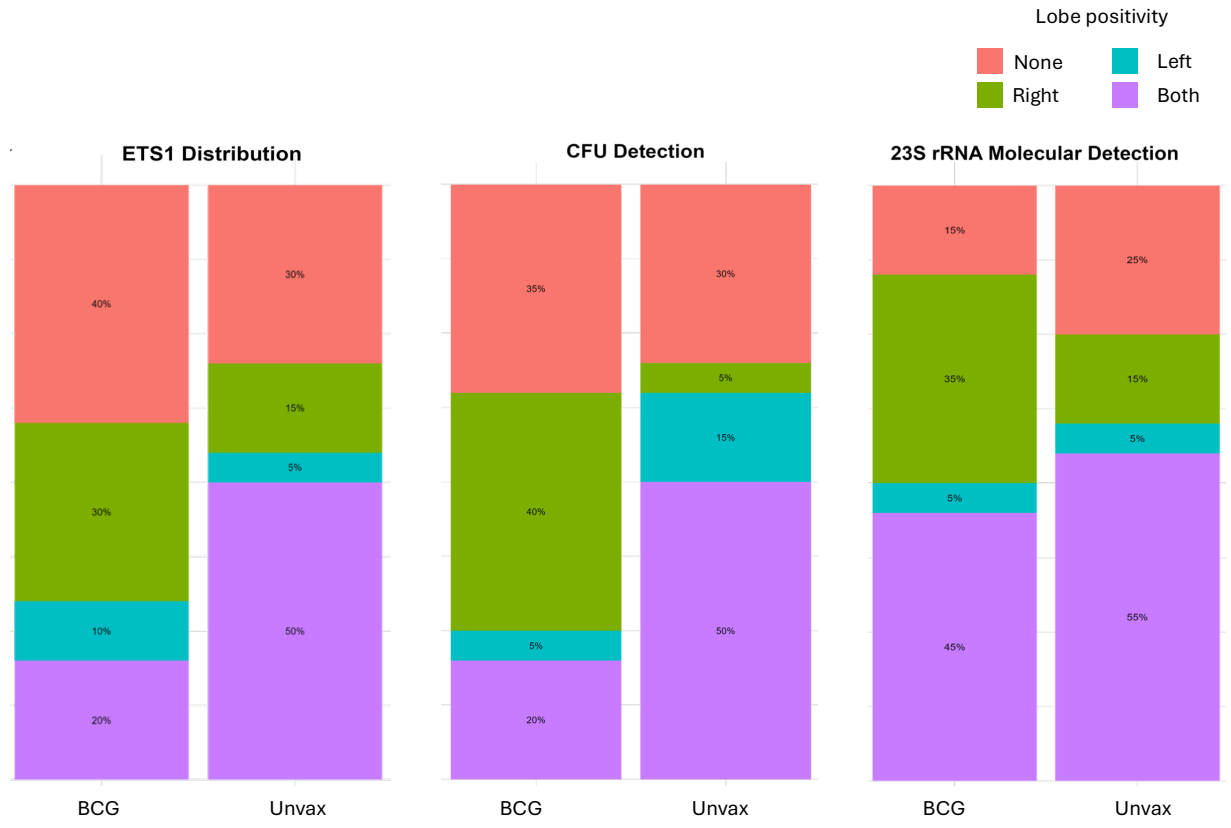

Figure 4. 1. CAMM molecular assays is sensitive in detecting low levels of Mtb in unvaccinated versus BCG vaccinated, ULD-infected mice. Unvaccinated or BCG vaccinated C3H mice were infected with ULD H37Rv and were harvested at day 28 p.i. Left lungs and right lungs were harvested for either CFU analysis or CAMM molecular assay. Percent of mice per group with Mtb detected in neither lung (salmon), right lung only (green), left lung only (teal), or both lungs (purple) for BCG vaccinated mice (left) or unvaccinated mice (right). Mtb lobe positivity was detected as ETS1 pre-rRNA (left), conventional CFU counts (middle), or stable 23S rRNA burden (right). Data courtesy of Nick Walter, Brendan Podell, and Greg Robertson.

4.2.2 Using the ULD model as a platform for pre-clinical vaccine testing

Our results using BCG in **Chapter 2** demonstrate that the ULD model can assess parameters of protection more relevant to clinical TB outcomes than transient reduction in bacterial burden. If mechanisms of protection can only be revealed using a physiologic ULD challenge model (as shown in **Chapter 3**), then it is critical to test vaccine candidates in a platform that will be able to sensitively measure these protective parameters. Thus, this work was foundational for establishing the ULD model as a platform for pre-clinical vaccine testing.

There are too many TB vaccine candidates in the pipeline to feasibly test all of them in NHP models or clinical trials. Therefore, it is essential to have a reliable pre-clinical platform that can identify the most promising candidates efficiently and cost-effectively. We have begun working with the Gates Foundation to test new vaccine candidates developed by biotechnology companies with promising results. We have also recently received funding to become a pre-clinical vaccine testing site. It is encouraging that this thesis work has the potential to accelerate the advancement of promising TB vaccine candidates into human clinical trials.

4.2.3 Dissecting types of CD8+ cells that contribute to BCG-mediated protection

In **Chapter 3**, we discovered that while CD4 T cells played major roles in control of lung burden and prevention of dissemination, CD8 T cells played a minor role in control of lung burden and a major role in prevention of infection. Naturally, the next question to answer is, what types of CD8+ cells could be responsible for this phenotype? We think a role for CD8 T cells in preventing infection of Mtb strains would happen early before robust Mtb replication occurs and hypothesize that innate-like non-classical CD8 T cells could be responsible.

In the CD8 depletion experiments, we confirmed by flow cytometry that CD8+ cDCs and effector CD4 T cells were not significantly depleted, ruling out the possibility that CD8+ cDCs directly or indirectly via CD4 T cells were responsible for this protection. However, we did not

include markers to look at other immune cell types that could express CD8. We therefore performed a flow cytometry experiment with unvaccinated or BCG vaccinated mice infected with CD Mtb and harvested at day 12 p.i. to explore BCG-induced immune cells that are responding early after infection (**Figure 4.2**). We included markers to look at NK cells and unconventional cell types including $\gamma\delta$ T cells, NKTs, and MAIT cells. We used a CD1d tetramer to identify NKTs and MR1 tetramer to identify MAIT cells. For each cell type, we looked at the numbers of overall IV- cells in the lung and found that BCG vaccinated mice had an increase in overall numbers of NK cells, $\gamma\delta$ T cells, NKTs, but not MAIT cells (**Figure 4.2**) and is consistent with the data from the scRNAseq experiment (**Figure 3.3**).

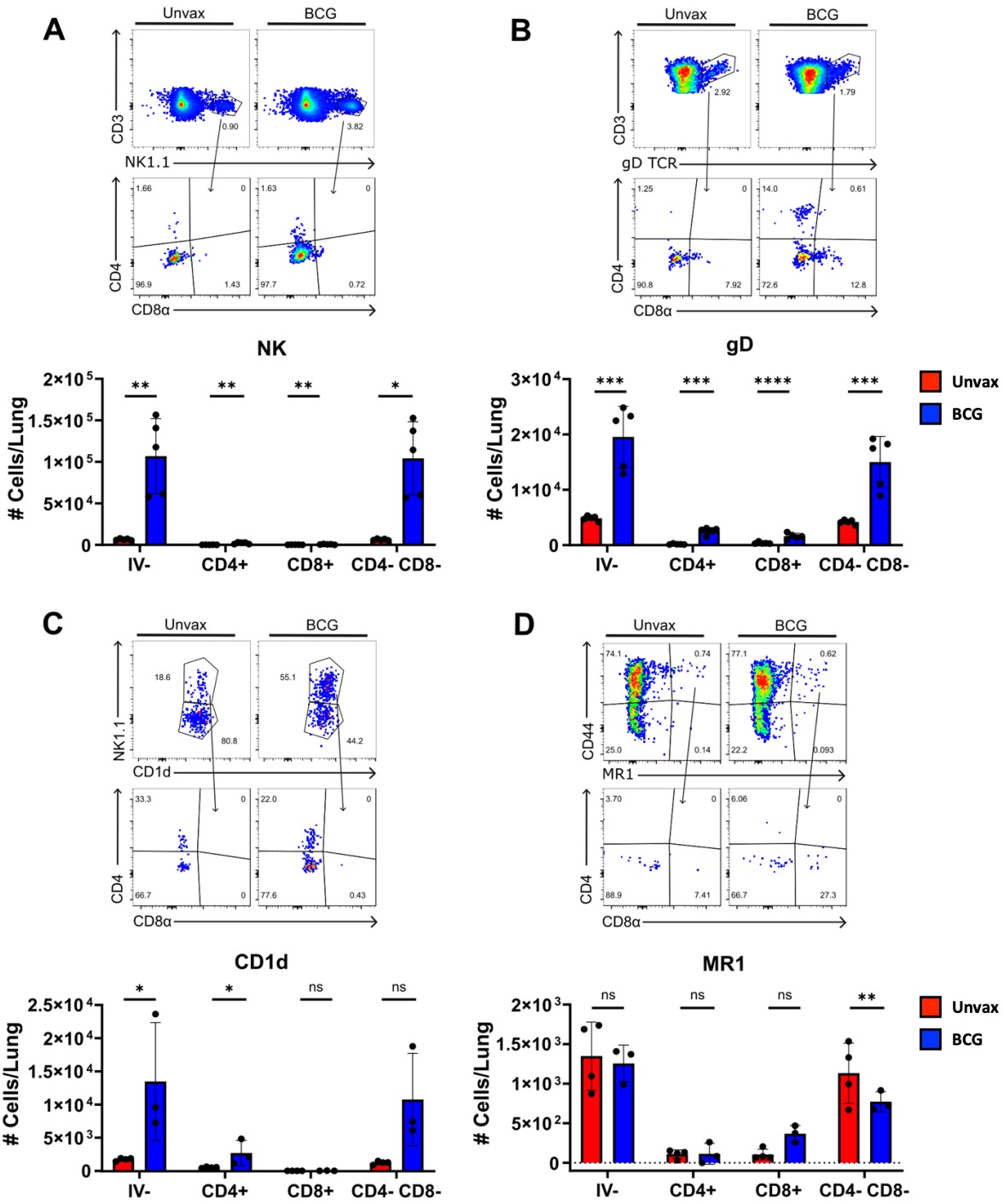

Figure 4. 2. BCG induces few CD4 or CD8-expressing innate-like cells responding early after Mtb infection. Unvaccinated or BCG vaccinated B6 mice were infected with CD mCherry-expressing H37Rv and lungs were harvested at day 12p.i. for flow cytometry analysis. Representative flow cytometry plots and quantification of IV- cells, CD4+ cells, CD8+ cells, and CD4- CD8- double negative (DN) cells for NK cells **(A)**, $\gamma\delta$ T cells **(B)**, CD1d-restricted NKT cells **(C)**, or MR1-restricted MAIT cells **(D)**. NK cell prior gating: lymphocytes, single cells, IV- live. $\gamma\delta$ T cell prior gating: lymphocytes, single cells, live, CD3+ dump-, IV-, $\gamma\delta$ TCR+. CD1d NKT prior gating: lymphocytes, single cells, live, CD3+ dump-, IV-, TCRb+, CD44+ CD1d+. MR1 MAIT prior gating: lymphocytes, single cells, live, CD3+ dump-, IV-, TCRb+. Significance was determined using unpaired t-test on GraphPad Prism. ns = not significant, *p<0.05, **p<0.01, ***p<0.001, ****p<0.0001.

We then determined which cells expressed CD4, CD8, or were double negative. BCG vaccinated mice had significantly more CD4+ NK cells and CD4+ $\gamma\delta$ cells (**Figure 4.2A-B**). There was also a trend towards more CD4+ CD1d-restricted NKTs that was not significant and there was no difference in the numbers of CD4+ MR1-restricted MAIT cells (**Figure 4.2C-D**). BCG vaccinated mice had significantly more CD8+ NK cells, CD8+ $\gamma\delta$ cells, and CD8+ MR1-restricted MAIT cells (**Figure 4.2A-C**). Interestingly, there were very few CD8+ CD1d-restricted NKTs regardless of vaccination (**Figure 4.2D**). It is important to note that the majority of each cell type were double negative, and there were only a few hundred to a few thousand of the single positive CD4+ or CD8+ cells (**Figure 4.2**). To our knowledge there is no known functional differences between the cells in these populations that express CD8 and those that do not. Thus, while we cannot rule out distinct immune contributions of the CD8-expressing cells within these innate populations, the fact that most of these cells do not express CD8 suggests that these cells are unlikely to be responsible for the protection revealed by CD8 depletion.

Next, we wanted to determine if non-classical CD8 T cells could be induced by BCG early after Mtb infection. Through the NIH tetramer facility, we obtained tetramers specific for the non-classically restricted H2M3 and Qa-1 CD8 T cells, two types of MHC Ib restricted CD8 T cells in mice. We found that BCG induces a larger population of H2M3-restricted CD8 T cells, and a smaller population of Qa-1 restricted CD8 T cells that respond to early lung infection after Mtb challenge (**Figure 4.3A**). In future work, we will further dissect the roles of classical versus non-classical CD8 T cells in BCG-mediated prevention of infection by taking advantage of H-2 $K^bD^{b-/-}$ mice that are deficient in classical MHC Ia restricted CD8 T cells but retain their non-classical MHC Ib restricted CD8 T cells. We confirmed in this flow cytometry experiment that the $K^bD^{b-/-}$ mice lack classically restricted TB10.4+ CD8 T cells even after BCG vaccination and that BCG induces both H2M3 and Qa-1 restricted CD8 T cells (**Figure 4.3B**). Future work will compare unvaccinated and BCG vaccinated $K^bD^{b-/-}$ mice infected with bar-coded ULD Mtb that are non-depleted or depleted with CD8 antibody to determine if BCG-induced non-classical CD8

T cells are required for prevention of infection, restriction of dissemination, and control of bacterial burden.

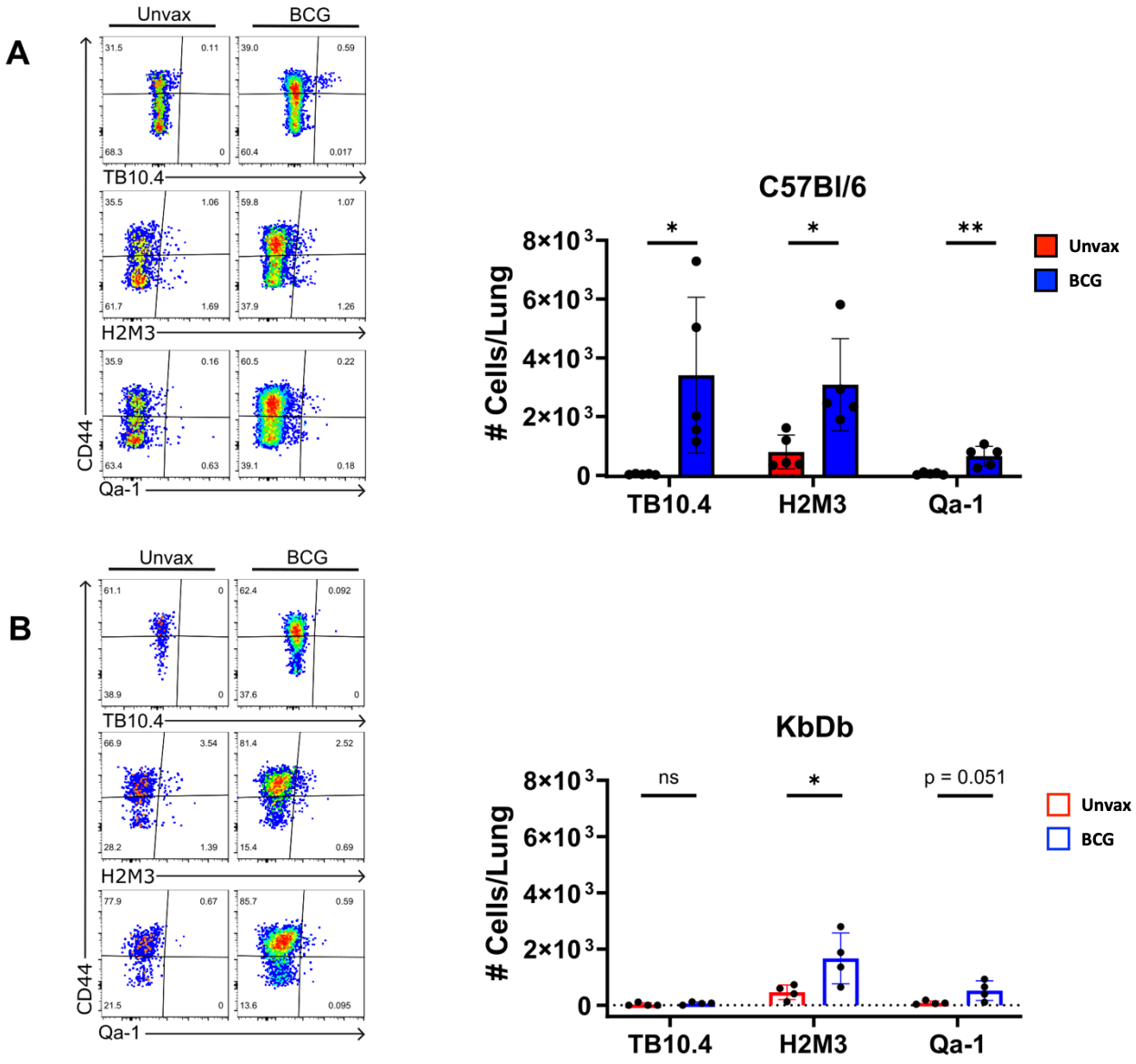

Figure 4. 3. BCG induces non-classical CD8 T responding early after Mtb infection in B6 and KbDb mice. Unvaccinated or BCG vaccinated B6 or $K^bD^{b-/-}$ mice were infected with CD mCherry-expressing H37Rv and lungs were harvested at day 12p.i. for flow cytometry analysis. Representative flow cytometry plots and quantification of TB10.4+, H2M3+, or Qa-1+ CD8 T cells for wild-type B6 mice **(A)** or $K^bD^{b-/-}$ mice **(B)**. Prior gating: lymphocytes, single cells, live, CD3+ dump-, IV-, TCRb+, and CD8a+ CD4-. Significance was determined using unpaired t-test on GraphPad Prism. ns = not significant, *p<0.05, **p<0.01.

4.3 Concluding remarks

Taking a step back, it is incredible that BCG, one of the oldest vaccines, has been used for over 100 years and is still widely administered at birth today because of its efficacy at preventing disseminated disease in infants and during childhood. Even so, TB immunity is complex and clearly BCG is not sufficient for reducing the global TB burden and the overall rates of mortality. New more effective TB vaccines are urgently needed, either to be used in conjunction with BCG or to boost BCG efficacy. Therefore, while BCG is an old vaccine, it is still highly relevant today, and it is crucial now more than ever to study BCG-mediated immunity to understand how to improve vaccine-mediated responses to better target clinically relevant TB outcomes.

The research in this dissertation highlights two important outcomes. First, this work used the ULD murine challenge model to identify novel parameters of vaccine-mediated protection including prevention of detectable infection, which has never been shown before in mice. Further, these findings set the stage for using the ULD model as a pre-clinical vaccine testing platform to accelerate testing and identification of the most promising vaccine candidates that should go to clinical trials. Second, this research uncovered distinct roles of CD4 and CD8 T cells in vaccine-mediated immunity against Mtb. Vaccine-induced CD8 T cells play a major role in prevention of infection and a minor role in control of lung burden while CD4 T cells play major roles in control of lung burden and BCG-mediated prevention of dissemination to the contralateral lung. These data could help identify immune responses that vaccine candidates should target and improve upon for better protection. Overall, the findings from this dissertation could therefore be key to accomplishing the larger goal of designing and accelerating the advancement of an effective TB vaccine.

References

1. WHO. 2024. Global Tuberculosis Report 2023: 1. TB disease burden, *on* WHO. https://www.who.int/teams/global-tuberculosis-programme/tb-reports/global-tuberculosis-report-2023/tb-disease-burden. Accessed September 19.
2. Butkeviciute E, Jones CE, Smith SG. 2018. Heterologous effects of infant BCG vaccination: potential mechanisms of immunity. Future microbiology 13:1193-1208.
3. Luca S, Mihaescu T. 2013. History of BCG Vaccine. Mædica 8:53-58.
4. Trunz BB, Fine PEM, Dye C. 2006. Effect of BCG vaccination on childhood tuberculous meningitis and miliary tuberculosis worldwide: a meta-analysis and assessment of cost-effectiveness. The Lancet (British edition) 367:1173-1180.
5. Colditz GA, Brewer TF, Berkey CS, Wilson ME, Burdick E, Fineberg HV, Mosteller F. 1994. Efficacy of BCG Vaccine in the Prevention of Tuberculosis: Meta-analysis of the Published Literature. JAMA : the journal of the American Medical Association 271:698-702.
6. Fine PEM. 1989. The BCG Story: Lessons from the Past and Implications for the Future. Reviews of infectious diseases 11:S353-S359.
7. Aronson NE, Santosham M, Comstock GW, Howard RS, Moulton LH, Rhoades ER, Harrison LH. 2004. Long-term Efficacy of BCG Vaccine in American Indians and Alaska Natives: A 60-Year Follow-up Study. JAMA : the journal of the American Medical Association 291:2086-2091.
8. Trauer JM, Kawai A, Coussens AK, Datta M, Williams BM, McBryde ES, Ragonnet R. 2021. Timing of Mycobacterium tuberculosis exposure explains variation in BCG effectiveness: a systematic review and meta-analysis. Thorax 76:1131-1141.
9. Dockrell HM, Smith SG. 2017. What Have We Learnt about BCG Vaccination in the Last 20 Years? Frontiers in immunology 8:1134-1134.
10. Vynnycky E, Fine PEM. 2000. Lifetime Risks, Incubation Period, and Serial Interval of Tuberculosis. American journal of epidemiology 152:247-263.
11. Behr MA, Kaufmann E, Duffin J, Edelstein PH, Ramakrishnan L. 2021. Latent Tuberculosis: Two Centuries of Confusion. American journal of respiratory and critical care medicine 204:142-148.
12. Behr MA, Edelstein PH, Ramakrishnan L. 2019. Is Mycobacterium tuberculosis infection life long? BMJ (Online) 367:l5770-l5770.
13. Coussens AK, Zaidi SMA, Allwood BA, Dewan PK, Gray G, Kohli M, Kredo T, Marais BJ, Marks G, Martinez L, Ruhwald M, Scriba TJ, Seddon JA, Tisile P, Warner DF, Wilkinson RJ, Esmail H, Houben RMGJ. 2024. International consensus classification of early tuberculosis states to guide research for improved care and prevention: A Delphi exercise. The lancet respiratory medicine 12:484-498.
14. CDC. 2023. Tuberculosis (TB), *on* CDC. https://www.cdc.gov/tb/about/index.html. Accessed September 19.

15. Rolo M, González-Blanco B, Reyes CA, Rosillo N, López-Roa P. 2023. Epidemiology and factors associated with Extra-pulmonary tuberculosis in a Low-prevalence area. Journal of clinical tuberculosis and other mycobacterial diseases 32:100377-100377.
16. Wells WF, Ratcliffe HL, Grumb C. 1948. On the mechanics of droplet nuclei infection; quantitative experimental air-borne tuberculosis in rabbits. American journal of hygiene 47:11-28.
17. Cohen SB, Gern BH, Delahaye JL, Adams KN, Plumlee CR, Winkler JK, Sherman DR, Gerner MY, Urdahl KB. 2018. Alveolar Macrophages Provide an Early Mycobacterium tuberculosis Niche and Initiate Dissemination. Cell Host & Microbe 24:439-446.e4.
18. Hussell T, Bell TJ. 2014. Alveolar macrophages: plasticity in a tissue-specific context. Nature reviews Immunology 14:81-93.
19. Zhai W, Wu F, Zhang Y, Fu Y, Liu Z. 2019. The Immune Escape Mechanisms of Mycobacterium Tuberculosis. International journal of molecular sciences 20:340.
20. Corleis B, Dorhoi A. 2020. Early dynamics of innate immunity during pulmonary tuberculosis. Immunology letters 221:56-60.
21. Blomgran R, Ernst JD. 2011. Lung Neutrophils Facilitate Activation of Naive Antigen-Specific CD4+ T Cells during Mycobacterium tuberculosis Infection. The Journal of immunology (1950) 186:7110-7119.
22. Dallenga T, Repnik U, Corleis B, Eich J, Reimer R, Griffiths GW, Schaible UE. 2017. M. tuberculosis-Induced Necrosis of Infected Neutrophils Promotes Bacterial Growth Following Phagocytosis by Macrophages. Cell host & microbe 22:519-530.e3.
23. Nouailles G, Dorhoi A, Koch M, Zerrahn J, Weiner J, Fae KC, Arrey F, Kuhlmann S, Bandermann SI, Loewe D, Mollenkopf H-J, Vogelzang A, Meyer-Schwesinger C, Mittrucker H-W, McEwen G, Kaufmann SHE. 2014. CXCL5-secreting pulmonary epithelial cells drive destructive neutrophilic inflammation in tuberculosis. The Journal of clinical investigation 124:1268-1282.
24. Ozaki T, Nakahira S, Tani K, Ogushi F, Yasuoka S, Ogura T. 1992. Differential Cell Analysis in Bronchoalveolar Lavage Fluid from Pulmonary Lesions of Patients with Tuberculosis. Chest 102:54-59.
25. Gern BH, Klas JM, Foster KA, Cohen SB, Plumlee CR, Duffy FJ, Neal ML, Halima M, Gustin AT, Diercks AH, Aderem A, Gale M, Aitchison JD, Gerner MY, Urdahl KB. 2024. CD4-mediated immunity shapes neutrophil-driven tuberculous pathology. Cold Spring Harbor Laboratory.
26. Cohen SB, Gern BH, Urdahl KB. 2022. The Tuberculous Granuloma and Preexisting Immunity. Annual review of immunology 40:589-614.
27. Tsai MC, Chakravarty S, Zhu G, Xu J, Tanaka K, Koch C, Tufariello J, Flynn J, Chan J. 2006. Characterization of the tuberculous granuloma in murine and human lungs: cellular composition and relative tissue oxygen tension. Cellular microbiology 8:218-232.
28. Ulrichs T, Kosmiadi GA, Trusov V, Jörg S, Pradl L, Titukhina M, Mishenko V, Gushina N, Kaufmann SHE. 2004. Human tuberculous granulomas induce peripheral

lymphoid follicle-like structures to orchestrate local host defence in the lung. The Journal of pathology 204:217-228.
29. Gern BH, Adams KN, Plumlee CR, Stoltzfus CR, Shehata L, Moguche AO, Busman-Sahay K, Hansen SG, Axthelm MK, Picker LJ, Estes JD, Urdahl KB, Gerner MY. 2021. TGFβ restricts expansion, survival, and function of T cells within the tuberculous granuloma. Cell host & microbe 29:594-606.e6.
30. Kauffman KD, Sallin MA, Sakai S, Kamenyeva O, Kabat J, Weiner D, Sutphin M, Schimel D, Via L, Barry CE, Wilder-Kofie T, Moore I, Moore R, Barber DL. 2018. Defective positioning in granulomas but not lung-homing limits CD4 T-cell interactions with Mycobacterium tuberculosis-infected macrophages in rhesus macaques. Mucosal immunology 11:462-473.
31. Ramakrishnan L. 2012. Revisiting the role of the granuloma in tuberculosis. Nature reviews Immunology 12:352-366.
32. Urdahl KB, Shafiani S, Ernst JD. 2011. Initiation and regulation of T-cell responses in tuberculosis. Mucosal Immunology 4:288-293.
33. Gallegos AM, Pamer EG, Glickman MS. 2008. Delayed protection by ESAT-6-specific effector CD4(+) T cells after airborne M-tuberculosis infection. The Journal of experimental medicine 205:2359-2368.
34. Reiley WW, Calayag MD, Wittmer ST, Huntington JL, Pearl JE, Fountain JJ, Martino CA, Roberts AD, Cooper AM, Winslow GM, Woodland DL. 2008. ESAT-6-specific CD4 T cell responses to aerosol Mycobacterium tuberculosis infection are initiated in the mediastinal lymph nodes. Proceedings of the National Academy of Sciences - PNAS 105:10961-10966.
35. Wolf AJ, Desvignes L, Linas B, Banaiee N, Tamura T, Takatsu K, Ernst JD. 2008. Initiation of the adaptive immune response to Mycobacterium tuberculosis depends on antigen production in the local lymph node, not the lungs. The Journal of experimental medicine 205:105-115.
36. Chandra P, Grigsby SJ, Philips JA. 2022. Immune evasion and provocation by Mycobacterium tuberculosis. Nature Reviews Microbiology 20:750-766.
37. Flory CM, Hubbard RD, Collins FM. 1992. Effects of in vivo T lymphocyte subset depletion on mycobacterial infections in mice. Journal of leukocyte biology 51:225-229.
38. Mogues T, Goodrich ME, Ryan L, LaCourse R, North RJ. 2001. The relative importance of T cell subsets in immunity and immunopathology of Airborne Mycobacterium tuberculosis infection in mice. The Journal of experimental medicine 193:271-280.
39. Esmail H, Riou C, du Bruyn E, Lai RP-J, Harley YXR, Meintjes G, Wilkinson KA, Wilkinson RJ. 2018. The Immune Response to Mycobacterium tuberculosis in HIV-1-Coinfected Persons. Annual review of immunology 36:603-638.
40. Lyadova IV, Panteleev AV. 2015. Th1 and Th17 Cells in Tuberculosis: Protection, Pathology, and Biomarkers. Mediators of Inflammation 2015:1-13.
41. Boisson-Dupuis S, Bustamante J, El-Baghdadi J, Camcioglu Y, Parvaneh N, El Azbaoui S, Agader A, Hassani A, El Hafidi N, Mrani NA, Jouhadi Z, Ailal F, Najib J, Reisli I, Zamani A, Yosunkaya S, Gulle-Girit S, Yildiran A, Cipe FE, …, Abel L. 2015.

Inherited and acquired immunodeficiencies underlying tuberculosis in childhood. Immunological reviews 264:103-120.
42. Flynn JL, Chan J, Triebold KJ, Dalton DK, Stewart TA, Bloom BR. 1993. An essential role for interferon γ in resistance to Mycobacterium tuberculosis infection. The Journal of experimental medicine 178:2249-2254.
43. Pearl JE, Saunders B, Ehlers S, Orme IM, Cooper AM. 2001. Inflammation and Lymphocyte Activation during Mycobacterial Infection in the Interferon-γ-Deficient Mouse. Cellular immunology 211:43-50.
44. Kagina BMN, Abel B, Scriba TJ, Hughes EJ, Keyser A, Soares A, Gamieldien H, Sidibana M, Hatherill M, Gelderbloem S, Mahomed H, Hawkridge A, Hussey G, Kaplan G, Hanekom WA. 2010. Specific T Cell Frequency and Cytokine Expression Profile Do Not Correlate with Protection against Tuberculosis after Bacillus Calmette-Guerin Vaccination of Newborns. American journal of respiratory and critical care medicine 182:1073-1079.
45. Majlessi L, Simsova M, Jarvis Z, Brodin P, Rojas M-Js, Bauche Cc, Nouzé Cm, Ladant D, Cole ST, Sebo P, Leclerc C. 2006. Increase in Antimycobacterial Th1-Cell Responses by Prime-Boost Protocols of Immunization Does Not Enhance Protection against Tuberculosis. Infection and Immunity 74:2128-2137.
46. Mittrücker H-W, Steinhoff U, Köhler A, Krause M, Lazar D, Mex P, Miekley D, Kaufmann SHE. 2007. Poor correlation between BCG vaccination-induced T cell responses and protection against tuberculosis. Proceedings of the National Academy of Sciences - PNAS 104:12434-12439.
47. Tameris M, Geldenhuys H, Luabeya AK, Smit E, Hughes JE, Vermaak S, Hanekom WA, Hatherill M, Mahomed H, McShane H, Scriba TJ. 2014. The Candidate TB Vaccine, MVA85A, Induces Highly Durable Th1 Responses. PloS one 9:e87340-e87340.
48. Cowley SC, Elkins KL. 2003. CD4(+) T cells mediate IFN-gamma-independent control of Mycobacterium tuberculosis infection both in vitro and in vivo. The Journal of immunology (1950) 171:4689-4699.
49. Gallegos AM, van Heijst JWJ, Samstein M, Su X, Pamer EG, Glickman MS. 2011. A Gamma Interferon Independent Mechanism of CD4 T Cell Mediated Control of M. tuberculosis Infection in vivo. PLoS pathogens 7:e1002052.
50. Van Dis E, Fox DM, Morrison HM, Fines DM, Babirye JP, McCann LH, Rawal S, Cox JS, Stanley SA. 2022. IFN-[gamma]-independent control of M. tuberculosis requires CD4 T cell-derived GM-CSF and activation of HIF-1[alpha]. PLoS pathogens 18:e1010721.
51. Maciag K, Plumlee CR, Cohen SB, Gern BH, Urdahl KB. 2024. Reappraising the Role of T Cell–Derived IFN-γ in Restriction of Mycobacterium tuberculosis in the Murine Lung. The Journal of immunology (1950) 213:339-346.
52. Yuk J-M, Kim JK, Kim IS, Jo E-K. 2024. TNF in Human Tuberculosis: A Double-Edged Sword. Immune network 24:e4-e4.
53. Sharma S, Kalia NP, Suden P, Chauhan PS, Kumar M, Ram AB, Khajuria A, Bani S, Khan IA. 2014. Protective efficacy of piperine against Mycobacterium tuberculosis. Tuberculosis (Edinburgh, Scotland) 94:389-396.

54. Tan Y, Tan Y, Li J, Hu P, Guan P, Kuang H, Liang Q, Yu Y, Chen Z, Wang Q, Yang Z, AiKeReMu D, Pang Y, Liu J. 2021. Combined IFN-γ and IL-2 release assay for detect active pulmonary tuberculosis: a prospective multicentre diagnostic study in China. Journal of translational medicine 19:289-289.
55. Aagaard C, Hoang TTKT, Izzo A, Billeskov R, Troudt J, Arnett K, Keyser A, Elvang T, Andersen P, Dietrich J. 2009. Protection and Polyfunctional T Cells Induced by Ag85B-TB10.4/IC31 (R) against Mycobacterium tuberculosis Is Highly Dependent on the Antigen Dose. PloS one 4:e5930-e5930.
56. Marín ND, París SC, Rojas M, García LF. 2013. Functional profile of CD4+ and CD8+ T cells in latently infected individuals and patients with active TB. Tuberculosis (Edinburgh, Scotland) 93:155-166.
57. Caccamo N, Guggino G, Joosten SA, Gelsomino G, Di Carlo P, Titone L, Galati D, Bocchino M, Matarese A, Salerno A, Sanduzzi A, Franken WPJ, Ottenhoff THM, Dieli F. 2010. Multifunctional $CD4^+$ T cells correlate with active Mycobacterium tuberculosis infection. European journal of immunology 40:2211-2220.
58. Day CL, Abrahams DA, Lerumo L, van Rensburg EJ, Stone L, O'Rie T, Pienaar B, de Kock M, Kaplan G, Mahomed H, Dheda K, Hanekom WA. 2011. Functional Capacity of Mycobacterium tuberculosis-Specific T Cell Responses in Humans Is Associated with Mycobacterial Load. The Journal of immunology (1950) 187:2222-2232.
59. Pantaleo G, Harari A, Rozot V, Enders FB, Perreau M, Stalder JM, Nicod LP, Cavassini M, Calandra T, Blanchet CL, Jaton K, Faouzi M, Day CL, Hanekom WA, Bart P-A. 2011. Dominant TNF-α + Mycobacterium tuberculosis -specific CD4 + T cell responses discriminate between latent infection and active disease. Nature medicine 17:372-376.
60. Qiu Z, Zhang M, Zhu Y, Zheng F, Lu P, Liu H, Graner MW, Zhou B, Chen X. 2012. Multifunctional CD4 T Cell Responses in Patients with Active Tuberculosis. Scientific reports 2:216.
61. Lindenstrom T, Knudsen NPH, Agger EM, Andersen P. 2013. Control of Chronic Mycobacterium tuberculosis Infection by CD4 KLRG1(-) IL-2-Secreting Central Memory Cells. The Journal of immunology (1950) 190:6311-6319.
62. Woodworth JS, Aagaard CS, Hansen PR, Cassidy JP, Agger EM, Andersen P. 2014. Protective CD4 T Cells Targeting Cryptic Epitopes of Mycobacterium tuberculosis Resist Infection-Driven Terminal Differentiation. The Journal of immunology (1950) 192:3247-3258.
63. Anderson KG, Mayer-Barber K, Sung H, Beura L, James BR, Taylor JJ, Qunaj L, Griffith TS, Vezys V, Barber DL, Masopust D. 2014. Intravascular staining for discrimination of vascular and tissue leukocytes. Nature protocols 9:209-222.
64. Sakai S, Kauffman KD, Schenkel JM, McBerry CC, Mayer-Barber KD, Masopust D, Barber DL. 2014. Cutting Edge: Control of Mycobacterium tuberculosis Infection by a Subset of Lung Parenchyma-Homing CD4 T Cells. The Journal of immunology (1950) 192:2965-2969.
65. Moguche AO, Shafiani S, Clemons C, Larson RP, Dinh C, Higdon LE, Cambier CJ, Sissons JR, Gallegos AM, Fink PJ, Urdahl KB. 2015. ICOS and Bcl6-dependent

pathways maintain a CD4 T cell population with memory-like properties during tuberculosis. Journal of Experimental Medicine 212:715-728.
66. Derrick SC, Yabe IM, Yang A, Morris SL. 2011. Vaccine-induced anti-tuberculosis protective immunity in mice correlates with the magnitude and quality of multifunctional CD4 T cells. Vaccine 29:2902-2909.
67. Forbes EK, Sander C, Ronan EO, McShane H, Hill AVS, Beverley PCL, Tchilian EZ. 2008. Multifunctional, High-Level Cytokine-Producing Th1 Cells in the Lung, but Not Spleen, Correlate with Protection against Mycobacterium tuberculosis Aerosol Challenge in Mice. The Journal of immunology (1950) 181:4955-4964.
68. Lindenstrom T, Agger EM, Korsholm KS, Darrah PA, Aagaard C, Seder RA, Rosenkrands I, Andersen P. 2009. Tuberculosis Subunit Vaccination Provides Long-Term Protective Immunity Characterized by Multifunctional CD4 Memory T Cells. The Journal of immunology (1950) 182:8047-8055.
69. Ballester M, Nembrini C, Dhar N, de Titta A, de Piano C, Pasquier M, Simeoni E, van der Vlies AJ, McKinney JD, Hubbell JA, Swartz MA. 2011. Nanoparticle conjugation and pulmonary delivery enhance the protective efficacy of Ag85B and CpG against tuberculosis. Vaccine 29:6959-6966.
70. Yuan X, Teng X, Jing Y, Ma J, Tian M, Yu Q, Zhou L, Wang R, Wang W, Li L, Fan X. 2015. live attenuated BCG vaccine overexpressing multistage antigens Ag85B and HspX provides superior protection against Mycobacterium tuberculosis infection. Applied microbiology and biotechnology 99:10587-10595.
71. Clemmensen HS, Knudsen NPH, Billeskov R, Rosenkrands I, Jungersen G, Aagaard C, Andersen P, Mortensen R. 2020. Rescuing ESAT-6 Specific CD4 T Cells From Terminal Differentiation Is Critical for Long-Term Control of Murine Mtb Infection. Frontiers in Immunology 11.
72. Torrado E, Cooper AM. 2010. IL-17 and Th17 cells in tuberculosis. Cytokine & growth factor reviews 21:455-462.
73. Gopal R, Rangel-Moreno J, Slight S, Lin Y, Nawar HF, Fallert Junecko BA, Reinhart TA, Kolls J, Randall TD, Connell TD, Khader SA. 2013. Interleukin-17-dependent CXCL13 mediates mucosal vaccine–induced immunity against tuberculosis. Mucosal Immunology 6:972-984.
74. Khader SA, Bell GK, Pearl JE, Fountain JJ, Rangel-Moreno J, Cilley GE, Shen F, Eaton SM, Gaffen SL, Swain SL, Locksley RM, Haynes L, Randall TD, Cooper AM. 2007. IL-23 and IL-17 in the establishment of protective pulmonary CD4+ T cell responses after vaccination and during Mycobacterium tuberculosis challenge. Nature Immunology 8:369-377.
75. Nikitina IY, Panteleev AV, Kosmiadi GA, Serdyuk YV, Nenasheva TA, Nikolaev AA, Gorelova LA, Radaeva TV, Kiseleva YY, Bozhenko VK, Lyadova IV. 2018. Th1, Th17, and Th1Th17 Lymphocytes during Tuberculosis: Th1 Lymphocytes Predominate and Appear as Low-Differentiated CXCR3(+)CCR6(+) Cells in the Blood and Highly Differentiated CXCR3(+/-) CCR6(-) Cells in the Lungs. The Journal of immunology (1950) 200:2090-2103.
76. Rakshit S, Ahmed A, Adiga V, Sundararaj BK, Sahoo PN, Kenneth J, D'Souza G, Bonam W, Johnson C, Franken KL, Ottenhoff TH, Finak G, Gottardo R, Stuart KD, De

Rosa SC, McElrath MJ, Vyakarnam A. 2019. BCG revaccination boosts adaptive polyfunctional Th1/Th17 and innate effectors in IGRA+ and IGRA- Indian adults. JCI insight 4.
77. Shanmugasundaram U, Bucsan AN, Ganatra SR, Ibegbu C, Quezada M, Blair RV, Alvarez X, Velu V, Kaushal D, Rengarajan J. 2020. Pulmonary Mycobacterium tuberculosis control associates with CXCR3- and CCR6-expressing antigen-specific Th1 and Th17 cell recruitment. JCI insight 5.
78. Leal IS, Smedegård B, Andersen P, Appelberg R. 2001. Failure to induce enhanced protection against tuberculosis by increasing T-cell-dependent interferon-γ generation. Immunology 104:157-161.
79. Elias D, Akuffo H, Britton S. 2005. PPD induced in vitro interferon gamma production is not a reliable correlate of protection against Mycobacterium tuberculosis. Transactions of the Royal Society of Tropical Medicine and Hygiene 99:363-368.
80. Lin PL, Flynn JL. 2015. CD8 T cells and Mycobacterium tuberculosis infection. Seminars in Immunopathology 37:239-249.
81. Stenger S, Hanson DA, Teitelbaum R, Dewan P, Niazi KR, Froelich CJ, Ganz T, Thoma-Uszynski S, Melián A, Bogdan C, Porcelli SA, Bloom BR, Krensky AM, Modlin RL. 1998. An Antimicrobial Activity of Cytolytic T Cells Mediated by Granulysin. Science (American Association for the Advancement of Science) 282:121-125.
82. Woodworth JS, Wu Y, Behar SM. 2008. Mycobacterium tuberculosis-Specific CD8+ T Cells Require Perforin to Kill Target Cells and Provide Protection In Vivo. The Journal of Immunology 181:8595-8603.
83. Silva BDdS, Trentini MM, da Costa AC, Kipnis A, Junqueira-Kipnis AP. 2014. Different phenotypes of CD8+ T cells associated with bacterial load in active tuberculosis. Immunology letters 160:23-32.
84. Cooper AM, Dsouza C, Frank AA, Orme IM. 1997. The course of Mycobacterium tuberculosis infection in the lungs of mice lacking expression of either perforin- or granzyme-mediated cytolytic mechanisms. Infection and Immunity 65:1317-1320.
85. Laochumroonvorapong P, Wang J, Liu CC, Ye WG, Moreira AL, Elkon KB, Freedman VH, Kaplan G. 1997. Perforin, a cytotoxic molecule which mediates cell necrosis, is not required for the early control of mycobacterial infection in mice. Infection and Immunity 65:127-132.
86. Behar SM, Dascher CC, Grusby MJ, Wang CR, Brenner MB. 1999. Susceptibility of mice deficient in CD1D or TAP1 to infection with Mycobacterium tuberculosis. The Journal of experimental medicine 189:1973-1980.
87. Joosten SA, Ottenhoff THM, Lewinsohn DM, Hoft DF, Moody DB, Seshadri C. 2019. Harnessing donor unrestricted T-cells for new vaccines against tuberculosis. Vaccine 37:3022-3030.
88. Kerksiek KM, Busch DH, Pilip IM, Allen SE, Pamer EG. 1999. H2-M3-restricted T cells in bacterial infection: Rapid primary but diminished memory responses. The Journal of experimental medicine 190:195-204.
89. Jensen PE, Sullivan BA, Reed-Loisel LM, Weber DA. 2004. Qa-1, a nonclassical class I histocompatibility molecule with roles in innate and adaptive immunity. Immunologic research 29:81-92.

90. Zeng L, Sullivan LC, Vivian JP, Walpole NG, Harpur CM, Rossjohn J, Clements CS, Brooks AG. 2012. A Structural Basis for Antigen Presentation by the MHC Class Ib Molecule, Qa-1b. The Journal of immunology (1950) 188:302-310.
91. Braud VM, Allan DSJ, O'Callaghan CA, Söderström K, D'Andrea A, Ogg GS, Lazetic S, Young NT, Bell JI, Phillips JH, Lanier LL, McMichael AJ. 1998. HLA-E binds to natural killer cell receptors CD94/NKG2A, B and C. Nature (London) 391:795-799.
92. Cotterill LA, Stauss HJ, Millrain MM, Pappin DJC, Rahman D, Canas B, Chandler P, Stackpoole A, Simpson E, Robinson PJ, Dyson PJ. 1997. Qa-1 interaction and T cell recognition of the Qa-1 determinant modifier peptide. European journal of immunology 27:2123-2132.
93. Borrego F, Ulbrecht M, Weiss EH, Coligan JE, Brooks AG. 1998. Recognition of human histocompatibility leukocyte antigen (HLA)-E complexed with HLA class I signal sequence-derived peptides by CD94/NKG2 confers protection from natural killer cell-mediated lysis. The Journal of experimental medicine 187:813-818.
94. McMurtrey C, Harriff MJ, Swarbrick GM, Duncan A, Cansler M, Null M, Bardet W, Jackson KW, Lewinsohn DA, Hildebrand W, Lewinsohn DM. 2017. T cell recognition of Mycobacterium tuberculosis peptides presented by HLA-E derived from infected human cells. PloS one 12:e0188288-e0188288.
95. La Manna MP, Orlando V, Prezzemolo T, Di Carlo P, Cascio A, Delogu G, Poli G, Sullivan LC, Brooks AG, Dieli F, Caccamo N. 2020. HLA-E-restricted CD8 + T Lymphocytes Efficiently Control Mycobacterium tuberculosis and HIV-1 Coinfection. American journal of respiratory cell and molecular biology 62:430-439.
96. Bian Y, Shang S, Siddiqui S, Zhao J, Joosten SA, Ottenhoff THM, Cantor H, Wang C-R. 2017. MHC Ib molecule Qa-1 presents Mycobacterium tuberculosis peptide antigens to CD8+ T cells and contributes to protection against infection. PLOS Pathogens 13:e1006384.
97. Paterson RL, La Manna MP, Arena De Souza V, Walker A, Gibbs-Howe D, Kulkarni R, Fergusson JR, Mulakkal NC, Monteiro M, Bunjobpol W, Dembek M, Martin-Urdiroz M, Grant T, Barber C, Garay-Baquero DJ, Tezera LB, Lowne D, Britton-Rivet C, Pengelly R, ..., Godinho LF. 2024. An HLA-E-targeted TCR bispecific molecule redirects T cell immunity against Mycobacterium tuberculosis. Proceedings of the National Academy of Sciences - PNAS 121:e2318003121.
98. van Meijgaarden KE, Haks MC, Caccamo N, Dieli F, Ottenhoff THM, Joosten SA. 2015. Human CD8(+) T-cells Recognizing Peptides from Mycobacterium tuberculosis (Mtb) Presented by HLA-E Have an Unorthodox Th2-like, Multifunctional, Mtb Inhibitory Phenotype and Represent a Novel Human T-cell Subset. PLoS pathogens 11:e1004671-e1004671.
99. Winchell CG, Nyquist SK, Chao MC, Maiello P, Myers AJ, Hopkins F, Chase M, Gideon HP, Patel KV, Bromley JD, Simonson AW, Floyd-O'Sullivan R, Wadsworth M, Rosenberg JM, Uddin R, Hughes T, Kelly RJ, Griffo J, Tomko J, ..., Flynn JL. 2023. CD8+ lymphocytes are critical for early control of tuberculosis in macaques. Journal of Experimental Medicine 220.
100. Chen CY, Huang D, Wang RC, Shen L, Zeng G, Yao S, Shen Y, Halliday L, Fortman J, Mcallister M, Estep J, Hunt R, Vasconcelos D, Du G, Porcelli SA, Larsen MH, Jacobs

WR, Haynes BF, Letvin NL, Chen ZW. 2009. A Critical Role for CD8 T Cells in a Nonhuman Primate Model of Tuberculosis. PLoS Pathogens 5:e1000392.
101. Simonson AW, Zeppa JJ, Bucsan AN, Chao MC, Pokkali S, Hopkins F, Chase MR, Vickers AJ, Sutton MS, Winchell CG, Myers AJ, Ameel CL, Kelly R, Krouse B, Hood LE, Li J, Lehman CC, Kamath M, Tomko J, ..., Flynn JL. 2024. CD4 T cells and CD8α+ lymphocytes are necessary for intravenous BCG-induced protection against tuberculosis in macaques. Cold Spring Harbor Laboratory.
102. Macchia I, Gauduin MC, Kaur A, Johnson RP. 2006. Expression of CD8α identifies a distinct subset of effector memory CD4⁺ T lymphocytes. Immunology 119:232-242.
103. Nikonenko BV, Apt AS, Mezhlumova MB, Avdienko VG, Yeremeev VV, Moroz AM. 1996. Influence of the mouse Bcg, Tbc-1 and xid genes on resistance and immune responses to tuberculosis infection and efficacy of bacille Calmette-Guerin (BCG) vaccination. Clinical and experimental immunology 104:37-43.
104. Maglione PJ, Xu J, Chan J. 2007. B Cells Moderate Inflammatory Progression and Enhance Bacterial Containment upon Pulmonary Challenge with Mycobacterium tuberculosis. Journal of Immunology 178:7222-7234.
105. Johnson CM, Cooper AM, Frank AA, Bonorino CBC, Wysoki LJ, Orme IM. 1997. Mycobacterium tuberculosis aerogenic rechallenge infections in B cell-deficient mice. Tubercle and lung disease 78:257-261.
106. Torrado E, Fountain JJ, Robinson RT, Martino CA, Pearl JE, Rangel-Moreno J, Tighe M, Dunn R, Cooper AM. 2013. Differential and Site Specific Impact of B Cells in the Protective Immune Response to Mycobacterium tuberculosis in the Mouse. PloS one 8:e61681-e61681.
107. Phuah J, Wong EA, Gideon HP, Maiello P, Coleman MT, Hendricks MR, Ruden R, Cirrincione LR, Chan J, Lin PL, Flynn JL. 2016. Effects of B Cell Depletion on Early Mycobacterium tuberculosis Infection in Cynomolgus Macaques. Infection and immunity 84:1301-1311.
108. Atzeni F, Batticciotto A, Masala IF, Talotta R, Benucci M, Sarzi-Puttini P. 2016. Infections and Biological Therapy in Patients with Rheumatic Diseases. The Israel Medical Association journal 18:164-167.
109. Liao T-L, Lin C-H, Chen Y-M, Chang C-L, Chen H-H, Chen D-Y. 2016. Different Risk of Tuberculosis and Efficacy of Isoniazid Prophylaxis in Rheumatoid Arthritis Patients with Biologic Therapy: A Nationwide Retrospective Cohort Study in Taiwan. PloS one 11:e0153217-e0153217.
110. Benard A, Sakwa I, Schierloh P, Colom A, Mercier I, Tailleux L, Jouneau L, Boudinot P, Al-Saati T, Lang R, Rehwinkel J, Loxton AG, Kaufmann SHE, Anton-Leberre V, O'Garra A, Del Carmen Sasiain M, Gicquel B, Fillatreau S, Neyrolles O, Hudrisier D. 2018. B Cells Producing Type I IFN Modulate Macrophage Polarization in Tuberculosis. American journal of respiratory and critical care medicine 197:801-813.
111. Kondratieva TK, Rubakova EI, Linge IA, Evstifeev VV, Majorov KB, Apt AS. 2010. B Cells Delay Neutrophil Migration toward the Site of Stimulus: Tardiness Critical for

Effective Bacillus Calmette-Guerin Vaccination against Tuberculosis Infection in Mice. The Journal of immunology (1950) 184:1227-1234.
112. Kozakiewicz L, Chen Y, Xu J, Wang Y, Dunussi-Joannopoulos K, Ou Q, Flynn JL, Porcelli SA, Jr WR, Chan J. 2013. B Cells Regulate Neutrophilia during Mycobacterium tuberculosis Infection and BCG Vaccination by Modulating the Interleukin-17 Response: e1003472. PLoS pathogens 9.
113. Dubois Cauwelaert N, Baldwin SL, Orr MT, Desbien AL, Gage E, Hofmeyer KA, Coler RN. 2016. Antigen presentation by B cells guides programing of memory CD4+ T-cell responses to a TLR4-agonist containing vaccine in mice. European journal of immunology 46:2719-2729.
114. Linge I, Dyatlov A, Kondratieva E, Avdienko V, Apt A, Kondratieva T. 2017. B-lymphocytes forming follicle-like structures in the lung tissue of tuberculosis-infected mice: Dynamics, phenotypes and functional activity. Tuberculosis (Edinburgh, Scotland) 102:16-23.
115. Chen Y, Bharrhan S, Xu J, Sharma T, Wang Y, Salgame P, Zhang J, Nargan K, Steyn AJC, Maglione PJ, Chan J. 2023. B cells promote granulomatous inflammation during chronic Mycobacterium tuberculosis infection in mice. PLOS Pathogens 19:e1011187.
116. Ordoñez C, Savage HP, Tarajia M, Rivera R, Weeks-Galindo C, Sambrano D, Riley L, Fernandez PL, Baumgarth N, Goodridge A. 2018. Both B-1a and B-1b cells exposed to Mycobacterium tuberculosis lipids differentiate into IgM antibody-secreting cells. Immunology 154:613-623.
117. Kunnath-Velayudhan S, Davidow AL, Wang H-Y, Molina DM, Huynh VT, Salamon H, Pine R, Michel G, Perkins MD, Xiaowu L, Felgner PL, Flynn JL, Catanzaro A, Gennaro ML. 2012. Proteome-Scale Antibody Responses and Outcome of Mycobacterium tuberculosis Infection in Nonhuman Primates and in Tuberculosis Patients. The Journal of infectious diseases 206:697-705.
118. de L. Costello AM, Kumar A, Narayan V, Akbar MS, Ahmed S, Abou-Zeid C, Rook GAW, Stanford J, Moreno C. 1992. Does antibody to mycobacterial antigens, including lipoarabinomannan, limit dissemination in childhood tuberculosis? Transactions of the Royal Society of Tropical Medicine and Hygiene 86:686-692.
119. Rijnink WF, Ottenhoff THM, Joosten SA. 2021. B-Cells and Antibodies as Contributors to Effector Immune Responses in Tuberculosis. Frontiers in immunology 12:640168-640168.
120. Abebe F, Bjune G. 2009. protective role of antibody responses during Mycobacterium tuberculosis infection. Clinical and experimental immunology 157:235-243.
121. Armstrong JA, Hart PD. 1975. Phagosome-lysosome interactions in cultured macrophages infected with virulent tubercle bacilli. Reversal of the usual nonfusion pattern and observations on bacterial survival. The Journal of experimental medicine 142:1-16.
122. Lu LL, Suscovich TJ, Fortune SM, Alter G. 2018. Beyond binding: antibody effector functions in infectious diseases. Nature reviews Immunology 18:46-61.

123. Belay M, Legesse M, Mihret A, Ottenhoff THM, Franken KL, Bjune G, Abebe F. 2016. IFN- γ and IgA against non-methylated heparin-binding hemagglutinin as markers of protective immunity and latent tuberculosis: Results of a longitudinal study from an endemic setting. The Journal of infection 72:189-200.
124. Dijkman K, Sombroek CC, Vervenne RAW, Hofman SO, Boot C, Remarque EJ, Kocken CHM, Ottenhoff THM, Kondova I, Khayum MA, Haanstra KG, Vierboom MPM, Verreck FAW. 2019. Prevention of tuberculosis infection and disease by local BCG in repeatedly exposed rhesus macaques. Nature medicine 25:255-262.
125. Darrah PA, Zeppa JJ, Maiello P, Hackney JA, Wadsworth nMH, Hughes TK, Pokkali S, Swanson nPA, Grant NL, Rodgers MA, Kamath M, Causgrove CM, Laddy DJ, Bonavia A, Casimiro D, Lin PL, Klein E, White AG, Scanga CA, ..., Seder RA. 2020. Prevention of tuberculosis in macaques after intravenous BCG immunization. Nature (London) 577:95-102.
126. Fletcher HA, Snowden MA, Landry B, Rida W, Satti I, Harris SA, Matsumiya M, Tanner R, O'Shea MK, Dheenadhayalan V, Bogardus L, Stockdale L, Marsay L, Chomka A, Harrington-Kandt R, Manjaly-Thomas Z-R, Naranbhai V, Stylianou E, Darboe F, ..., McShane H. 2016. T-cell activation is an immune correlate of risk in BCG vaccinated infants. Nature communications 7:11290-11290.
127. Tsuji S, Matsumoto M, Takeuchi O, Akira S, Azuma, Hayashi A, Toyoshima K, Seya T. 2000. Maturation of Human Dendritic Cells by Cell Wall Skeleton of Mycobacterium bovis Bacillus Calmette-Guérin: Involvement of Toll-Like Receptors. Infection and Immunity 68:6883-6890.
128. Sugisaki K, A M Dannenberg, Jr., Abe Y, Tsuruta J, Su WJ, Said W, Feng L, Yoshimura T, Converse PJ, Mounts P. 1998. Nonspecific and immune-specific up-regulation of cytokines in rabbit dermal tuberculous (BCG) lesions. Journal of leukocyte biology 63:440-450.
129. Marchant A, Goetghebuer T, Ota MO, Wolfe I, Ceesay SJ, De Groote D, Corrah T, Bennett S, Wheeler J, Huygen K, Aaby P, McAdam KPWJ, Newport MJ. 1999. Newborns Develop a Th1-Type Immune Response to Mycobacterium bovis Bacillus Calmette-Guerin Vaccination. The Journal of immunology (1950) 163:2249-2255.
130. Ravn P, Boesen H, Pedersen BK, Andersen P. 1997. Human T cell responses induced by vaccination with Mycobacterium bovis bacillus Calmette-Guerin. The Journal of immunology (1950) 158:1949-1955.
131. Smith SG, Kleinnijenhuis J, Netea MG, Dockrell HM. 2017. Whole Blood Profiling of Bacillus Calmette-Guerin-Induced Trained Innate Immunity in Infants Identifies Epidermal Growth Factor, IL-6, Platelet-Derived Growth Factor-AB/BB, and Natural Killer Cell Activation. Frontiers in immunology 8:644-644.
132. Cheng S-C, Quintin J, Cramer RA, Shepardson KM, Saeed S, Kumar V, Giamarellos-Bourboulis EJ, Martens JHA, Rao NA, Aghajanirefah A, Manjeri GR, Li Y, Ifrim DC, Arts RJW, van der Meer BMJW, Deen PMT, Logie C, O'Neill LA, Willems P, ..., Netea MG. 2014. mTOR- and HIF-1α–mediated aerobic glycolysis as metabolic basis for trained immunity. Science (American Association for the Advancement of Science) 345:1579-1579.

133. Kleinnijenhuis J, Quintin J, Preijers F, Joosten LAB, Ifrim DC, Saeed S, Jacobs C, van Loenhout J, de Jong D, Stunnenberg HG, Xavier RJ, van der Meer JWM, van Crevel R, Netea MG. 2012. Bacille Calmette-Guérin induces NOD2-dependent nonspecific protection from reinfection via epigenetic reprogramming of monocytes. Proceedings of the National Academy of Sciences - PNAS 109:17537-17542.
134. Delahaye JL, Gern BH, Cohen SB, Plumlee CR, Shafiani S, Gerner MY, Urdahl KB. 2019. Cutting Edge: Bacillus Calmette-Guérin-Induced T Cells Shape Mycobacterium tuberculosis Infection before Reducing the Bacterial Burden. The Journal of immunology (1950) 203:807-812.
135. Nemes E, Geldenhuys H, Rozot V, Rutkowski KT, Ratangee F, Bilek N, Mabwe S, Makhethe L, Erasmus M, Toefy A, Mulenga H, Hanekom WA, Self SG, Bekker L-G, Ryall R, Gurunathan S, Diazgranados CA, Andersen P, Kromann I, ..., Hatherill M. 2018. Prevention of M. tuberculosis Infection with H4:IC31 Vaccine or BCG Revaccination. New England Journal of Medicine 379:138-149.
136. Arbues A, Aguilo JI, Gonzalo-Asensio J, Marinova D, Uranga S, Puentes E, Fernandez C, Parra A, Cardona PJ, Vilaplana C, Ausina V, Williams A, Clark S, Malaga W, Guilhot C, Gicquel B, Martin C. 2013. Construction, characterization and preclinical evaluation of MTBVAC, the first live-attenuated M. tuberculosis -based vaccine to enter clinical trials. Vaccine 31:4867-4873.
137. Tameris M, Mearns H, Penn-Nicholson A, Gregg Y, Bilek N, Mabwe S, Geldenhuys H, Shenje J, Luabeya AKK, Murillo I, Doce J, Aguilo N, Marinova D, Puentes E, Rodríguez E, Gonzalo-Asensio J, Fritzell B, Thole J, Martin C, ..., Veldsman A. 2019. Live-attenuated Mycobacterium tuberculosis vaccine MTBVAC versus BCG in adults and neonates: a randomised controlled, double-blind dose-escalation trial. The lancet respiratory medicine 7:757-770.
138. Hess J, Miko D, Catic A, Lehmensiek V, Russell DG, Stefan HEK. 1998. Mycobacterium bovis Bacille Calmette-Guerin Strains Secreting Listeriolysin of Listeria monocytogenes. Proceedings of the National Academy of Sciences - PNAS 95:5299-5304.
139. Farinacci M, Weber S, Kaufmann SHE. 2012. The recombinant tuberculosis vaccine rBCG Δ ureC::hly + induces apoptotic vesicles for improved priming of CD4+ and CD8+ T cells. Vaccine 30:7608-7614.
140. Stylianou E, Griffiths KL, Poyntz HC, Harrington-Kandt R, Dicks MD, Stockdale L, Betts G, McShane H. 2015. Improvement of BCG protective efficacy with a novel chimpanzee adenovirus and a modified vaccinia Ankara virus both expressing Ag85A. Vaccine 33:6800-6808.
141. Pinpathomrat N, Bull N, Pasricha J, Harrington-Kandt R, McShane H, Stylianou E. 2021. Using an effective TB vaccination regimen to identify immune responses associated with protection in the murine model. Vaccine 39:1452-1462.
142. Mustafa AS. 2021. Adjuvants and Antigen-Delivery Systems for Subunit Vaccines against Tuberculosis. Vaccines (Basel) 9:972.
143. Kaufmann SHE, Weiner J, Von Reyn CF. 2017. Novel approaches to tuberculosis vaccine development. International Journal of Infectious Diseases 56:263-267.

144. Saini V, Raghuvanshi S, Talwar GP, Ahmed N, Khurana JP, Hasnain SE, Tyagi AK, Tyagi AK. 2009. Polyphasic Taxonomic Analysis Establishes Mycobacterium indicus pranii as a Distinct Species. PloS one 4:e6263-e6263.
145. Sharma SK, Katoch K, Sarin R, Balambal R, Jain NK, Patel N, Murthy KJR, Singla N, Saha PK, Khanna A, Singh U, Kumar S, Sengupta A, Banavaliker JN, Chauhan DS, Sachan S, Wasim M, Tripathi S, Dutt N, ..., Rani R. 2017. Efficacy and Safety of Mycobacterium indicus pranii as an adjunct therapy in Category II pulmonary tuberculosis in a randomized trial. Scientific reports 7:3354-12.
146. Penn-Nicholson A, Geldenhuys H, Burny W, van der Most R, Day CL, Jongert E, Moris P, Hatherill M, Ofori-Anyinam O, Hanekom W, Bollaerts A, Demoitie M-A, Kany Luabeya AK, De Ruymaeker E, Tameris M, Lapierre D, Scriba TJ. 2015. Safety and immunogenicity of candidate vaccine M72/AS01E in adolescents in a TB endemic setting. Vaccine 33:4025-4034.
147. Van Der Meeren O, Hatherill M, Nduba V, Wilkinson RJ, Muyoyeta M, Van Brakel E, Ayles HM, Henostroza G, Thienemann F, Scriba TJ, Diacon A, Blatner GL, Demoitié M-A, Tameris M, Malahleha M, Innes JC, Hellström E, Martinson N, Singh T, ..., Tait DR. 2018. Phase 2b Controlled Trial of M72/AS01E Vaccine to Prevent Tuberculosis. The New England journal of medicine 379:1621-1634.
148. Tait DR, Hatherill M, Van Der Meeren O, Ginsberg AM, Van Brakel E, Salaun B, Scriba TJ, Akite EJ, Ayles HM, Bollaerts A, Demoitié M-A, Diacon A, Evans TG, Gillard P, Hellström E, Innes JC, Lempicki M, Malahleha M, Martinson N, ..., Roman F. 2019. Final Analysis of a Trial of M72/AS01E Vaccine to Prevent Tuberculosis. The New England journal of medicine 381:2429-2439.
149. Tkachuk AP, Gushchin VA, Potapov VD, Demidenko AV, Lunin VG, Gintsburg AL. 2017. Multi-subunit BCG booster vaccine GamTBvac: Assessment of immunogenicity and protective efficacy in murine and guinea pig TB models. PloS one 12:e0176784.
150. Tkachuk AP, Bykonia EN, Popova LI, Kleymenov DA, Semashko MA, Chulanov VP, Fitilev SB, Maksimov SL, Smolyarchuk EA, Manuylov VA, Vasina DV, Gushchin VA, Gintsburg AL. 2020. Safety and Immunogenicity of the GamTBvac, the Recombinant Subunit Tuberculosis Vaccine Candidate: A Phase II, Multi-Center, Double-Blind, Randomized, Placebo-Controlled Study. Vaccines (Basel) 8:652.
151. Orme IM, Ordway DJ. 2016. Mouse and Guinea Pig Models of Tuberculosis. Microbiology spectrum 4.
152. Plumlee CR, Duffy FJ, Gern BH, Delahaye JL, Cohen SB, Stoltzfus CR, Rustad TR, Hansen SG, Axthelm MK, Picker LJ, Aitchison JD, Sherman DR, Ganusov VV, Gerner MY, Zak DE, Urdahl KB. 2021. Ultra-low Dose Aerosol Infection of Mice with Mycobacterium tuberculosis More Closely Models Human Tuberculosis. Cell host & microbe 29:68-82.e5.
153. Nemeth J, Olson GS, Rothchild AC, Jahn AN, Mai D, Duffy FJ, Delahaye JL, Srivatsan S, Plumlee CR, Urdahl KB, Gold ES, Aderem A, Diercks AH. 2020. Contained Mycobacterium tuberculosis infection induces concomitant and heterologous protection. PLoS pathogens 16:e1008655-e1008655.

154. Plumlee CR, Barrett HW, Shao DE, Lien KA, Cross LM, Cohen SB, Edlefsen PT, Urdahl KB. 2023. Assessing vaccine-mediated protection in an ultra-low dose Mycobacterium tuberculosis murine model. PLoS pathogens 19:e1011825-e1011825.
155. Balasubramanian V, Wiegeshaus EH, Taylor BT, Smith DW. 1994. Pathogenesis of tuberculosis: pathway to apical localization. Tubercle and Lung Disease 75:168-178.
156. Donald PR, Diacon AH, Lange C, Demers AM, von Groote-Biddlingmeier F, Nardell E. 2018. Droplets, dust and guinea pigs: an historical review of tuberculosis transmission research, 1878-1940. The international journal of tuberculosis and lung disease 22:972-982.
157. Jacobs AL. 1941. Infective dose in pulmonary tuberculosis. Tubercle 22:266-271.
158. Colditz GA, Berkey CS, Mosteller F, Brewer TF, Wilson ME, Burdick E, Fineberg HV. 1995. The efficacy of bacillus Calmette-Guérin vaccination of newborns and infants in the prevention of tuberculosis : meta-analyses of the published literature. Pediatrics (Evanston) 96:29-35.
159. Mangtani P, Abubakar I, Ariti C, Beynon R, Pimpin L, Fine PEM, Rodrigues LC, Smith PG, Lipman M, Whiting PF, Sterne JA. 2014. Protection by BCG Vaccine Against Tuberculosis: A Systematic Review of Randomized Controlled Trials. Clinical infectious diseases 58:470-480.
160. Abubakar I, Pimpin L, Ariti C, Beynon R, Mangtani P, Sterne JAC, Fine PEM, Smith PG, Lipman M, Elliman D, Watson JM, Drumright LN, Whiting PF, Vynnycky E, Rodrigues LC. 2013. Systematic review and meta-analysis of the current evidence on the duration of protection by bacillus Calmette-Guerin vaccination against tuberculosis. Health technology assessment (Winchester, England) 17:1-372.
161. Schrager LK, Vekemens J, Drager N, Lewinsohn DM, Olesen OF. 2020. The status of tuberculosis vaccine development. The Lancet infectious diseases 20:e28-e37.
162. Karp CL, Wilson CB, Stuart LM. 2015. Tuberculosis vaccines: barriers and prospects on the quest for a transformative tool. Immunological reviews 264:363-381.
163. Cardona P-J, Williams A. 2017. Experimental animal modelling for TB vaccine development. International journal of infectious diseases 56:268-273.
164. Bloom BR, Modlin RL. 2016. Mechanisms of Defense against Intracellular Pathogens Mediated by Human Macrophages. Microbiology spectrum 4.
165. Mollenkopf H-J, Kursar M, Kaufmann SHE. 2004. Immune Response to Postprimary Tuberculosis in Mice: Mycobacterium tuberculosis and Miycobacterium bovis bacille Calmette-Guérin Induce Equal Protection. The Journal of infectious diseases 190:588-597.
166. Vidal SJ, Sellers D, Yu J, Wakabayashi S, Sixsmith J, Aid M, Barrett J, Stevens SF, Liu X, Li W, Plumlee CR, Urdahl KB, Martinot AJ, Barouch DH. 2023. Attenuated Mycobacterium tuberculosis vaccine protection in a low-dose murine challenge model. iScience 26:106963-106963.
167. Balasubramanian V, Wiegeshaus EH, Smith DW. 1994. Mycobacterial Infection in Guinea Pigs. Immunobiology (1979) 191:395-401.

168. Wood R, Morrow C, Barry CE, Bryden WA, Call CJ, Hickey AJ, Rodes CE, Scriba TJ, Blackburn J, Issarow C, Mulder N, Woodward J, Moosa A, Singh V, Mizrahi V, Warner DF. 2016. Real-Time Investigation of Tuberculosis Transmission: Developing the Respiratory Aerosol Sampling Chamber (RASC). PloS one 11:e0146658-e0146658.
169. Dinkele R, Gessner S, Patterson B, McKerry A, Hoosen Z, Vazi A, Seldon R, Koch A, Warner DF, Wood R. 2024. Persistent Mycobacterium tuberculosis bioaerosol release in a tuberculosis-endemic setting. iScience 27:110731.
170. Fennelly KP, Martyny JW, Fulton KE, Orme IM, Cave DM, Heifets LB. 2004. Cough-generated Aerosols of Mycobacterium tuberculosis: A New Method to Study Infectiousness. American journal of respiratory and critical care medicine 169:604-609.
171. Nduba V, Njagi LN, Murithi W, Mwongera Z, Byers J, Logioia G, Peterson G, Segnitz RM, Fennelly K, Hawn TR, Horne DJ. 2024. Mycobacterium tuberculosis cough aerosol culture status associates with host characteristics and inflammatory profiles. Nature communications 15:7604-15.
172. Fennelly KP, Jones-Lopez EC, Ayakaka I, Kims S, Menyha H, Kirenga B, Muchwa C, Joloba M, Dryden-Peterson S, Reilly N, Okwera A, Elliott AM, Smith PG, Mugerwa RD, Eisenach KD, Ellner JJ. 2012. Variability of Infectious Aerosols Produced during Coughing by Patients with Pulmonary Tuberculosis. American journal of respiratory and critical care medicine 186:450-457.
173. Theron G, Limberis J, Venter R, Smith L, Pietersen E, Esmail A, Calligaro G, te Riele J, de Kock M, van Helden P, Gumbo T, Clark TG, Fennelly K, Warren R, Dheda K. 2020. Bacterial and host determinants of cough aerosol culture positivity in patients with drug-resistant versus drug-susceptible tuberculosis. Nature medicine 26:1435-1443.
174. Acuna-Villaorduna C, Schmidt-Castellani LG, Marques-Rodrigues P, White LF, Hadad DJ, Gaeddert M, Ellner JJ, Fennelly KP, Palaci M, Dietze R, Jones-Lopez EC. 2018. Cough-aerosol cultures of Mycobacterium tuberculosis in the prediction of outcomes after exposure. A household contact study in Brazil. PloS one 13:e0206384-e0206384.
175. Jones-López EC, Acuña-Villaorduña C, Ssebidandi M, Gaeddert M, Kubiak RW, Ayakaka I, White LF, Joloba M, Okwera A, Fennelly KP. 2016. Cough Aerosols of Mycobacterium tuberculosis in the Prediction of Incident Tuberculosis Disease in Household Contacts. Clinical infectious diseases 63:10-20.
176. Donald PR, Diacon AH, Thee S. 2021. Anton Ghon and His Colleagues and Their Studies of the Primary Focus and Complex of Tuberculosis Infection and Their Relevance for the Twenty-First Century. Respiration 100:557-567.
177. Lin PL, Ford CB, Coleman MT, Myers AJ, Gawande R, Ioerger T, Sacchettini J, Fortune SM, Flynn JL. 2014. Sterilization of granulomas is common in active and latent tuberculosis despite within-host variability in bacterial killing. Nature medicine 20:75-79.
178. Martin CJ, Cadena AM, Leung VW, Lin PL, Maiello P, Hicks N, Chase MR, Flynn JL, Fortune SM. 2017. Digitally Barcoding Mycobacterium tuberculosis Reveals In Vivo Infection Dynamics in the Macaque Model of Tuberculosis. mBio 8.

179. O'Grady F, Riley RL. 1963. Experimental Airborne Tuberculosis. Advances in Tuberculosis Research 12:150-190.
180. Riley RL, Mills CC, Nyka W, Weinstock N, Storey PB, Sultan LU, Riley MC, Wells WF. 1959. AERIAL DISSEMINATION OF PULMONARY TUBERCULOSIS A TWO-YEAR STUDY OF CONTAGION IN A TUBERCULOSIS WARD. American Journal of Hygiene 70:185-196.
181. Kline SE, Hedemark LL, Davies SF. 1995. Outbreak of Tuberculosis among Regular Patrons of a Neighborhood Bar. The New England journal of medicine 333:222-227.
182. Sultan L, Nyka W, Mills C, O'Grady F, Wells W, Riley RL. 1960. Tuberculosis disseminators. A study of the variability of aerial infectivity of tuberculous patients. The American review of respiratory disease 82:358-369.
183. Ypma RJF, Altes HK, van Soolingen D, Wallinga J, van Ballegooijen WM. 2013. A Sign of Superspreading in Tuberculosis: Highly Skewed Distribution of Genotypic Cluster Sizes. Epidemiology (Cambridge, Mass) 24:395-400.
184. Mayer-Barber Katrin D, Andrade Bruno B, Barber Daniel L, Hieny S, Feng Carl G, Caspar P, Oland S, Gordon S, Sher A. 2011. Innate and Adaptive Interferons Suppress IL-1α and IL-1β Production by Distinct Pulmonary Myeloid Subsets during Mycobacterium tuberculosis Infection. Immunity (Cambridge, Mass) 35:1023-1034.
185. Fine PEM. 1988. BCG vaccination against tuberculosis and leprosy. British medical bulletin 44:691-703.
186. Lu LL, Smith MT, Yu KKQ, Luedemann C, Suscovich TJ, Grace PS, Cain A. 2019. IFN-[gamma]-independent immune markers of Mycobacterium tuberculosis exposure. Nature medicine 25:977.
187. Hansen SG, Zak DE, Xu G, Ford JC, Marshall EE, Malouli D, Gilbride RM, Hughes CM, Ventura AB, Ainslie E, Randall KT, Selseth AN, Rundstrom P, Herlache L, Lewis MS, Park H, Planer SL, Turner JM, Fischer M, ..., Picker LJ. 2018. Prevention of tuberculosis in rhesus macaques by a cytomegalovirus-based vaccine. Nature medicine 24:130-143.
188. Beura LK, Hamilton SE, Bi K, Schenkel JM, Odumade OA, Casey KA, Thompson EA, Fraser KA, Rosato PC, Filali-Mouhim A, Sekaly RP, Jenkins MK, Vezys V, Haining WN, Jameson SC, Masopust D. 2016. Normalizing the environment recapitulates adult human immune traits in laboratory mice. Nature (London) 532:512-516.
189. Ma S, Morrison R, Hobbs SJ, Farrow-Johnson J, Rustad TR, Sherman DR. 2018. Network stress test reveals novel drug potentiators in Mycobacterium tuberculosis. Cold Spring Harbor Laboratory.
190. Hu Z, Wong K-W, Zhao H-M, Wen H-L, Ji P, Ma H, Wu K, Lu S-H, Li F, Li Z-M, Shu T, Xu J-Q, Lowrie DB, Fan X-Y. 2017. Sendai Virus Mucosal Vaccination Establishes Lung-Resident Memory CD8 T Cell Immunity and Boosts BCG-Primed Protection against TB in Mice. Molecular therapy 25:1222-1233.
191. Moliva JI, Hossfeld AP, Canan CH, Dwivedi V, Wewers MD, Beamer G, Turner J, Torrelles JB. 2018. Exposure to human alveolar lining fluid enhances Mycobacterium bovis BCG vaccine efficacy against Mycobacterium tuberculosis infection in a CD8(+) T-cell-dependent manner. Mucosal immunology 11:968-978.

192. Nandakumar S, Kannanganat S, Posey JE, Amara RR, Sable SB. 2014. Attrition of T-Cell Functions and Simultaneous Upregulation of Inhibitory Markers Correspond with the Waning of BCG-Induced Protection against Tuberculosis in Mice. PLoS ONE 9:e113951.
193. Jaron B, Maranghi E, Leclerc C, Majlessi L. 2008. Effect of Attenuation of Treg during BCG Immunization on Anti-Mycobacterial Th1 Responses and Protection against Mycobacterium tuberculosis. PLoS ONE 3:e2833.
194. Man K, Miasari M, Shi W, Xin A, Henstridge DC, Preston S, Pellegrini M, Belz GT, Smyth GK, Febbraio MA, Nutt SL, Kallies A. 2013. The transcription factor IRF4 is essential for TCR affinity-mediated metabolic programming and clonal expansion of T cells. Nature immunology 14:1155-U79.
195. Cao J, Liao S, Zeng F, Liao Q, Luo G, Zhou Y. 2023. Effects of altered glycolysis levels on CD8+ T cell activation and function. Cell Death & Disease 14.
196. Liu S, Liao S, Liang L, Deng J, Zhou Y. 2023. The relationship between CD4+ T cell glycolysis and their functions. Trends in Endocrinology & Metabolism 34:345-360.
197. Kühtreiber WM, Tran L, Kim T, Dybala M, Nguyen B, Plager S, Huang D, Janes S, Defusco A, Baum D, Zheng H, Faustman DL. 2018. Long-term reduction in hyperglycemia in advanced type 1 diabetes: the value of induced aerobic glycolysis with BCG vaccinations. npj Vaccines 3.
198. Kühtreiber WM, Takahashi H, Keefe RC, Song Y, Tran L, Luck TG, Shpilsky G, Moore L, Sinton SM, Graham JC, Faustman DL. 2020. BCG Vaccinations Upregulate Myc, a Central Switch for Improved Glucose Metabolism in Diabetes. iScience 23:101085.
199. Sutton MS, Bucsan AN, Lehman CC, Kamath M, Pokkali S, Magnani DM, Seder R, Darrah PA, Roederer M. 2024. Antibody-mediated depletion of select leukocyte subsets in blood and tissue of nonhuman primates. Frontiers in immunology 15:1359679-1359679.
200. Addison EG, North J, Bakhsh I, Marden C, Haq S, Al-Sarraj S, Malayeri R, Wickremasinghe RG, Davies JK, Lowdell MW. 2005. Ligation of CD8α on human natural killer cells prevents activation-induced apoptosis and enhances cytolytic activity. Immunology 116:354-361.
201. Garcillã¡N B, Marin AVM, Jimã©Nez-Reinoso AS, Briones AC, Muã±Oz-Ruiz M, Garcã-A-Leã^{3}N MAJ, Gil J, Allende LM, Martã-Nez-Naves E, Toribio MAL, Regueiro JR. 2015. Î^{3}Î´ T Lymphocytes in the Diagnosis of Human T Cell Receptor Immunodeficiencies. Frontiers in Immunology 6.
202. Nel I, Bertrand L, Toubal A, Lehuen A. 2021. MAIT cells, guardians of skin and mucosa? Mucosal immunology 14:803-814.
203. Sharma M, Zhang S, Niu L, Lewinsohn DM, Zhang X, Huang S. 2020. Mucosal-Associated Invariant T Cells Develop an Innate-Like Transcriptomic Program in Anti-mycobacterial Responses. Frontiers in Immunology 11.
204. Hoft DF, Brown RM, Roodman ST. 1998. Bacille Calmette-Guérin Vaccination Enhances Human γδ T Cell Responsiveness to Mycobacteria Suggestive of a Memory-Like Phenotype. The Journal of Immunology 161:1045-1054.

205. Caruso AM, Serbina N, Klein E, Triebold K, Bloom BR, Flynn JL. 1999. Mice Deficient in CD4 T Cells Have Only Transiently Diminished Levels of IFN-γ, Yet Succumb to Tuberculosis. The Journal of Immunology 162:5407-5416.
206. Drain PK, Bajema KL, Dowdy D, Dheda K, Naidoo K, Schumacher SG, Ma S, Meermeier E, Lewinsohn DM, Sherman DR. 2018. Incipient and Subclinical Tuberculosis: a Clinical Review of Early Stages and Progression of Infection. Clinical microbiology reviews 31.